## NOTICE

The quality of this microform is heavily dependent upon the quality of the original thesis submitted for microfilming. Every effort has been made to ensure the highest quality of reproduction possible.

If pages are missing, contact the university which granted the degree.

Some pages may have indistinct print especially if the original pages were typed with a poor typewriter ribbon or if the university sent us an inferior photocopy.

Reproduction in full or in part of this microform is governed by the Canadian Copyright Act, R.S.C. 1970, c. C-30, and subsequent amendments.

## AVIS

La qualité de cette microforme dépend grandement de la qualité de la thèse soumise au microfilmage. Nous avons tout fait pour assurer une qualité supérieure de reproduction.

S'il manque des pages, veuillez communiquer avec l'université qui a conféré le grade.

La qualité d'impression de certaines pages peut laisser à désirer, surtout si les pages originales ont été dactylographiées à l'aide d'un ruban usé ou si l'université nous a fait parvenir une photocopie de qualité inférieure.

La reproduction, même partielle, de cette microforme est soumise à la Loi canadienne sur le droit d'auteur, SRC 1970, c. C-30, et ses amendements subséquents.

ISBN 0-315-59157-9

# Characterization of Traps by Deep Level Transient Spectroscopy in GaAs Epitaxial Layers Grown by Close-Spaced Vapor Transport

Sylvain Bourassa

A Thesis

in

The Department

of

Electrical Engineering

Presented in Partial Fulfillment of the Requirements
for the Degree of Master of Engineering at
Concordia University
Montréal, Québec, Canada

January 1990

## ABSTRACT

### CHARACTERIZATION OF TRAPS BY DEEP LEVEL TRANSIENT SPECTROSCOPY IN GaAs EPITAXIAL LAYERS GROWN BY CLOSE-SPACED VAPOR TRANSPORT

Sylvain Bourassa

Two methods to characterize gallium arsenide (GaAs) Schottky barrier diodes are presented in this thesis. The GaAs epitaxial layers have been grown by the close-spaced vapor transport (CSVT) technique. The first method presented is the capacitance-voltage (C-V) measurement. The second method is the current-voltage (I-V) measurement.

The characterization by the C-V measurement and the I-V measurement are the prerequisite for the deep level transient spectroscopy (DLTS) technique used to characterize deep level traps in a GaAs semiconductor material. It is found that when the characterization of the diode corresponds to the required specification, the DLTS technique can be used.

The DLTS measurement uses the change in capacitance of a Schottky barrier diode under reverse bias. From these various capacitance transients measured, the apparent activation energy, the capture cross section and the concentration of deep levels are found in a GaAs sample. Two particular deep level traps have been found in those

samples; EL2 and ELCS1. For the above methods and technique outlined, theoretical and experimental considerations are presented.

Finally, the results obtained by characterization of GaAs epitaxial layers found by DLTS are presented. The probable causes of error involved in the DLTS measurements are discussed. Then a model for the EL2 trap concentration in GaAs epitaxial layers is proposed. According to this model, it is shown that the EL2 concentration is function of the possible off-stoichiometry variation with the deposition temperature for epitaxial layers grown by CSVT.

## REMERCIEMENTS

Je tiens à exprimer ma gratitude au Professeur B.A. Lombos pour m'avoir choisi dans son equipe de recherche et de m'avoir prêté confiance à l'utilisation des équipements de laboratoire de Physique des Solides du Département de Genie Electrique à l'Universite Concordia de Montréal. Je le remercie vivement pour les nombreux conseils et discussions scientifiques qui ont permis la réalisation de ce rapport.

Je remercie également les Professeurs M. Rouzeyre et M. Averous de l'Université des Sciences et Techniques du Languedoc a Montpellier (France), de m'avoir acceuilli dans leur laboratoires de Physique. Leur acceuil m'a permi d'obtenir les premiers résultats experimentaux a la réalisation de ce projet.

J'exprime ma reconnaissance au Dr. T. Bretagnon et au Dr. A Jean pour leurs nombreux conseils théorique et pratique lors de l'acquisition des resultats expérimentaux a l'Universite Concordia.

TABLE OF CONTENTS


| | Page |
|---|---|
| LIST OF TABLES | x |
| LIST OF FIGURES | xi |
| Chapter | |
| 1.0 INTRODUCTION | 1 |
| 2.0 BASIC DEFINITIONS ON CRYSTALLINE STRUCTURE FOR GaAs | 5 |
| 2.1 Crystal lattice and point defect | 5 |
| 2.1.1 The crystal lattice | 5 |
| 2.1.2 Point defects | 6 |
| 2.2 Shallow and Deep Level States in Semiconductors | 7 |
| 2.2.1 Shallow levels | 8 |
| 2.2.2 Deep levels | 8 |
| 3.0 GENERAL CONSIDERATIONS AND EXPERIMENTAL DESCRIPTIONS OF SCHOTTKY BARRIERS | 9 |
| 3.0.0 Introduction | 9 |
| 3.1 Capacitance-Voltage Characteristics of a Schottky Barrier | 11 |
| 3.1.1 Space charge region of an SKB | 11 |
| 3.1.2 Experimental Considerations | 15 |
| 3.2 Current-Voltage Characteristics of a Schottky Barrier | 17 |
| 3.2.1 Current Characteristic | 17 |
| 3.2.2 Practical methods to find Rs, Rsh, n, Io and $\phi b$ | 18 |
| 3.2.3 Experimental considerations | 21 |

3.2.4 Comparison of the barrier height $\phi b$ between C(V) and I(V) measurements ..... ..... 22

3.3 Practical Consideration of Schottky Barrier Fabrication ..... 24

3.3.1 Practical considerations for ohmic contacts. 24

3.3.2 Practical considerations for metal-semiconductor junction ..... 24

4.0 CHARACTERIZATION OF DEEP LEVELS AND EXPERIMENTAL DESCRIPTIONS ..... ..... 27

4.0.0 Introduction ..... 27

4.1 Some General Definitions ..... 28

4.1.1 General equation of occupation of a defect state ..... 28

4.1.2 General definition of capture rate of free carriers ..... 30

4.1.3 Definition of emission rate of a carrier trapped ..... 32

4.1.4 Emission rate at thermal equilibrium ..... 32

4.2 Schottky Barrier Taking Deep Levels Into Account .. 35

4.2.1 Determination of the transition region ..... 35

4.2.2 Determination of the capacitance variation . 37

4.2.3 Capacitive measurements method ..... 40

4.2.4 DLTS method analysis ... ..... .. .... 41

4.2.5 Arrhenius plot ... ..... ... 42

4.3 Experimental Description for Finding S(T)/Co, Ea and $N_T$ ..... 44

4.3.1 Experimental considerations for capacitance transient measurement ..... 44

4.3.2 Experimental procedures for finding Ea ..... 49

4.3.3 Summary of experimental procedure for finding all parameters and $N_T$ ..... 51

5.0 RESULTS AND DISCUSSIONS ..... 53

5.0.0 Introduction ..... 53

5.1.0 Determination of free carrier concentration and barrier height ..... 54

5.2 Apparent Activation Energy Ea ..... 64

5.2.1 Identification of deep trap levels ..... 64

5.2.2 Probable causes of error in finding Ea ..... 72

5 3 Experimental Results ..... 76

5.4 n, Io, Vb, Rs and Rsh measurements ..... 82

5.4.1 Plots of $N_D$ vs $\phi b$ and Js vs $\phi b$ ..... 84

5.4 2 Plots of EL2 vs $\phi b$ and ELCS1 vs $\phi b$ ..... 90

5.4.3 Comparison for Vb from C(V) and for $\phi b$ from I(V) measurement ..... 93

5.5 Experimental Observations on EL2 and ELCS1 Traps .. 94

5.5.1 Proposed model for EL2 deep donor trap ..... 104

5 5.2 Application of the EL2 Model to CSVT epitaxial growth ..... 109

5.5.3 The 300K trap ELCS1 ..... 113

6.0 CONCLUSIONS ..... 114

REFERENCES ..... 117

APPENDIX I

List of Symbols and Results for all Samples ..... ..... 123

APPENDIX II.

Space charge region derivation for a Schottky barrier ..... 149

APPENDIX III

The image force barrier lowering ..... 154

APPENDIX IV

Emission rate at thermal equilibrium ..... 155

APPENDIX V

Determination of the transition region λ ..... ..... 158

APPENDIX VI

Determination of ΔC/Co ..... ..... 159

APPENDIX VII

Arrhenius Plot and Rate Window ..... ..... ..... 162

APPENDIX VIII

Summary on epitaxial layer grown by CSVT technique ..... .. 165

APPENDIX IX

Results for temperature regulator for DLTS ..... 167

APPENDIX X

Schottky barrier fabrication ..... ... .... ..... 172

# LIST OF TABLES


| TABLE | | Page |
|---|---|---|
| 5.1 | Diameter found from the Talysurf ..... | 59 |
| 5.2 | Error found in $N_D$ according to a change in diameter D .. | 61 |
| 5.3 | Temperature with corresponding rate window for fig. 5.7. | 67 |
| 5.4 | Several measurements of apparent activation energy for EL2 ..... | 67 |
| 5.5 | Comparison for ELCS1 trap found at different laboratories ..... ..... | 70 |
| 5.6 | Apparent activation energies for peaks shown in fig. 5.8 | 71 |
| 5.7 | Error between theoretical and experimental temperature measurements ..... | 73 |
| 5.8 | Results for sample R16 ..... | 78 |
| 5.9 | Results for sample B46 ..... | 79 |
| 5.10 | Results for sample B51 ..... | 80 |
| I.1 | Results for all samples studied ..... | 128 |
| IX.1 | Readings for R at the cryostat tail and at the sample .. | 167 |
| IX.2 | Results from circuit of fig. IX.1 ..... | 168 |

LIST OF FIGURES


| Figure | | Page |
|---|---|---|
| 2.1 | Important lattice structures ..... | 5 |
| 2.2 | Point defects in a binary AB compound semiconductor .... | 7 |
| 3.1 | Band diagram for the junction at equilibrium ($\phi_m > \phi_s$) ... | 13 |
| 3.2 | Typical C(V) and $1/C(V)^2$ plots ..... | 14 |
| 3.3 | C(V) measurement flow chart ..... | 16 |
| 3.4 | Equivalent circuit of a non-ideal diode ..... | 19 |
| 3.5 | Measured I-V characteristic & ln(I) vs V ..... | 21 |
| 3.6 | Flow chart of I(V) measurement ..... | 23 |
| 4.1 | The basic process of carrier generation and recombination through traps ..... | 29 |
| 4.2 | Schottky barrier under reverse bias ..... | 36 |
| 4.3 | Voltage pulse applied to a Schottky barrier & corresponding change in capacitance ..... | 38 |
| 4.4 | Space charge region and charge distribution of a Schottky barrier under reverse bias ..... | 39 |
| 4.5 | Experimental sequence for capacitance measurements ..... | 41 |
| 4.6 | DLTS peak due to a change in capacitance transient ..... | 43 |
| 4.7 | Experimental setup for the measurement of S(T)/Co by DLTS ..... | 45 |
| 4.8 | Flow chart of DLTS by sampling ..... | 46 |
| 4.9 | Example for variables to entered initially ..... | 47 |
| 4.10 | Flow chart of the DLTS spectrum ..... | 50 |
| 4.11 | Flow chart of Arrhenius plot ..... | 51 |
| 5.1 | C(V) measurement ..... | 55 |
| 5.2 | $1/C(V)^2$ measurement ..... | 56 |

| | | |
|---|---|---|
| 5.3 | Typical curves from the Talysurf ..... | 58 |
| 5.4 | Capacitance circuit measurement ..... | 63 |
| 5.5 | Typical DLTS spectrum ..... | 66 |
| 5.6 | DLTS peaks for different rate window (for EL2) ..... | 66 |
| 5.7 | Arrhenius plot allowing to find Ea ..... | 68 |
| 5.8 | DLTS spectrum for sample D374 ..... | 71 |
| 5.9 | Examples of thermal speed as function of the temperature | 75 |
| 5.10 | An example of experimental curves of ln(I) vs V ..... | 82 |
| 5.11 | Graph of $N_D$ vs $\phi_b$ for samples D369 through D378 ..... | 85 |
| 5.12 | Graph of Js vs $\phi_b$ for samples D369 through D378 ..... | 87 |
| 5.13 | Graph of $N_D$ vs $\phi_b$ for samples B39 through B60 ..... | 88 |
| 5.14 | Graph of $N_D$ vs $\phi_b$ for samples R2 through R16 ..... | 89 |
| 5.15 | Graph of $N_T$(EL2) vs $\phi_b$ for samples R and B series ..... | 91 |
| 5.16 | Graph of $N_T$(ELCS1) vs $\phi_b$ for samples R and B series .... | 92 |
| 5.17 | DLTS spectra of the CSVT epitaxial layers ..... | 93 |
| 5.18 | Graph of $N_T$ vs the distance from the junction (sample R16) ..... | 98 |
| 5.19 | Graph of $N_T$ vs the distance from the junction (sample B46) ..... | 99 |
| 5.20 | Graph of $N_T$ vs the distance from the junction (sample B51) ..... | 100 |
| 5.21 | Graph of $N_T$(ELCS1) vs the substrate temp. (series R & B) | 101 |
| 5.22 | Graph of $N_T$(EL2) vs the substrate temp. (series R & B).. | 102 |
| 5.23 | Graph of $N_D$ vs the substrate temp. (series R & B) ..... | 103 |
| 5.24 | Formation for EL2 complex ..... | 104 |
| 5.25 | Representation of EL2 formation ..... | 106 |

5.26 Diagram for compensation in GaAs crystal ..... 107

5.27 $N_T$(EL2) vs $V_{Ga}$ concentration ..... 111

5.28 $N_T$(ELCS1) vs $N_d$ for samples AL, AU and As ..... 112

II.1 Schematic representation of a Schottky barrier ..... 152

III.1 Diagram of the image force lowering of the barrier ..... 154

VIII.1 Diagram of the CSVT system ..... 166

IX.1 Temperature Regulator for DLTS ..... 171

# 1.0 INTRODUCTION

In the early 1980's, with the advent of new technologies in solid state devices, scienlists and industries were turned towards the gallium arsenide (GaAs) semiconductor (SC) devices because of the interesting features presented over silicon (Si) devices.

There are several advantages for using GaAs. For example one of the interesting feature, is that GaAs have a wider band gap than Si allowing operation over a wider temperature range. Furthermore, GaAs provides a semi-insulating substrate which is ideal for planar device technology by ion implantation as a way of introducing dopants (1). The semi-insulating (SI) nature of the GaAs as a substrate ($\rho > 10^8$ ohm-cm) allows for the isolation of adjacent devices on the same substrate and to reduce parasitic capacitance in metal-semiconductor field-effect transistor (MESFET's) (2). Such MESFET devices are suitable for building integrated circuits (IC's) in semiconductors since they are easy to build and relies on reverse biased Schottky diode formed between the gate and the SC (3).

Finally, another interesting feature for using GaAs, is the high speed that it can provide because of the high mobility of GaAs material (1). For example GaAs transistor gates switch faster than Si transistor to transistor logic (TTL) gates since the minority carrier recombination lifetime is in the range of micro second for Si and in the range of pico second for GaAs. Further more, when operating at the same speeds as Si gates, GaAs gates require less power (3)(4).

The past research being made on GaAs and the reasons stated above bring our interests to study the interesting properties of the crystal.

In this thesis we will study the deep level traps on GaAs epitaxial layer grown by closed spaced vapor transport (CSVT) technique on SI GaAs substrate and GaAs substrate doped with Si (5).

The study of deep levels for GaAs samples is made by the deep level transient spectroscopy (DLTS) technique. The DLTS is a measurement technique used to evaluate the apparent activation energies, the concentrations of deep levels in SC's and their capture cross section. This measurement technique requires a computer system and a $p^+n$ junction or a Schottky barrier diode for the measurement. $p^+$ n junctions and Schottky barriers junctions are frequently used as test devices to study basic material properties since they are easy to fabricate and they allow one to see the type of defect easily (majority or minority carriers), depending on the type of semiconductor used (n type or p type).

Schottky barrier diodes are referred to as rectifying contacts. A Schottky barrier is a metal-semiconductor junction. The junction creates a bending of the semiconductor energy bands near the interface. This bending of the bands produces a depletion region which has a certain capacitance. If a bias is applied to the Schottky barrier, the bending of the energy bands will be changed, modifying the depletion layer width thus its capacitance.

The DLTS technique uses the change in capacitance of the biased junction as a basis for the measurement. Capacitance transients are measured as a function of temperature. As the temperature increases, more levels become ionized. These ionized levels modify the aspect of the capacitance transient since more free carriers are generated. From these changing capacitance transients, the concentrations and energy

levels due to impurities or defect structures of the crystal can be calculated (6).

For the study and characterization of GaAs epitaxial layer, this report is divided into four parts. In the first part, some general definitions are given on GaAs crystalline structure, point defects, shallow and deep level states in a semiconductor (SC).

The second part considers the Schottky barrier capacitance since the variation of the capacitance with voltages under reverse bias will allow the determination of the concentration of shallow donors or acceptors. These will be used to evaluate the concentration of deep levels as it is discussed in the following chapter. Furthermore, in that chapter the characteristics of the diode is examined in order to verify if it can be used for further experiments. The characteristics of the diode is found by the current-voltage measurements. In both cases, the theoretical basis are given and the experimental descriptions follow.

Then in the third part, the characterization of deep levels is studied followed by the experimental descriptions. This third chapter presents first some general definitions on capture rates and emission rates of carriers. Then the theory on capacitive measurements method is described which leads to the DLTS measurement method used in practice. The DLTS measurement on a GaAs sample will allow to find the apparent activation energies by using the Arrhenius plot, and the total trap concentration.

Finally, in the last part, the results obtained by characterization of the GaAs samples found by DLTS measurements are analyzed, discussed and compared with published data. At first, the

probable causes of error involved in the DLTS measurements are evaluated. Then a proposed model for EL2 trap is described and it will be shown that its concentration is function of the possible off-stoichiometry variation with the deposition temperature for epitaxial layers grown by CSVT. Then the report is terminated by a brief conclusion.

## 2.0 BASIC DEFINITIONS ON CRYSTALLINE STRUCTURE FOR GaAs

### 2.1 Crystal lattice and point defect

#### 2.1.1 The crystal lattice

The three dimensional periodic arrangement of atoms in a crystal is called the lattice (7). Some important SC such Si and GaAs have *diamond* and *zincblende* lattice structures as shown in figure 2.1 respectively. These lattice structures are characterized by tetrahedral coordination. As it can be seen in the figure, each atom is surrounded by four equidistant nearest neighbors which lie at the corner of a tetrahedron (8).

The diamond and the zincblende lattices can be considered as two interpenetrating face-centered cubic lattices. For diamond lattice, such as Si, all the atoms are Si. In a zincblende lattice, such as GaAs, the cation sub lattice is gallium (Ga) and the anion sub lattice is arsenic (As) (8).

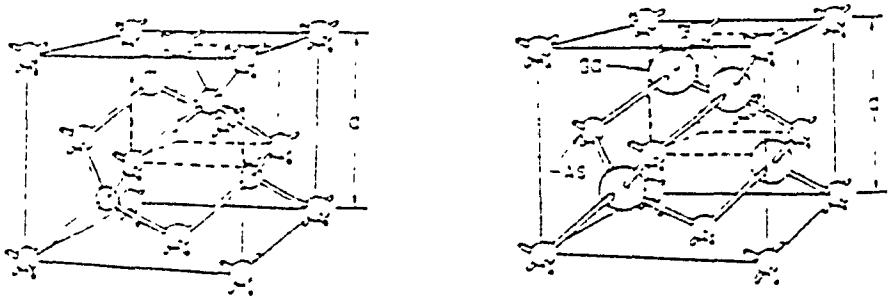

a) Diamond (C, Ge, Si, etc) b) Zincblende (GaAs, GaP, etc)

Fig. 2.1 Important lattice structures

2.1.2 Point defects

We have seen in section 2.1.1 an example of perfect GaAs crystal lattice, but in reality all crystals deviate from perfection. These imperfections or defects of the crystal have important consequences in material properties. They might give rise to localized energy states (9)(10).

The crystallographic defects that give rise to localized energy states in the crystal are called point defects. Point defects in a crystal are lattice flaws that cause interruptions in the lattice periodicity (11)(12). A schematic representation of simple point defects in a binary AB compound crystal semiconductor such as GaAs is shown in figure 2.2 (13) where the cation sub lattice is represented by A and the anion sublattice is represented by B. The different types of point defects are described below. Clearly, vacancies $V_A$ and $V_B$ of sub lattice A and B respectively are shown by rectangles numbered by 1 and 2 respectively. An anti site $B_A$ is an atom of sub lattice B taking the place of an atom of the regular sub lattice A (rectangle #3). An anti site $A_B$ is the contrary of $B_A$ (rectangle #4). The substitutional impurity $I_B$ is a foreign atom I taking the place of an atom of the regular sub lattice B (rectangle #5). A complex $I_A + V_B$ is an impurity $I_A$ with a vacancy $V_B$ (rectangle #6). Finally a complex $V_B + B_A$ is a vacancy $V_B$ and anti site $B_A$ (rectangle #7).

In a semiconductor there are two basic types of lattice disorder, the Frenkel defect and the Schottky defect. The Frenkel defect is a vacancy created by the removal of an atom from a lattice site and it is subsequently positioned interstitially (14)(15). The Schottky defect is the same as the Frenkel defect except that the atom is a missing one

instead being placed interstitially.

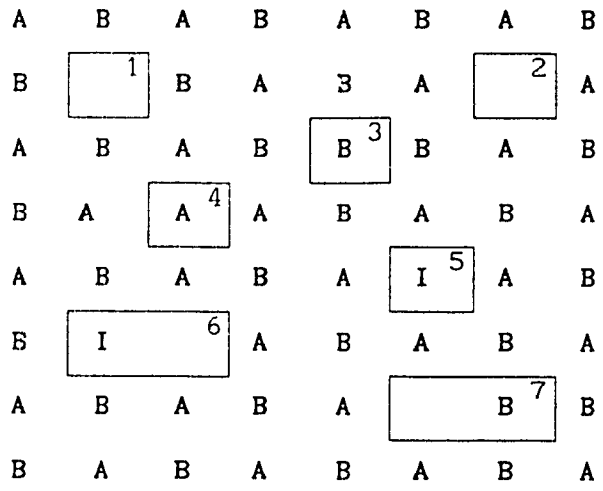


**Figure 2.2 Point defects in a binary AB compound semiconductor**

**1) vacancy $V_A$ 2) vacancy $V_B$ 3) anti site $B_A$ 4) anti site $A_B$**

**5) substitutional impurity $I_B$ 6) $I_A$+$V_B$ complex 7) $V_A$+$B_A$ complex.**

## 2.2 Shallow and Deep Level States in Semiconductors

It has been mentioned above that defects in a crystal might give rise to localized energy states. Besides the imperfections of the crystal, lattice defects can be created voluntary by adding foreign atoms to the host lattice (16). This will introduce electronic energy states into the forbidden gap of an SC. These are the so called *defect states* (17).

This section introduces two categories of defect state: the shallow level impurities and the deep level impurities. The deep level state will be studied extensively in a subsequent chapter.

### 2.2.1 Shallow levels

In general, shallow states are located near their related band edges: near the valence band (VB) for acceptor impurities and near the conduction band (CB) for donor impurities. In fact a shallow state is defined by kT greater than the ionization energy level Ei for a donor in an n-type SC. Here k is the Boltzmann constant and T is the absolute temperature. Thus at room temperature (T=300K), kT=26meV where we have a shallow level if Ei is less than 26meV. The ionization energy of shallow state can be described by the effective mass approximation theory (16)(17) or by the modified hydrogenic model that can be found in reference (18). Shallow impurities are widely used in SC technology for modifying the amount and type of electrical conductivity of an extrinsic SC material. This is the basis of device fabrication such as diodes, transistors and integrated circuits.

### 2.2.2 Deep levels

As opposed to shallow levels, deep levels states are located at considerable distances from a band edge: in this case kT should be less than the energy level Ei. It would require a higher energy for an electron to go from the deep level to the conduction band. Thus at room temperature we have a deep level for Ei greater than 26meV. For GaAs references (19)(20) show a table giving the doping impurities that will cause shallow or deep levels in this material. For example, Si is an amphoteric impurity in GaAs, but it has been shown experimentally that Si would be a shallow donor in this material with an activation energy equal to 0.002eV (21). On the other hand chromium (Cr) is a deep acceptor in GaAs with an activation energy equal to 0.63eV (19).

# 3.0 GENERAL CONSIDERATIONS AND EXPERIMENTAL DESCRIPTIONS OF SCHOTTKY BARRIERS

## 3.0.0 Introduction

This chapter is divided into three main sections. The first section deals with the capacitance of a Schottky barrier (SKB). The second section is involved in finding the characteristics of the SKB and the last one gives some practical considerations for SKB fabrication.

The capacitance of an SKB is of fundamental importance in the characterization of a GaAs sample for two reasons. The first reason is that the variation of the junction capacitance of an SKB with reverse bias voltage applied to the junction, usually denoted by C(V), will allow one to find the shallow donor concentration $N_D$ of an n-type GaAs SC sample under investigation.[1] The shallow donor concentration will be used in turn for the calculation of the deep level trap concentration. Furthermore, C(V) might be used to calculate the barrier height Vb that gives some additional information on the quality of SKBs as it will be explained in the following. The second reason is that the junction capacitance of an SKB is used since the DLTS technique is based on the change in capacitance of the biased junction.

The characteristics of an SKB is determined by using the current as function of voltage measurements of the junction. This is denoted by I(V) With this measurement method several information on the diode

---

[1] The shallow acceptor concentration $N_A$ for an p-type SC can be found also, if the case may be.

can be found such as the barrier height $\phi_b$, the ideality factor n, the reverse saturation current Io, the series resistance Rs and the shunt resistance Rsh.

The knowledge of $\phi_b$ is required to determine if the DLTS measurements should be performed. As an example, the EL2 DLTS signal peak is strongly dependent on the SKB $\phi_b$ between 0.62eV to 0.82eV (22) For $\phi_b$ less than 0.62eV the DLTS measurements fail to show the EL2 signal. For $\phi_b$ greater than 0.82eV, the EL2 DLTS signal is measured with confidence since it is not altered anymore.

The ideality factor n indicates the current conduction mode of an SKB (23). n is usually between one and two. If n is close to one for low free carrier concentration, the current conduction mode is done by thermionic emission for which an SKB is in good condition for DLTS measurements.

The reverse saturation current Io indicates the current of the diode under reverse bias before the breakdown voltage occurs. If the reverse current under reverse bias voltage is maintained fairly constant until breakdown occurs (i.e. no leakage current added), the diode can be used for DLTS experiments. The leakage current have an influence on $\phi_b$ thus it may affect the measurement of the trap concentration. Furthermore, Rs and Rsh may be found, indicating if they model practical diodes, since our diodes should have low values for series resistance Rs in order to prevent ohmic loss from the junction resistance and have large value for shunt resistance Rsh in order to prevent leakage current (24)(25).

Finally, the third section describes some practical considerations for an SKB fabrication. At first, ohmic contacts are

made on the SC and an evaporation of metal on the SC using Al-Pd metalization is described in order to obtained diodes with the best characterization as possible, as it was mentioned above.

## 3.1 Capacitance-Voltage Characteristics of a Schottky Barrier

For our experimental results, it is necessary to know the free carrier concentration $N_D$ or $N_A$ of an SC, and the barrier height Vb of the metal-semiconductor junction. In order to do so, it is required to know the capacitance of the junction under reverse bias voltage applied.

### 3.1.1 Space charge region of an SKB

An n-type Schottky barrier is a metal-semiconductor junction where the work function of the metal $\phi_m$ is greater than the work function of the SC $\phi_s$ ($\phi_m > \phi_s$). Its basic band diagram at equilibrium is shown in figure 3.1. The contact potential is represented by qVi (eV) and the barrier height is represented by Vb (eV). The barrier height Vb is equal to the sum of qVi and $\phi_n$ ($Vb = qVi + \phi_n$) where $\phi_n$ is the difference between Ec and Efs ($\phi_n = Ec - Efs$) (26) where Ec is the energy level at the conduction band and Efs is the Fermi level.

The width of the space charge region W with a voltage bias applied is given by (27)

$$W = \left(\frac{2\epsilon_s}{qN_D}[Vi - kT/q - V]\right)^{1/2} \qquad (3.1)$$

where Vi is the contact potential, V is the external bias applied, $\epsilon_s$

is the SC permitivity [2], $N_D$ is the shallow donor concentration[3], k is the Boltzmann constant and T is the temperature in Kelvin. The derivation of the above equation is given in appendix II.

The width of the depletion region at zero bias (Wo) is obtained when V is equal to zero. For forward bias (V = Vf), W decreases below Wo and for a reverse bias (V = Vr), W increases above Wo.

By the known relation C=dQ/dV where C is the capacitance, Q the charge density and V the voltage, and equation 3.1, the junction capacitance is found as (27)(28)

$$C_j = \frac{\epsilon_s S}{W} = S\left[\frac{q\epsilon_s}{2[V_i-(kT/q)-V]}N_D\right]^{1/2} \qquad (3.2)$$

where S is the surface area of the junction and the other parameters have the same meaning as before.[4]

Is is clear here that the reverse bias condition forms a parallel plate capacitor comprising a layer of dielectric thickness W and dielectric constant $\epsilon_s$ between two conducting electrodes (28).

The capacitance of equation 3.2 can easily be measured as

---

[2] $\epsilon_s = \epsilon\epsilon_o$ where $\epsilon$ = 13.2 for GaAs and $\epsilon_o$ = 8.854 X $10^{-14}$ F/cm.

[3] Actually the free carrier concentration for an n-type GaAs sample is given by $N_D$ since $N_D >> N_A$.

[4] The derivation of equation 3.2 is given in appendix II

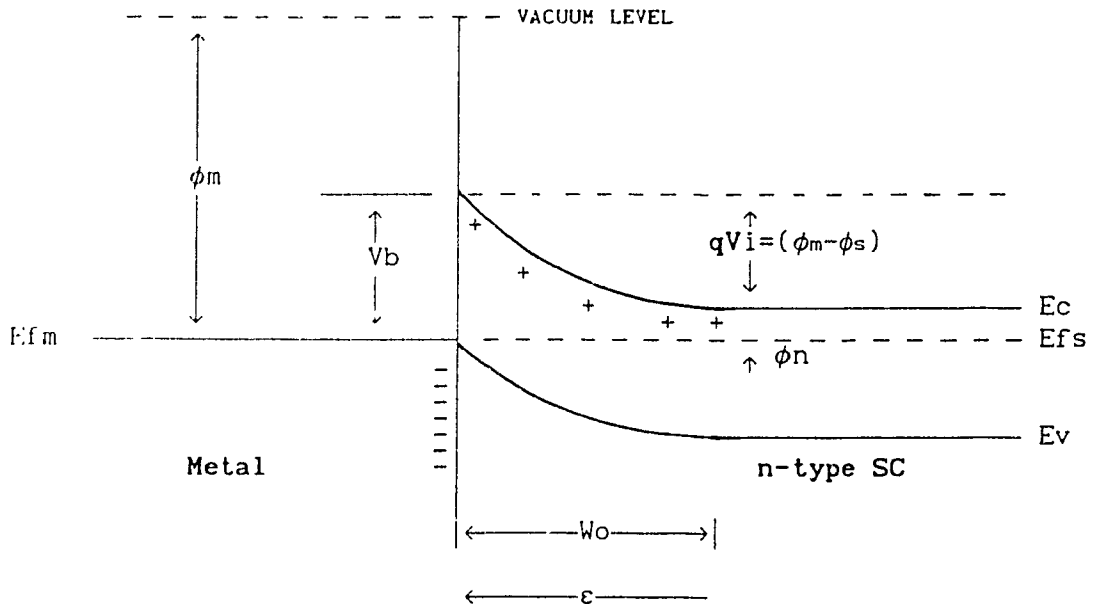


Fig. 3.1 Band diagram for the junction at equilibrium ($\phi_m > \phi_s$). n-type metal-semiconductor junction.

function of the reverse bias V = -Vr. This equation can be rewritten as (27) (29)

$$\frac{1}{C^2} = \frac{1}{S^2} \frac{2(Vi - kT/q - V)}{q\epsilon_s N_D} \qquad (3.3)$$

and the plot of $1/C^2$ as function of V is a straight line whose slope and intercept can be used to determine the doping concentration $N_D$ and the barrier height Vb. In fact, equation 3.3 takes the form of a straight line y = ax + b where y is $1/C^2$, x is V, a is the slope and b is the intercept with the y axis. Thus taking the slope of equation 3.3 we get

$$-\frac{d(1/C^2)}{dV} = \frac{1}{S^2} \frac{2}{q\epsilon_s N_D} \qquad (3.4)$$

where the doping concentration is found as

$$N_D = \frac{1}{S^2}\frac{2}{q\epsilon_s}\left[\frac{-1}{d(1/C^2)/dV}\right] \qquad (3.5)$$

The intercept of the straight line (equation 3.3) with the voltage axis gives the barrier height Vb (30).

Figure 3.2 shows typical C(V) and $1/C(V)^2$ plots. Figure 3.2a is drawn from equation 3.2 and figure 3.2b from equation 3.3. From figure 3.2b, if the doping concentration $N_D$ is not uniform in the SC, the plot $1/C^2$ will not be linear. Therefore, one has to choose two points P1 and P2 for the best linear fit. The slope of linear fits (i.e. $N_D$'s) may be different for points P1 to P2 and P2 to P3. It happens in some experimental cases that the concentration $N_D$ is slightly different for different reverse bias voltage applied (i.e. to points P1, P2 and P2, P3).

The best linear fit to points P1 to P2 or P2 to P3 can be found by the least square method (31).

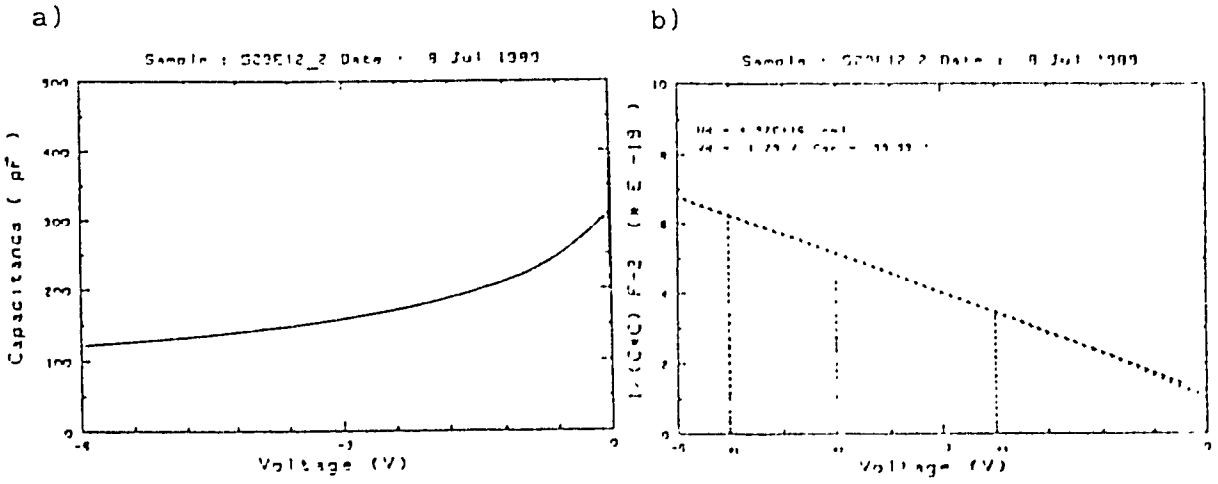


Fig. 3.2 Typical C(V) and $1/C(V)^2$ plots

3.1.2 Experimental Considerations

In practice, to find Nd and Vb, we use a computer HP 300, a programmable multimeter HP 3455A, and a programmable capacitance-meter HP 4280A. The sample is inserted on the tip tail inside the cryostat so that the measurements are being performed under vacuum. This way, measurements are made under insulated conditions. The simplified flow chart of the computer program used to measure the capacitance C(V) of Schottky barriers is shown in figure 3.3 (32). At the beginning, the computer reads from the operator the voltage range to be measured. Then, the capacitance meter (C-meter) performs the capacitance measurement for the range of voltage chosen and stores the values in its own buffer. Then the capacitance meter transfers the data to the computer upon request. Afterwards, the operator may choose to plot C(V) measured as shown in figure 3.2a, or may choose to plot $1/C^2$ shown in figure 3.2b.

The operator chooses two points P1 and P2; the program does the linear fit in this range of points chosen in order to find **a** and **b** (from the line y=ax+b) from the least square method (31). Thus **a** is the slope $d(1/C^2)/dV$ which is substituted in equation 3.5 in order to get Nd Finally Vb is found by the intersection of the strait line with the voltage axis (i.e. when y=0). Thus Vb is given as **-b/a.**

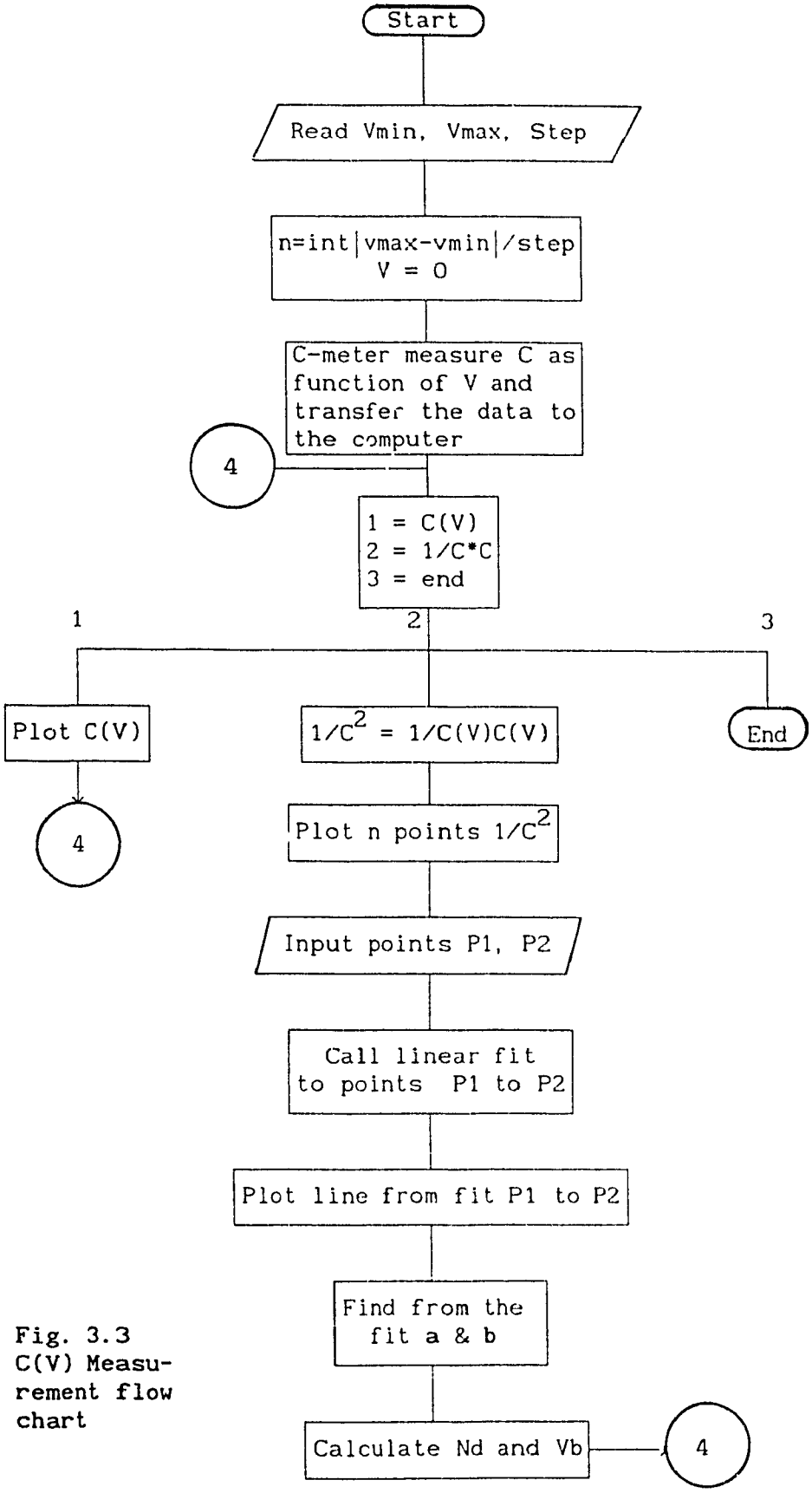


**Fig. 3.3 C(V) Measurement flow chart**

## 3.2 Current-Voltage Characteristics of a Schottky Barrier

Another interesting way to find the barrier height[5] $\phi_b$ is to use the I(V) characteristics of a Schottky barrier. Moreover, the measurement of I as function of V will allow us to find the characteristics of a non ideal diode such as the series resistance, the shunt resistance, the saturation current and the ideality factor.

### 3.2.1 Current Characteristic

The current of a practical metal-semiconductor diode made on high mobility semiconductor such GaAs is mainly due to thermionic emission of electrons over the barrier (23)(30) and the current I as function of the applied bias V is given by the relation

$$I = Io\left[e^{qV/nkT} - 1\right] \qquad (3.6)$$

where n is the diode ideality factor and Io is the reverse saturation current. For an *ideal* Schottky barrier with the doping concentration ranging from $10^{15}$ to $10^{17}$ $cm^{-3}$, the ideality factor n equals unity and the current flows only due to thermionic emission (23). For this case Io is written as

$$Io = SA^{*}T^{2}e^{(-\phi_b/kT)} \qquad (3.7)$$

---

[5] When we use the I(V) measurement method, we will use $\phi b$ instead of Vb (in C(V) measurement) in order to differentiate the barrier height found by one method or the other.

where $\phi_b$ is the barrier height (eV) and $A^*$ is the effective Richardson constant of the semiconductor given by 7.8 $Acm^{-2}K^{-2}$ for GaAs (37)(38). The other values have their usual meaning.

The barrier height $\phi_b$ in equation 3.7 may not be negligible and is dependent on the bias applied and the shallow donor concentration $N_D$. This is due to the effect of the image force barrier lowering. The image force barrier lowering known as the Schottky effect can be understood by referring to appendix V. The barrier height is therefore lowered by an amount (39)(40)

$$\Delta\phi_b = \left[\frac{q^3 N_D}{8\pi^2 \epsilon_s^3}(Vi - V)\right]^{1/4} \qquad (3.8)$$

where $\epsilon_s$ is the permitivity of the SC and V is the applied voltage. The other values have their usual meaning.

3.2.2 Practical methods to find Rs, Rsh, n, Io and $\phi_b$

Here we describe a practical and convenient method to find Rs, Rsh, n, and Io. To start off with, the theoretical equation 3.6 can be rewritten as (41)

$$I = Io\, e^{(qV/nkT)}\,(1 - e^{-qV/nkT}) \qquad (3.9)$$

For the case of a non-ideal Schottky barrier, the series resistance Rs from ohmic loss due to the junction resistance and the shunt resistance from the leakage currents are added to the ideal case of equation 3.6 (25). Thus equation 3.6 becomes

$$I = \left[ Io\left( e^{(q/nkT)(V-IRs)} - 1 \right) + \frac{V}{Rsh} \right] \qquad (3.10)$$

where the equivalent circuit is shown in figure 3.4. For this circuit, the current I from equation 3.10 is equal to Imes (the current flowing out of the non-ideal diode). Then V is equal to Vtheo the voltage of the ideal diode and (V-IRs) is the measured voltage Vmes at the non-ideal diode terminals. The current flowing out of the ideal diode is Itheo. Thus it can be seen that the measured values Imes and Vmes are related with the junction values Itheo and Vtheo by the following expressions (41)

$$Imes = Itheo + Gsh * Vtheo \qquad (3.11a)$$

$$Vmes = Vtheo + Rs * Imes \qquad (3.11b)$$

Thus equations 3.9 and 3.11 can be used to determine Io, n, Rs and Rsh.

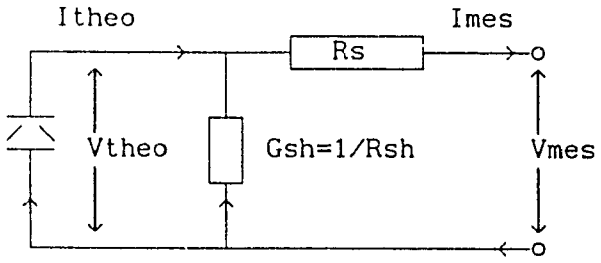


**Fig. 3.4 Equivalent circuit of a non-ideal diode**

The values of n and Io can be determined accurately from the regression linear line (41). Equation 3.9 is written as

$$\ln\left[ \frac{I}{\left(1 - e^{-qV/nkT}\right)} \right] = \ln(Io) + qV/nkT \qquad (3.12)$$

This equation takes the form as $y = ax + b$, where $x = V$ and $y = \ln(I)$ for $V > 3kT$ (42). This equation is a straight line with slope **a** (i.e. **a** is obtained by differentiating the voltage V with respect to ln(I) in equation 3.12) and with **b** the intercept with the y axis when $V = 0$ corresponding to the ideal diode equation.

In practice, the I-V characteristics of a practical Schottky diode is measured as shown in figure 3.5a. Then the natural logarithm of the measured current is taken as function of the measured voltage. The linear part of the I-V characteristics measured as shown in figure 3.5b correspond to the theoretical diode given by equation 3.9. Thus two points P1 and P2 are chosen from that linear part and the best linear fit is performed in order to find the values of **a** and **b** from the line $y = ax + b$ (31).

By comparing **a** and **b** with equation 3.12, we find Io and n directly as (41)(42)

$$Io = e^{b} \tag{3.13a}$$

and

$$n = q/(akT) \tag{3.13b}$$

As shown in figure 3.5b, the non linear parts are the series resistance Rs and the shunt resistance Rsh. In order to find Rs, we take the maximum measured current I and we substitute it in equation 3.11b in order to get

$$Rs = \frac{Vmes - Vtheo}{Imes} = \frac{Vmes - \{(\ln(Imes) - b)/a\}}{Imes} \tag{3.14}$$

where Vtheo is obtained from **a**, **b** and ln(Imes).

In a similar way Rsh is found using equation 3.11a. Therefore,

$$Rsh = \frac{Vmes}{Imes - 10^{(a\ Vmes + b)}} \qquad (3.15)$$

a) b)

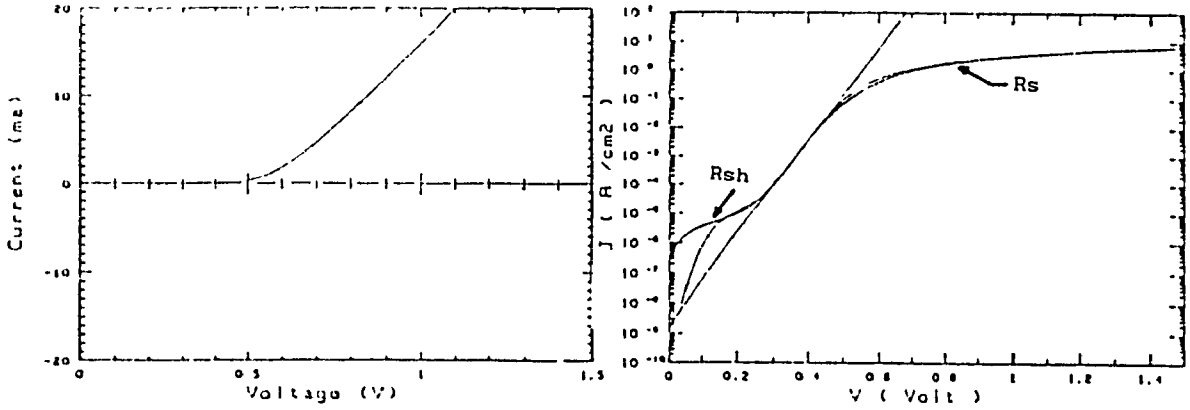


Fig. 3.5 a) Measured I-V characteristic b) ln(I) vs V

3.2.3 Experimental considerations

In order to get the experimental results for n, Io, Rs and Rsh, we use the computer HP, a programmable multimeter as described before, a generator HP S116A and a scanner Keithley 706. The simplified flow chart of the computer program is shown in figure 3.6 (32). The sample is placed inside the cryostat as before. This time there is a set of resistors, chosen by the scanner, placed in series with the diode, and the voltage V across R selected by the scanner is read. The current flowing through the diode is simply I = V/R. This is repeated up to the required values of N found from Vmin and Vmax. During this

process the value of I and V are recorded in an array and the plot is performed at the same time.

Then, the plot ln(I) vs V is performed. Two points P1 and P2 are chosen in the linear part of the plot in order to get the values of **a** and **b** from the regression line. Finally, the values of n and Io are found using equations 3.13, $\phi_b$ is then found using equation 3.7 and Rs and Rsh are found by equations 3.14 and 3.15 respectively.

### 3.2.4 Comparison of the barrier height $\phi_b$ between C(V) and I(V) measurements

So far we discussed two ways to find the barrier height $\phi_b$: one with the C(V) measurement and the other with the I(V) measurement. In the first case, the barrier height is measured by a method which does not require movement of the electron over the barrier, therefore, the value of $\phi_b$ is not altered by the image force lowering. In the case of the I(V) measurement, the electron is moved over the barrier that makes $\phi_b$ lowered by the image force (39). Therefore, the barrier heights obtained by the C(V) method are larger than those obtained from the I(V) measurement (43).

It is observe that in many cases the barrier height from the I(V) measurement could be close to the one from the C(V) measurement if the former is multiplied by the ideality factor n (43). We will discuss the experimental differences between $\phi_b$ and Vb in section 5.4.3.

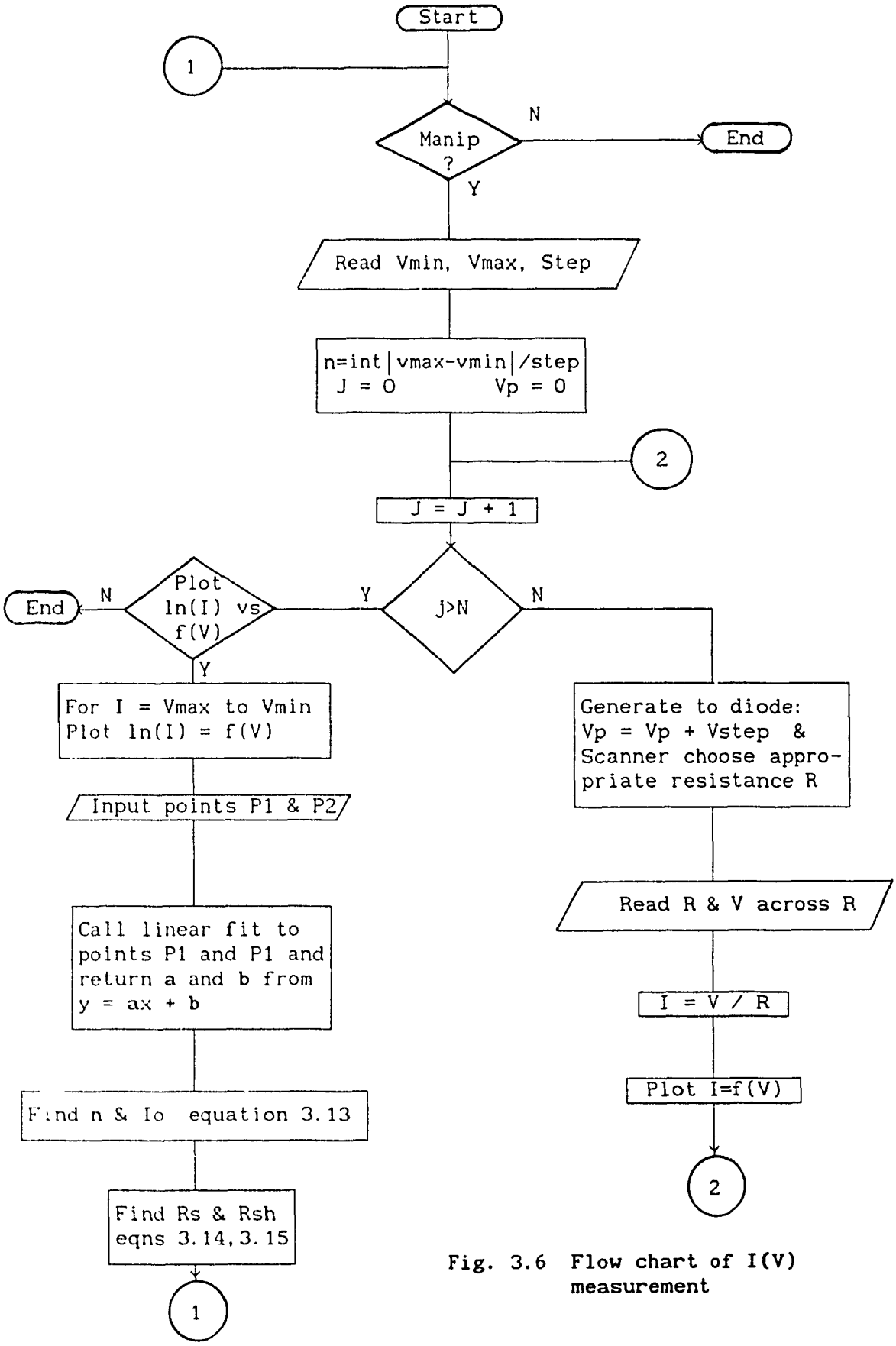


**Fig. 3.6 Flow chart of I(V) measurement**

## 3.3 Practical Consideration for Schottky Barrier Fabrication

The process used to make a Schottky barrier with a good ideality factor n is described here. Appendix X gives the steps for the fabrication of a Schottky diode and the section below explains the reasons for obtaining good diodes.

### 3.3.1 Practical considerations for ohmic contacts

As stated before, for low doping concentration ($N_D < 10^{17} cm^{-3}$), the current over the barrier is mainly due to thermionic emission. In this case the junction resistance is independent of doping and is minimized for low barrier height.

For contact with high doping concentration ($N_D > 10^{17} cm^{-3}$), the tunneling process dominates and the junction resistance depends largely on it. Thus for high doping concentration, low barrier height must be used to obtain low values of junction resistance (44).

The methods used to make ohmic contacts is described in appendix X. For our experimental purpose, we evaporated small area of indium on our GaAs samples. Then the contacts were made by alloying at the corresponding eutectic temperature (500°C) into the SC under hydrogen for two minutes (44). The ohmic contacts are then verified with the curve tracer.

### 3.3.2 Practical considerations for metal-semiconductor junction

According to the theory described in section 3.2.1, an ideal diode has an ideality factor n equals to one. But in practice, when such a diode is fabricated, this ideality factor n may be greater than one due to the image force lowering of the barrier and due to the presence of a

thin insulating interface layer (23).

For the case where $\Delta\phi_b$ is negligible, the ideality factor **n** of the diode may depend on the surface quality of the diode before a metallic evaporation is being performed on the GaAs sample. Therefore, maximum care is taken during the diode fabrication in order to get the surface of the sample as clean as possible.

In order to obtain Schottky diodes with **n** as close to one (typically; $1<n<1.1$), it is necessary to obtain interfaces electrically and thermally stable. This can be done by using the Al-Pd metalization system because of the weak reaction with GaAs (45).

In this process, the sample is cleaned using classical degreasing in trichloroethane, acetone and methanol, and dipped in hydrofluoridric acid (HF) in order to remove any oxides on its surface (45) if the case may be. Then the palladium (Pd) is deposited on the sample where circular areas of 0.8 mm of diameter have been defined with a photo lithographic process using negative photo resist. This deposition is obtained by dipping the sample into an activator solution containing hydrofluoridric acid, acetic acid an $PdCl_2$ involving the reduction of $Pd^+$ ions to metallic Pd by galvanic displacement.

Furthermore, before the sample is dipped into the activator, the sample is immersed into pure hydrochloric acid (HCl) in order to remove the oxides left on its surface. Then it is dipped into deionized water in order to remove the acids from the surface so it does not interfere with the solution.

Finally, an aluminum (Al) evaporation is performed under $10^{-6}$ Torr (or $1.33X10^{-4}$ Pa) vacuum in order to make a good contact between both Pd and Al. With the ohmic contacts and the Al-Pd deposited on the GaAs

samples, the Schottky barriers are verified with the curve tracer first. Then they are characterized with C(V) and I(V) measurements as described in previous sections.

# 4.0 CHARACTERIZATION OF DEEP LEVELS AND EXPERIMENTAL DESCRIPTIONS

## 4.0.0 Introduction

The aim of this chapter is to describe the experimental methods to find the apparent activation energy Ea and the total trap concentration $N_T$ from deep level centers referred to as trap at can be present in semiconductor materials. In order to describe how to find these two parameters, we take the general case for an n-type SC containing only shallow donors and simple monovalent deep donors as an example, as it is described in references (16) and (46).

The shallow donor concentration $N_D$ can easily be found with the C(V) measurement method as described in the previous chapter with the use of a Schottky barrier (SKB). In this chapter we still use an SKB as a test device, but this time by taking deep levels into account.

The SKB is initially under reverse bias where all shallow and deep levels above the Fermi-level are ionized. This correspond to a junction capacitance Co. At this initial condition, we have the total trap concentration Nr and the shallow donors ionized. When an electrical pulse is applied to the SKB (decreasing the depletion layer width) which is still under reverse bias, there will be less deep levels ionized above the Fermi level; that is there will be a fraction of the total trap concentration $N_T$ at time t that will be occupied by electrons. This is denoted by $n_T(t)$. For this case, the traps capture electrons from the conduction band since the capture rate dominates while the shallow donors remains ionized. The amount of the trap that will not be occupied by electrons at time t will be denoted

by $\{N_T - n_T(t)\}$.

When the pulse has elapsed, the initial reverse bias condition tends to take place (i.e. the depletion layer width increases to its original width). Since there are now electrons trapped, and the system tends to reach the equilibrium, the electrons will be remitted back to the conduction band since the emission rate dominates. As it will be seen in details in this chapter, the emission rate is temperature dependent and it has an effect on the variation of $n_T(t)$. Therefore, by the variation of $n_T(t)$, a corresponding capacitance transient C(t) can be measured experimentally. The values of C(t) is thus normalized to $\Delta C/C_0$ as it will be shown later on.

Experimentally, we measure the capacitance transients at instants $t_1$ and $t_2$ with a scan in temperature ranging from about 80K to 400K. Then we take the maximum peak height at a temperature $T_M$ to determine the total trap concentration $N_T$, and then we vary times $t_1$ and $t_2$ in order to get different values of $T_M$. The latter will allow to find $E_a$. Before going further, in section 4.1 we give some general definitions on capture rate and emission rate in order to apply it to SKBs in section 4.2.

## 4.1 Some General Definitions

### 4.1.1 General equation of occupation of a defect state

In this subsection, we show the electronic transition between the conduction band Ec, the valence band Ev and a deep level trap $E_T$. The general rate equations governing the occupation of a defect state of total trap concentration $N_T$ (17) are given by

$$\frac{dn_T(t)}{dt} = K_n\{N_T - n_T(t)\} - e_n n_T(t) - K_p n_T(t) + e_p\{N_T - n_T(t)\} \quad (4.1)$$

where $n_T(t)$ is the concentration of defects occupied by electrons at time t, $\{N_T - n_T(t)\}$ is the concentration of defects that are not occupied by electrons at time t, $e_n$ is the emission rate for electrons, $e_p$ is the emission rate for holes and $K_n$ and $K_p$ are the probabilities per unit time that a defect captures an electron and a hole respectively. Figure 4.1 shows the diagram of the electronic transition between the bands and level $E_T$ at thermal equilibrium (47)(48). The single level generation and recombination through traps

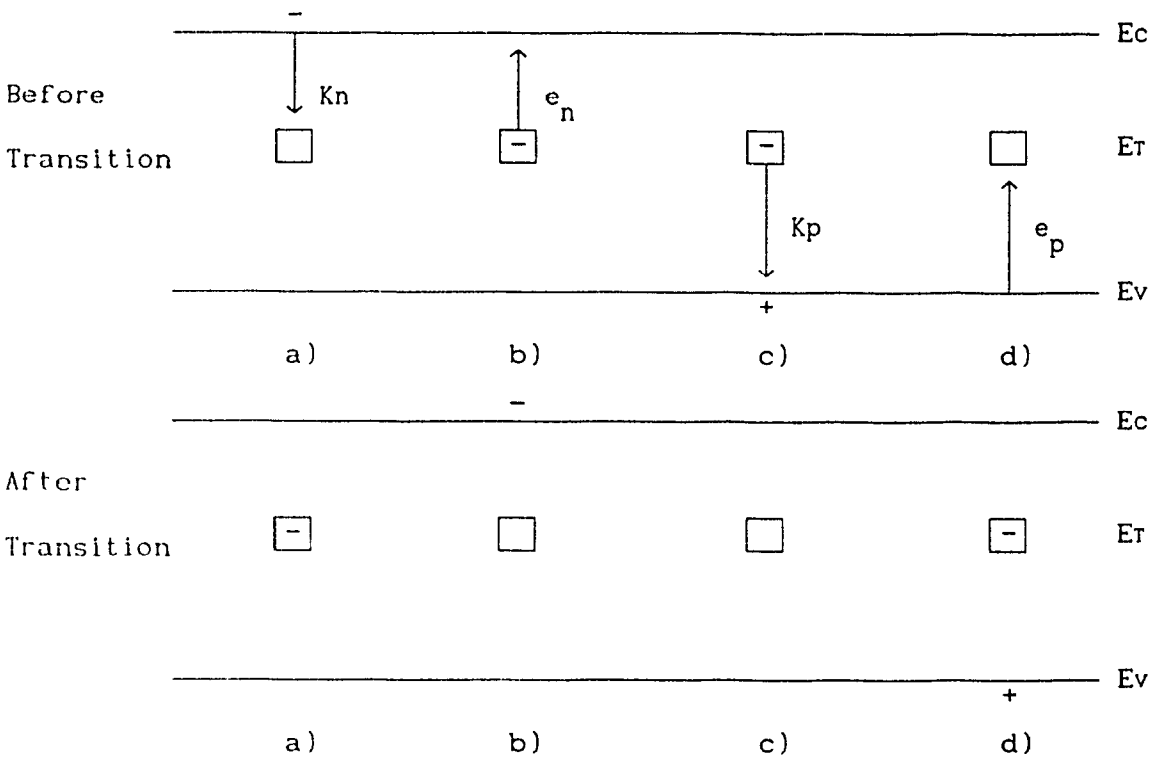


**Fig. 4.1 The basic process of carrier generation and recombination through traps a) electron capture, b) electron emission, c) hole capture, d) hole emission.**

can be described by four processes as shown in the figure. Those are a) the electron capture, b) the electron emission, c) the hole capture, and d) the hole emission. The direction of the arrow indicates the direction of the transition.

In general, for a given deep center it is assumed that (16)(17) one of the emission rate has to be much larger than the other. Thus deep level centers are classified as *electron traps* when $K_n >> K_p$ by the condition $e_n >> e_p$ and a *hole trap* when $K_p >> K_n$ by the condition $e_p >> e_n$ (49)(50). Note that an electron trap is a majority carrier trap in n-type material and a minority carrier trap in p-type material.

4.1.2 General definition of capture rate of free carriers

A deep defect has a specific capture cross section $\sigma_n$ and $\sigma_p$ for capturing electrons and holes respectively. For example, for a deep defect, $\sigma_n$ describes (50)

$$N_D^+ + (e)_{CB}^- \longrightarrow N_D \qquad (4.2a)$$

and $\sigma_p$ describes

$$N_A^- + (h)_{VB}^+ \longrightarrow N_A \qquad (4.2b)$$

where $N_D^+$ is an ionized donor, $N_D$ is a neutral donor, $N_A^-$ is an ionized acceptor, $N_A$ is a neutral acceptor, $(e)_{CB}^-$ is an electron from the conduction band and $(h)_{VB}^+$ is a hole from the valence band.

The capture rate Kn of a flaw for an electron trap is given by the probability per unit time that a defect captures an electron from the

conduction band proportional to the concentration $n$ of electrons[1] in the band (17)(51), thus

$$K_n = C_n n \tag{4.3}$$

where $C_n$ ($cm^3/s$) is the coefficient captures of electrons and is given by

$$C_n = \sigma_n \langle V_{thn} \rangle \tag{4.4}$$

where $\langle V_{thn} \rangle$ is the average thermal velocity of electrons which is given by (51)

$$\langle V_{thn} \rangle = \{3kT/m_n^*\}^{1/2} \tag{4.5}$$

where $m_n^*$ is the electron mass effective, k is the Boltzmann constant and T is the temperature. Note that for an electron trap, the capture rate from the conduction band to the defect occurs according to the following relationships;

$$\frac{dn_T(t)}{dt} = K_n n_T(t) \tag{4.6}$$

where $dn_T(t)/dt$ is the rate of change of the concentration of flaws occupied by electrons, for capturing electrons.

---

[1] Replace n by p in all equations and "electron" by "hole for a hole trap.

4.1.3 Definition of emission rate of a carrier trapped

For the case of an electron trap, the carrier emission from the defect to the conduction band occurs with the probability per unit time $e_n$ ($sec^{-1}$). Thus, the rate of change in the concentration of defects occupied by electrons with respect to time for emitting electrons from the trap level to the conduction band is given by (17)(52)

$$\frac{dn_T(t)}{dt} = -e_n n_T(t) \qquad (4.7)$$

4.1.4 Emission rate at thermal equilibrium

An electron trap exchanges carriers with the conduction band and a hole trap exchanges carriers with the valence band. For the case of an electron trap, equation 4.1 can be rewritten as (17)(52)

$$\frac{dn_T(t)}{dt} = nC_n\{N_T - n_T(t)\} - e_n n_T(t) \qquad (4.8)$$

From equation 4.8, assuming steady state we obtain the emission rate at thermal equilibrium as

$$e_n = 1/\tau_n = N_c\sigma_n\langle V_{thn}\rangle g_n^* e^{-(E_D/kT)} \qquad (4.9)$$

where $E_D$ is the Gibbs free energy of transition, $g_n^*$ is the degeneracy factor[2] and $N_c$ is the effective density of state. The determination

---

[2] $g_n^* = g_e/g_f$ for a nondegenerated condition; $g_e$ and $g_f$ are statistical weights of the flaw electronic configuration when "empty" and "filled" with the electron.

of equation 4.9 is given in appendix IV where $N_c$ is given.

For most SC, the quantity $E_D$ is expected to be temperature dependent (53). Thus, the information relative to a transition may appear in terms of enthalpy ($\Delta H_n$) and entropy ($\Delta S_n$) of the transition rather than expression $E_D$ directly. Thus the relation for the three thermodynamic functions are related by (53)(54)

$$\Delta H_n = E_D + T\Delta S_n \qquad (4.10)$$

where T is the temperature. Equation 4.9 can thus be rewritten as

$$e_n = N_c\sigma_n\langle V_{th_n}\rangle g_n^* \left[e^{\Delta S_n/k}\right]\left[e^{-\Delta H_n/kT}\right] \qquad (4.11a)$$

or

$$e_n = T^2\sigma_n\alpha\beta X_n\, e^{-\Delta H_n/kT} \qquad (4.11b)$$

where $\alpha$ includes the constant terms in the density of states ($N_c=\alpha T^{3/2}$), $\beta$ includes the constant terms in the average thermal velocity ($\langle V_{th_n}\rangle=\beta T^{1/2}$) and $X_n$ includes the entropy and the degeneracy factor ($X_n=g_n^* e^{\Delta S_n/k}$).

Experimentally the thermal activation energy $\Delta H_n$ can be determined approximately from equation 4.11b as

$$T^2/e_n \approx Ae^{\Delta H_n/kT} \qquad (4.12)$$

by taking a plot of $\log(T^2/e_n)$ as function of $(1/T)$ where $A=(\sigma_n\alpha\beta X_m)^{-1}$

(In section 4.2.5, we will give the procedure for finding the activation energy).

Now, since $E_D$ varies non linearly with the temperature, as shown in reference (54), and if this non linearity may be small enough, the emission probability can be rewritten as

$$e_n \approx CT^2 \, e^{-Ea/kT} \qquad (4.13)$$

over a reasonably broad temperature range of measurement, where $C=(\sigma_n \alpha \beta Xm)$ and Ea is the apparent (or effective) thermal energy[3]. Thus Ea indicates a value for $\Delta Hn$ for somewhere near the center of that measured range. Thus when $E_D$ declines in a non linear way with rising temperature, any value deduced for Ea will tend to exceed $E_D$ of any temperature. Therefore, it is assumed that the emission probability can be approximated for low temperature variation in $E_D$ as

$$e_n = 1/\tau_n \approx Nc\sigma_n \langle Vthn \rangle g_{ne}^{*} \, e^{-(Ea/kT)} \qquad (4.14)$$

meaning that the experimental measurement for the apparent activation energy Ea will be somewhat a bit higher than $E_D$.

Similarly, for a hole trap we obtain;

$$e_p = 1/\tau_p \approx Nv\sigma_p \langle Vthp \rangle (g_p^{*})^{-1} \, e^{(-Ea/kT)} \qquad (4.15)$$

---

[3] We have written Ea instead $E_{eff}$ for convenience.

## 4.2 Schottky Barrier Taking Deep Levels Into Account

This section considers the equations of a Schottky barrier taking deep level traps into account as shown in figure 4.2. Those equations will allow the determination of the transition region $\lambda$ and the variation in capacitance $\Delta C/C_0$ (capacitance transients) from the variation of the trap concentration $n_T(t)$ occupied by electrons. From the capacitance transient the DLTS technique will then be applied in order to find Ea and $N_T$ experimentally in the next section.

### 4 2.1 Determination of the transition region

Let us consider an n-type Schottky barrier under reverse bias by a voltage qV with a shallow donor $N_D$, and a deep level located at $(E_c-E_T)$ within the band gap with total trap concentration $N_T$. This is shown in figure 4.2a. Furthermore, we consider the charge distribution $\rho(x)$ constant assuming that $N_D$ and $N_T$ are completely ionized above the Fermi level and the semiconductor is uniformly doped (55). The charge distribution is shown in figure 4.2b. The transition region $\lambda$ can be found by solving Poisson's equation

$$\frac{d^2V}{dx^2} = -\frac{q}{\epsilon_s}[N_D] \qquad (4.16)$$

where q is the charge of an electron, $\epsilon_s$ is the SC permitivity, $N_D$ is the shallow donor concentration, and where $\lambda$ is defined in the space charge region as shown in figure 4.2. Thus, solving the above equation from x equals $(W-\lambda)$ to W we find $\lambda$ (56) given as[4]

---

[4] The derivation of the transition region is derived in appendix V.

$$\lambda = \left[\frac{2\epsilon_s}{q^2 N_D}(E_F - E_T)\right]^{1/2} \qquad (4.17)$$

The value of $E_F$ can be calculated from $n_o = n_i e^{(E_F - E_i)/kT}$ where for the SC material used, $n_i$ is the intrinsic carrier concentration, $E_i$ is the intrinsic Fermi level and $n_o$ is the shallow donor concentration ($n_o = N_D$) (57). The apparent activation energy ($E_a \approx E_T$) is determined experimentally. Therefore, knowing $N_D$ which is determined from C(V) measurement and Ea, $\lambda$ can easily be found.

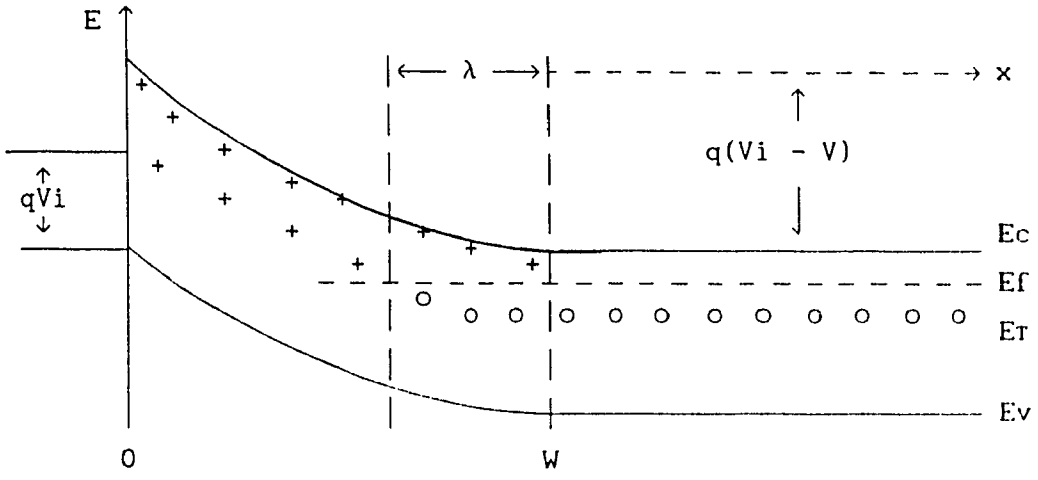


a) Diagram of a Schottky barrier with a deep level

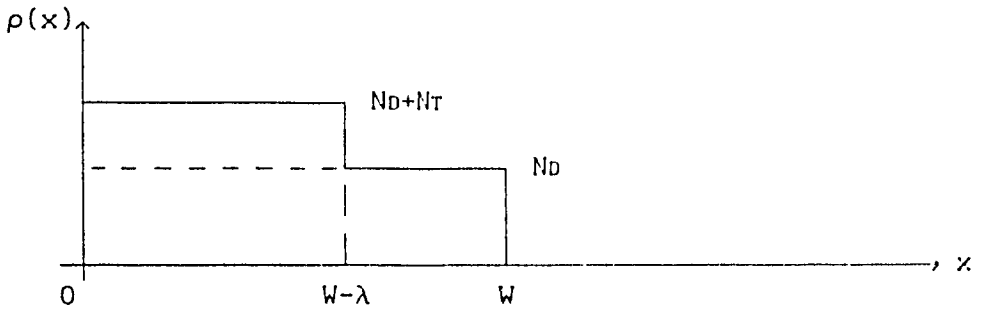


b) Charge distribution

**Fig. 4.2 Schottky barrier under reverse bias**

4.2.2 Determination of the capacitance variation

Here we take the general case for an n-type SC containing shallow donors and simple monovalent deep donors as an example in order to find the variation in capacitance $\Delta C/C_o$. Initially, the Schottky barrier is under a constant reverse bias $V_o$ which is considered as the equilibrium case before time $t_{-1}$ as shown in figure 4.3a. After time $t_{-1}$, a positive pulse from $V_o$ to $V_1$ is applied, where $V_o$ and $V_1$ are both negative values since the operation is performed under reverse bias. The pulse has a duration $\Delta t = t_0 - t_{-1}$ (sec.).

At $V_o$ we consider that the trap is empty from 0 to $(W_o-\lambda_o)$ as shown by (+'s) in figure 4.4a since the monovalent deep donor trap is ionized as indicated in the figure, as well as the shallow one. The voltage pulse $V_1$ causes the filling of the trap with electrons from $(W_o-\lambda_o)$ to $(W_1-\lambda_1)$ as shown by (o's) in figure 4.4b since the capture rate $K_n$ dominates. Therefore, electrons from the conduction band has been captured by the trap. Thus, solving the differential equation 4.6 from $t_{-1}$ to $t_0$ (figure 4.3) we obtain the equation of the filling of the defect (capture of electrons) as

$$n_{T_t}(t) = N_T\, e^{K_n \Delta t} \qquad (4.18)$$

At $t_{0+}$ the trap begins to empty according to the law of equation 4.7. Thus solving equation 4.7 from $t_0$ to $t_\infty$ where $t_\infty$ correspond to enough time so that the trap is completely empty (that is return to $V_o$), we obtain the equation of the emptying of the defect (emission of electrons back to the conduction band) as

$$n_{T_e}(t) = N_T(1 - e^{-t/\tau_n}) \qquad (4.19)$$

Thus the variation of charges $n_{T_e}(t)$ corresponds to an increasing value of capacitance C(t) as shown in figure 4.3b. Note that the emptying of the trap defect is done by thermal relaxation (since $\tau_n$ is temperature dependent) and it takes much longer time to empty than filling by an electric pulse.

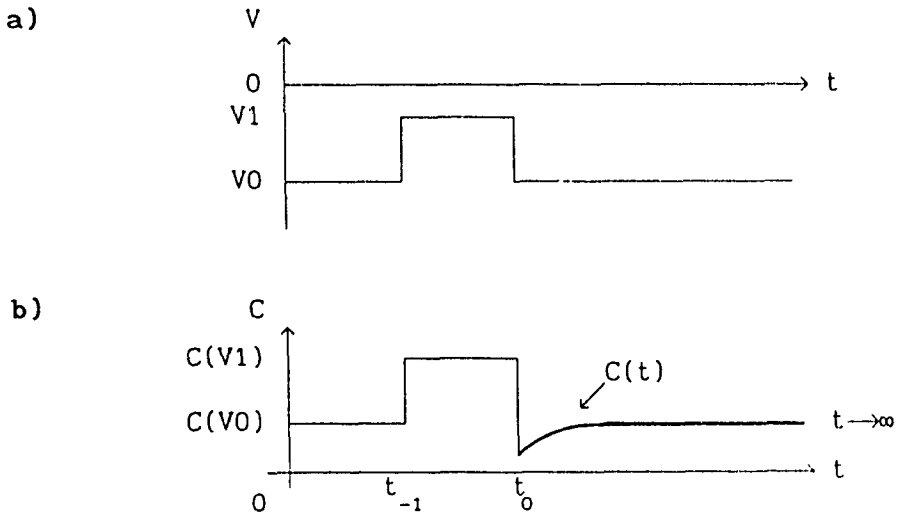


**Fig. 4.3 a) Voltage pulse applied to a Schottky barrier b) Corresponding change in capacitance**

The variation in capacitance C(t) is normalized to $\Delta C/C_0$ and is found by solving Poisson's equation with the limits shown in figure 4.4c where $\Delta C=(C(t)-C_0)$ and $C_0$ correspond to C(V0) shown in figure 4.3b (58). Thus we have

$$V(t) = \int_0^{W_0} x\frac{q}{\epsilon_s}N_D\,dx + \int_0^{W_1-\lambda_1} x\frac{q}{\epsilon_s}N_T\,dx + \int_{W_1-\lambda_1}^{W_0-\lambda_0} x\frac{q}{\epsilon_s}N_T(1-e^{-t/\tau_n})\,dx \qquad (4.20)$$

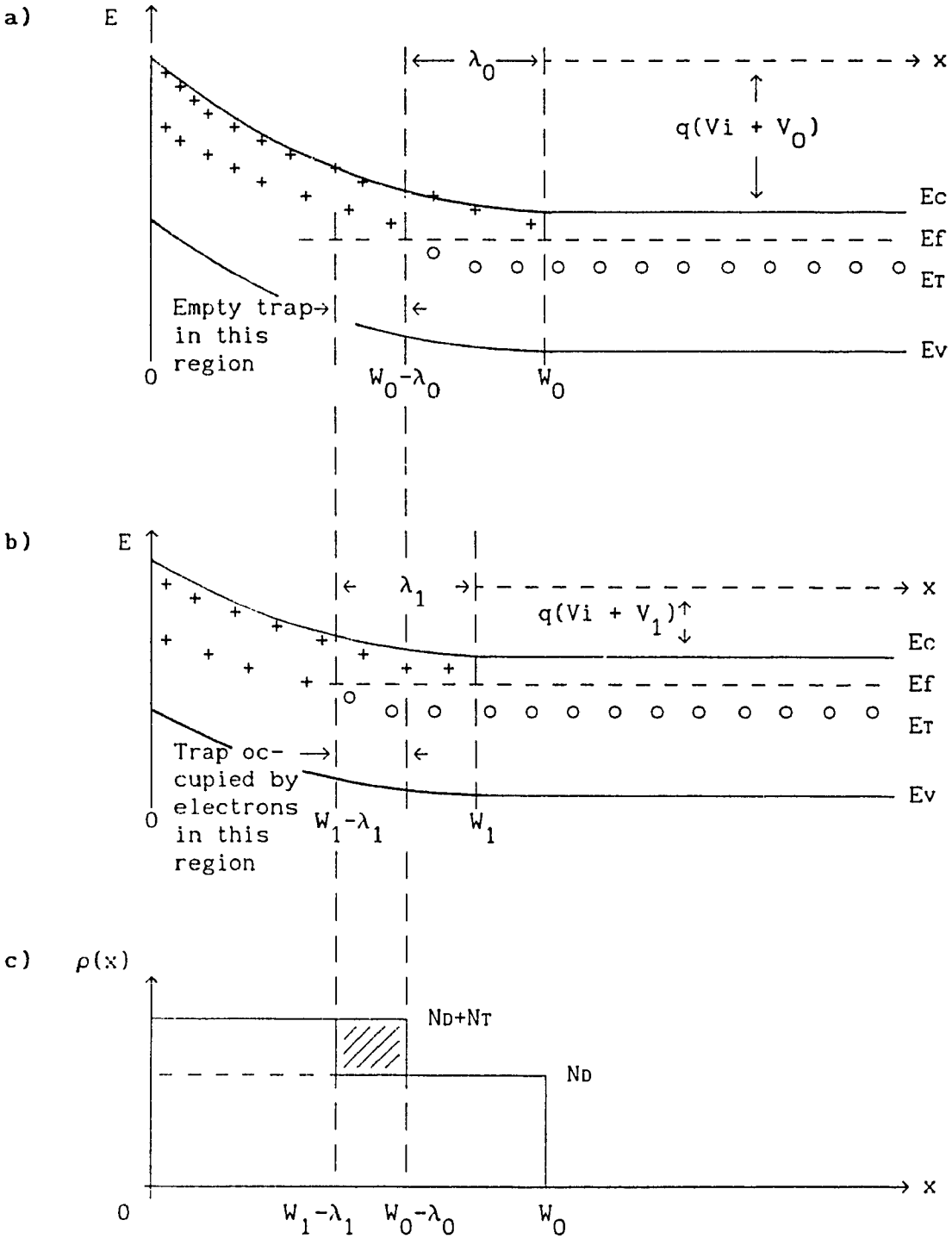


Fig. 4.4
Space charge region and charge distribution of a Schottky barrier under reverse bias; o⟶ filled trap with an electron and +⟶ empty trap. a) At Vo, b) At Vi c) Charge distribution.

By solving the above equation we obtain the required result of $\Delta C/C_0$ which is given by (58)

$$\frac{\Delta C}{C_0} = \frac{C - C_0}{C_0} = \frac{N_T}{2N_D} \frac{\{(W_0-\lambda_0)^2-(W_1-\lambda_1)^2\}}{W_0^2} (1-e^{-t/\tau_n}) \qquad (4.21)$$

which is the normalized variation of the capacitance between $(W_1-\lambda_1)$ and $(W_0-\lambda_0)$ due to trap defect when a bias pulse is applied to the Schottky barrier under reverse bias[5]. The above equation can be simplified further since $\lambda_{0,1}$ are small to as compare to $W_{0,1}$. Thus if $N_D$ is uniformly distributed, $\lambda_0 = \lambda_1 = \lambda$ we have (56)

$$\frac{\Delta C}{C_0} = \frac{N_T}{2N_D} \frac{\{(W_0-\lambda)^2-(W_1-\lambda)^2\}}{W_0^2} (1-e^{-t/\tau_n}) \qquad (4.22)$$

4.2.3 Capacitive measurement method

The principle on capacitive measurement method starts off with a system in equilibrium; that is a Schottky barrier under reverse bias at $V_0$ corresponding to $C_0$. A series of electric pulses applied to the Schottky barrier (external disturbances) will cause the system to be out of equilibrium during the pulse $\Delta t$ as it can be seen in figure 4.5a. After each electrical pulse, transients in capacitance occur as shown in figure 4.5b. The shape of these transients will change with a constant increase in temperature (figure 4.5c) if a deep defect is present in the SC material since the emission rate $e_n$ is temperature dependent. These transients are thus measured experimentally

---

[5] The derivation of equation 4.22 is given in appendix VI.

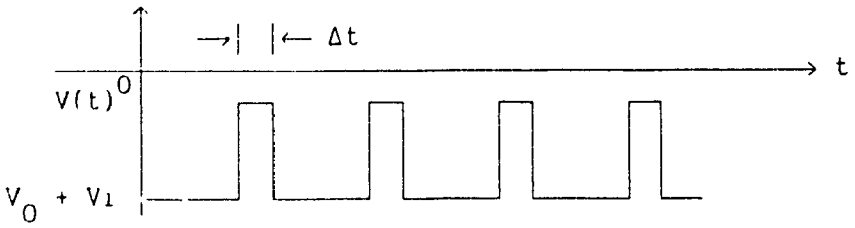


a) Electrical pulses

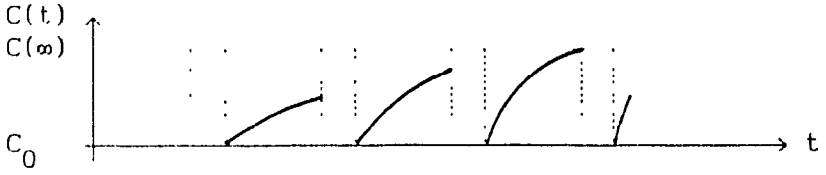


b) Transient of capacitance

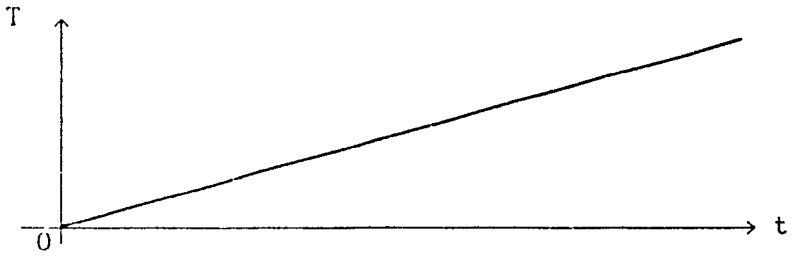


c) Thermal stimuli

Fig. 4.5 Experimental sequence for capacitance measurements

4.2.4 DLTS method analysis

The DLTS method introduced by D. V. Lang in 1974 (6) consists in measuring the difference in capacitance transients of figure 4.5b at times $t_1$ and $t_2$ as it is shown on the left hand side of figure 4.6. The difference in capacitance transients is given by (50) the function

$$S(T) = C(t_2) - C(t_1) \qquad (4.23)$$

where S(T) is the plot of $C(t_2)-C(t_1)$ as function of the temperature T

as shown on the right hand side of figure 4.6. The normalized value S(T)/Co can easily be calculated by substituting equation 4.22 into 4.23 in order to get (60)

$$\frac{S(T)}{Co} = \frac{C(t_2) - C(t_1)}{Co} = \left[\frac{N_T}{2N_D}\,\frac{\{(W_o-\lambda)^2-(W_1-\lambda)^2\}}{W_o^2}\right](e^{-t_1/\tau_n} - e^{-t_2/\tau_n}) \qquad (4.24)$$

By fixing times $t_1$ and $t_2$ we obtain a window constant in time (6), and if the temperature increase linearly with time, for a given defect, equation 4.24 will give rise to a DLTS peak where the maximum is located at a temperature $T_M$ as shown in figure 4.6.

In order to find $T_M$, one has to differentiate equation 4.24 with respect to the temperature (taking equation 4.13 into account) and equate it to zero so we obtain the *rate window* $\tau_n = 1/e_n$ as (6)(60)[6]

$$\tau_n = \frac{t_2 - t_1}{\ln(t_2/t_1)} \qquad (4.25)$$

By varying times $t_1$ and $t_2$, the rate window $\tau_n$ will change accordingly, thus shifting the DLTS peak on the temperature axis as suggested by equation 4.24. The snift in the DLTS peak will allow the determination of the effective activation energy.

### 4 2.5 Arrhenius plot

When a deep level trap is characterized by its energy level $E_a$ and its capture cross section $\sigma_n$, we may say that we have its signature

---

[6] This equation is derived in appendix VII

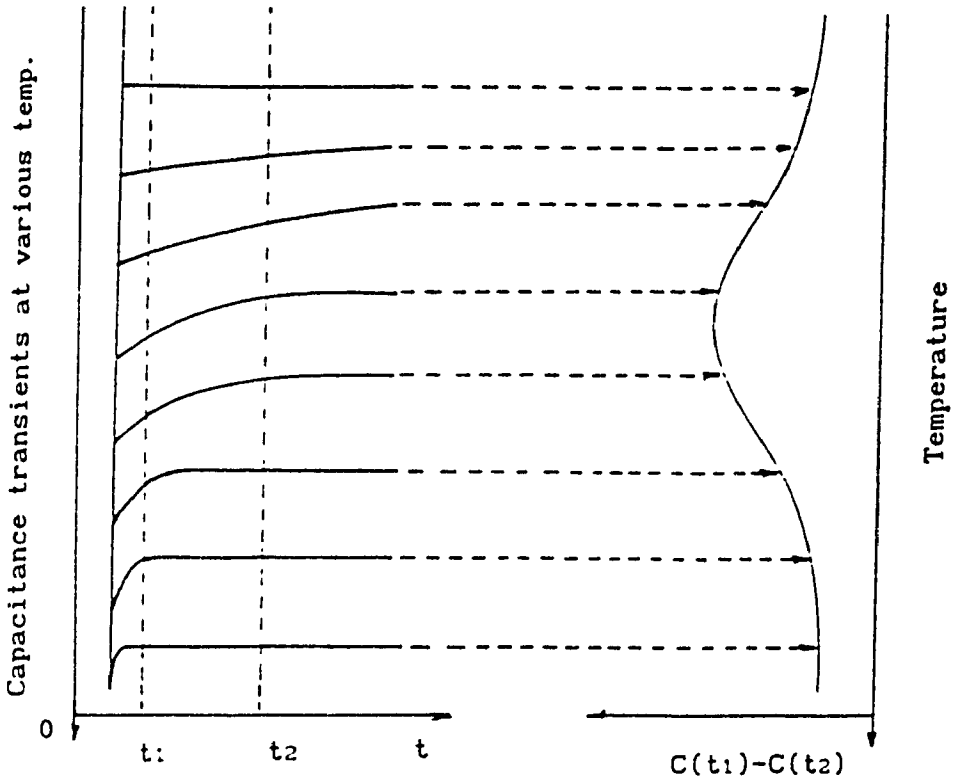


Fig. 4.6 DLTS peak due to a change in capacitance transient

(6). The signature of a trap energy level Ea is found by the Arrhenius plot. In this subsection we will see how to find the energy of activation Ea of a given trap when a DLTS measurement have been performed on a semiconductor sample.

By the relation $1/\tau_n$ given by equation 4.14 we find from appendix VII that this equation can be written as

$$\ln(\tau_n T^2) = \frac{Ea}{kT} - \ln\{\alpha\beta\sigma_n\} \qquad (4.26)$$

where Ea is the apparent activation energy, k the Boltzmann constant, T the temperature, $\alpha$ and $\beta$ are constant, $\tau_n = 1/e_n$ and $\sigma_n$ is the capture cross section. Note that the second term of the right hand side in equation 4.26 is independent of the temperature. In fact, equation

4.26 is a straight line of the form y = ax + b where x represents 1/T. The slope is then given by

$$a = Ea/k \qquad (4.27a)$$

and the intercept is

$$b = -\ln\{\alpha\beta\sigma_n\} \qquad (4.27b)$$

which cuts the y axis. We recall here that a and b can be found by equations from the linear fit.

Thus, the Arrhenius plot (6); $\ln(\tau_n T^2)$ vs (1000/T) allows one to find the activation energy Ea of the deep level trap by taking the slope of the line, and the capture cross section by the intercept of the line with the y axis.

## 4.3 Experimental Description for Finding S(T)/Co Ea and Nt

In this section, we describe the experimental procedure to find the capacitance transient S(T)/Co, the apparent activation energy Ea and the total trap concentration Nt.

### 4.3.1 Experimental considerations for capacitance transients measurement

The measurement of the peak S(T)/Co described in subsection 4.2.4 is performed with the same equipment as described in sections 3.1.2 and 3.2.4 where four electronic apparatus have been added. For a good visualization of the experimental measurement S(T)/Co by DLTS, a

schematic is shown in figure 4.7. The HP computer, the multimeter, the capacitance meter (61)[7] and the pulse generator, are shown; where an oscilloscope has been added in order to visualize the pulse height and the time duration if necessary. A printer and a plotter have been added also in order to get the print out of the initial conditions given by the operator and the plot of the final result of S(T)/Co; and finally, a power supply is connected to the heating element inside the cryostat in order to heat it up. The sample is then placed on the tip tail inside of the cryostat where the temperature may be changed from liquid nitrogen (77K) to approximately 400K under vacuum.

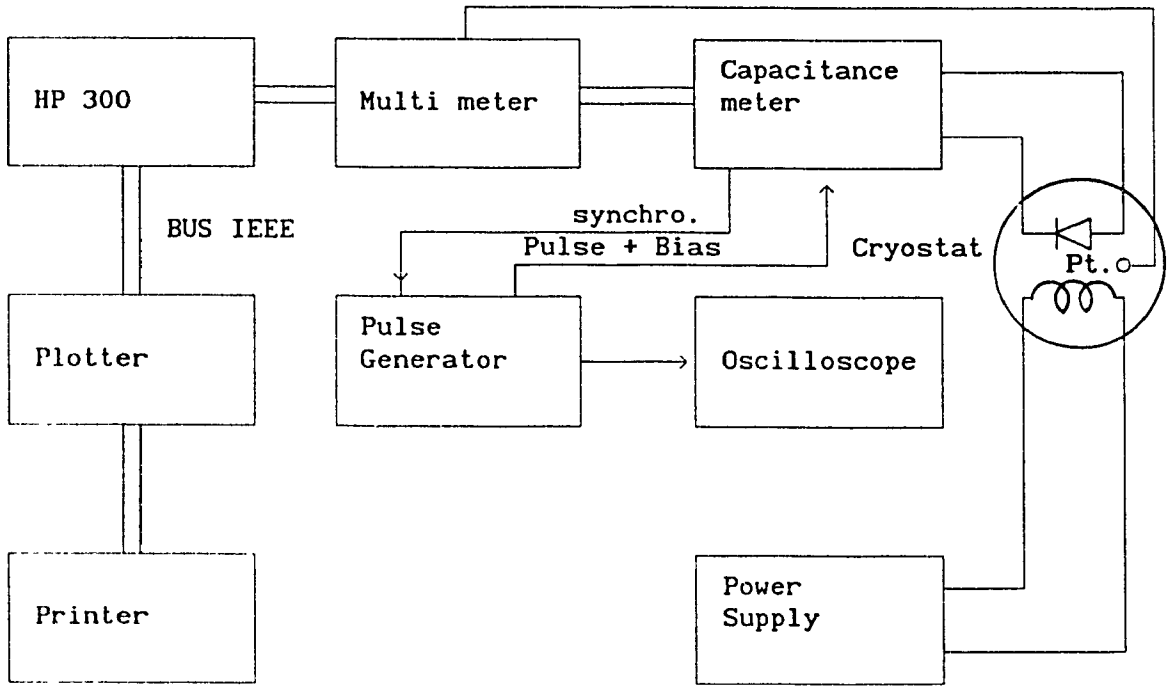


Fig. 4.7 Experimental setup for the measurement of S(T)/Co by DLTS

[7] The capacitance-meter manual gives some indications for setting up fig. 4.7, and gives also some programming techniques.

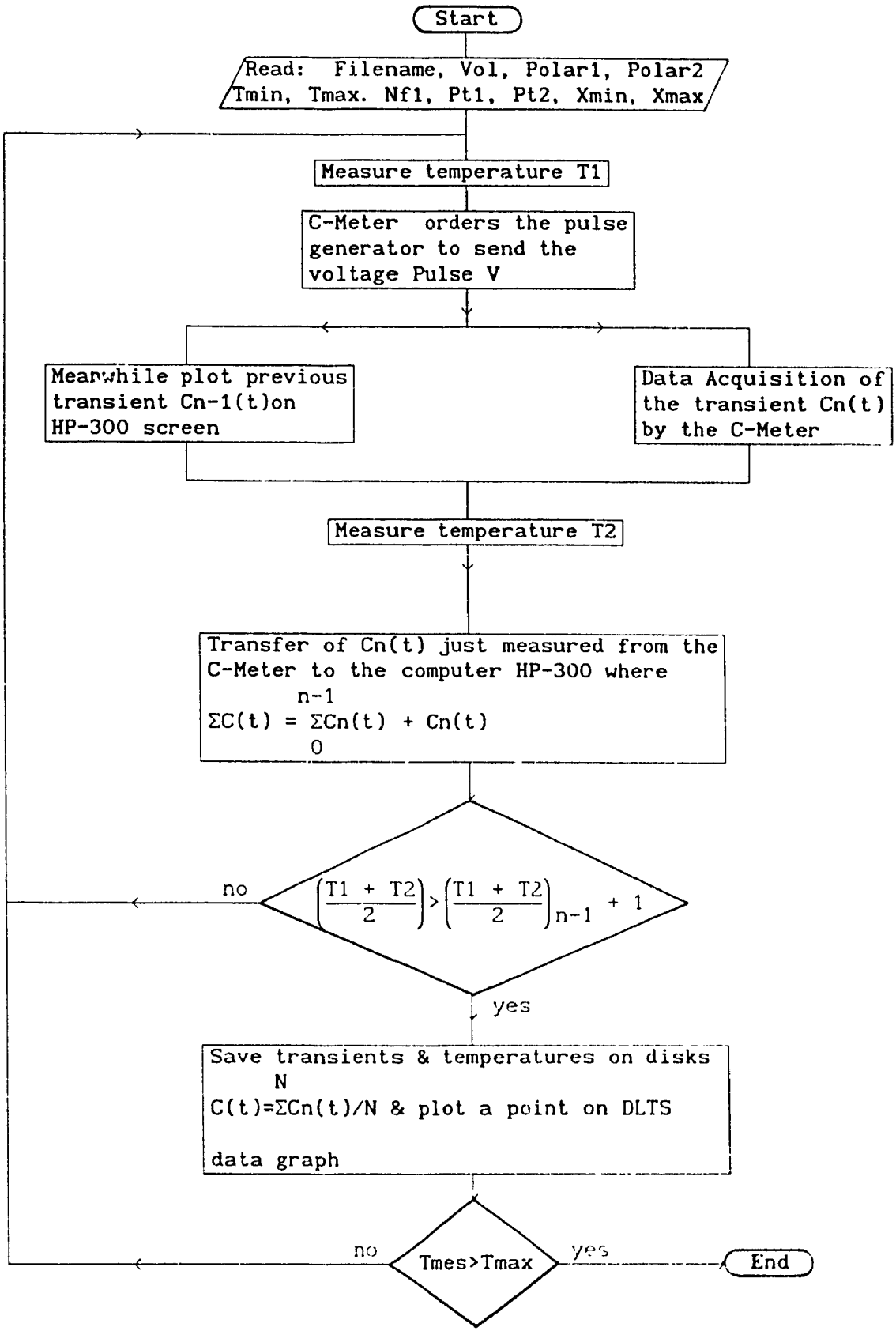


Fig. 4.8 Flow chart of DLTS by sampling

The principle of operation of the S(T)/Co measurement by DLTS is shown by the simplified flow chart in figure 4.8 above (61). The first step of the program allows the operator to enter all the parameters for the DLTS measurement. The reverse constant DC bias (Polar1) and the pulse height (Polar2) are entered (recall fig. 4.5a). Then the number of sampling points N for each capacitance transient is entered where N can range from 1 to 600. The pulse width in milliseconds and the time Td between two sampling points are also entered. Finally points Pt1 and Pt2 from figure 4.6 are entered in order to choose the rate window during the experiment. Figure 4.9 shows an example of one transient with variables to be entered initially that are stored in a data file by the computer.

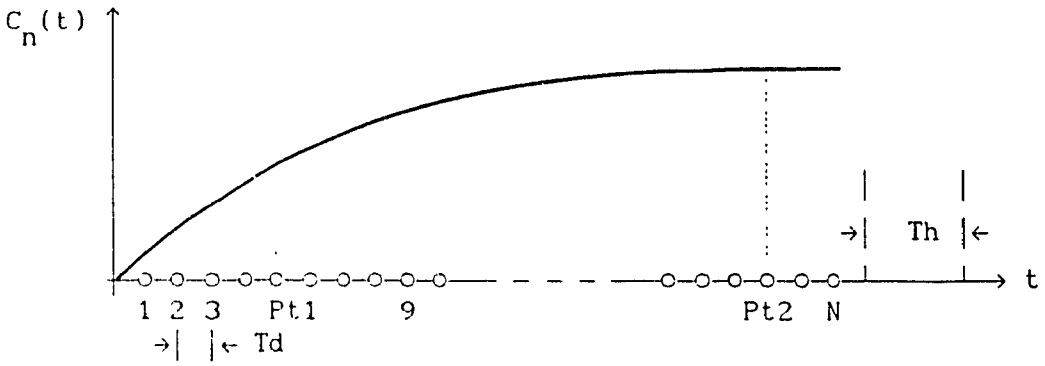


**Fig. 4.9 Example for variables to be entered initially**

The minimum temperature Tmin and the maximum temperature Tmax have to be entered in order to give the range of temperature the experiment is to be performed. Finally, the number of transients recorded in the file Nf1 (approximately 300) has to be set up by the operator, and the vertical lower bound Xmin and upper bound Xmax of the DLTS peak has to be set up before the experiment runs.

Thus a binary data file is created with file name (Name$) in volume VOL of the mass storage unit chosen by the operator. Hence the binary data file can store all capacitance transients and temperature values for the entire temperature scan.

After the parameters has been entered, the computer measures a temperature $T_1$. The temperature is measured with the platinum (Pt) resistance (R) installed inside the tip tail of the cryostat. The computer program ask the multimeter to get in ohmmeter mode so the resistance R can be read. The corresponding temperature due to the resistance read at that instant is given by the third order polynomial;

$$T = 31.5 + 23.5R + 0.002161R^2 - 3.58 \times 10^{-6}R^3 \qquad (4.28)$$

derived from the sensor specification.

Then the capacitance meter orders the pulse generator, which is controlled by the HP-300 computer, to trigger the pulse (Fig. 4.5a). After the pulse duration, the capacitance meter enters N points of the transient into its buffer. Meanwhile, the computer can plot the previous transient $C_{n-1}(t)$ on the screen of the HP-300.

Once this has been achieved, a second measurement of temperature $T_2$ is performed and then, the transfer of transient $C_n(t)$ measured from capacitance meter to the computer HP-300 is performed where all the transients $C_n(t)$ are going to be stored in the computer buffer in array C(t).

Then the previous average temperature plus $1^{\circ}C$ set by the operator is compared with the actual average temperature. If Tav is greater

than Tav-1 + 1°C, the transients and the temperatures data are saved on disks and a point is plotted on the S(T)/Co vs T° graph. If not, another measurement of T1 is performed and the process continue as indicated by the flow chart.

Here the program stops when the measure of temperature is greater than Tmax set at the beginning. When the computer has finished to perform its data acquisition, the DLTS peak(s) is (are) usually shown on the plotter and all transients and temperatures are stored on the disk for further purposes as it will be seen shortly.

4.3.2 Experimental procedures for finding Ea

In practice a computer program called DLTS spectrum reads the capacitance transients and the corresponding temperatures T stored on the disk (transient on the left hand side shown in figure 4.6) to transfer them into an array C(t,T). Then from C(t,T), the value of the experimental signal curve is plotted for *n* different times t1 and t2 as follows (right hand side of figure 4.6);

$$\frac{S(T)}{Co} = \frac{C(t_2) - C(t_1)}{Co} \left(e^{-t_1/\tau_n} - e^{t_2/\tau_n}\right)^{-1} \qquad (4.29)$$

where the experimental values of [{C(t2) - C(t2)} / Co] has been multiplied by $(e^{-t_1/\tau_n} - e^{t_2/\tau_n})^{-1}$ in order to find the total trap concentration $N_T$ directly as it will be seen shortly. The term on the right hand side bracket is a correction factor. Thus the result will give *n* different peaks with the same height shifted in temperature, where the maximum peaks are found at $T_M$ where $M = 1$ to *n* for this case.

For example, the operator can choose the values of t2 as ten times

$t_1$ where $t_1$ can take five values such as 2, 3, 4, 5, 6. Therefore, it is obvious that the rate window $\tau_n$ given by equation 4.25 will change accordingly giving five different values for $T_M$ for five corresponding DLTS peaks. The flow chart of figure 4.10 summarizes well the above statements of the experimental procedure.

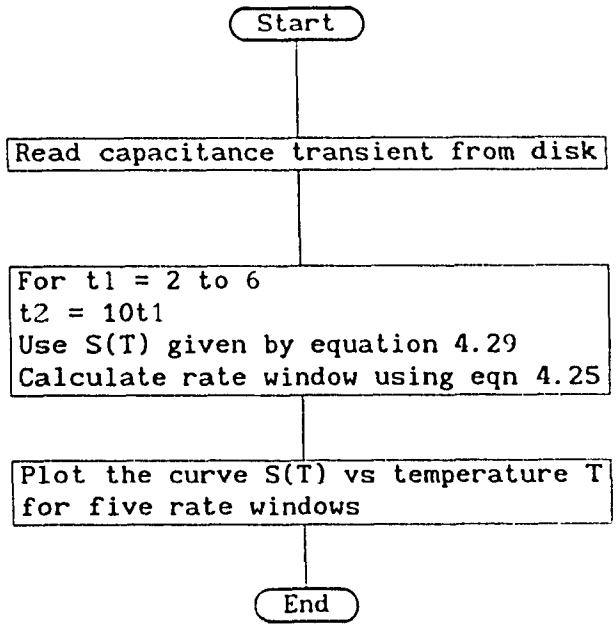


Fig. 4.10 Flow chart of the DLTS spectrum

The apparent activation energy Ea for this example is found knowing the peaks of $S(T_M)$ for five different rate windows. Therefore, a program called Arrhenius plot, enters all five temperature $T_M$ with their respective emission rate $\tau_n$ and perform the plot $\ln(\tau_n T^2)$ vs (1000/T) as shown by the flow chart of figure 4.11.

Then the linear fit is used (31) in order to find a and b from the straight line $y = ax + b$ as before and equations in 4.27a and 4.27b are used to find Ea and $\sigma_n$ respectively.

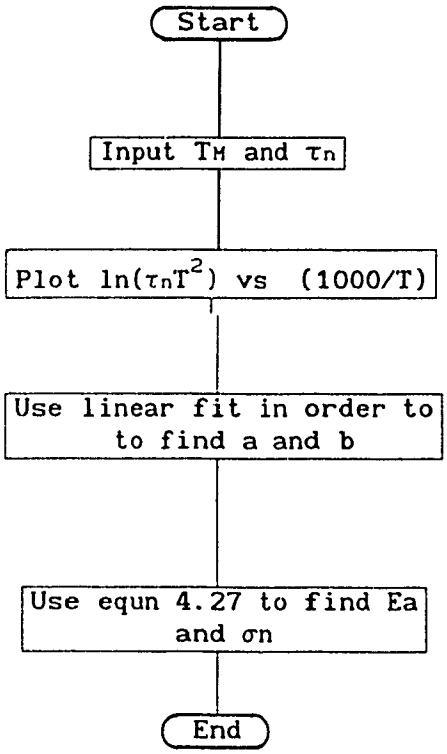


**Fig. 4.11 Flow chart for Arrhenius plot**

4.3.3 Summary of experimental procedure for finding all parameters and $N_T$

The very first thing to do to find all the parameters is to find $N_D$ using the C(V) method as explained in section 3.3.1. Then we have to perform the DLTS experiment as described in section 4.3.1 where the flow chart of figure 4.8 summarizes it well. At this point all the capacitance transients are stored on the disk.

The second step is to find the energy of activation Ea and the capture cross section $\sigma_n$ of the trap of interest with the Arrhenius plot as described in section 4.3.2 with the help of the flow charts of figures 4.10 and 4.11.

Then the transition region $\lambda$ can be found using equation 4.17 and

the values of $W_0$ and $W_1$ can be found from $C_0$ and $C_1$ measured by the capacitance meter respectively by the relation $W = \varepsilon S/C$. Finally, the total trap concentration $N_T$ can be found using equation 4.29 (with the help of equation 4.24) by taking $S(T_M)$ which is the maximum height of the experimental peak. Therefore,

$$N_T = 2S(T_M)N_D \left[\frac{\{(W_0-\lambda)^2-(W_1-\lambda)^2\}}{W_0^2}\right]^{-1} \qquad (4.30)$$

where the values have their usual their usual meaning.

# 5.0 RESULTS AND DISCUSSIONS

## 5.0.0 Introduction

In this chapter we discuss the deep level traps found in GaAs epitaxial layer by DLTS measurement technique under different conditions where all the detailed results are given in appendix I. The epitaxial layers were grown by the CSVT technique (5)(62) as described in appendix VIII The samples labeled with letters R, B, E, AL, AU and AS had their epitaxial layer fabricated in our laboratory at Concordia University in Montréal and those labeled with letter D were fabricated at INRS Energie in Varenne Québec.

The sources and substrates used for the epitaxial layer growth in samples labeled R, B and E were both (100) direction undoped SI GaAs. For samples labeled AL, AU and AS, the source was undoped SI GaAs (100) direction and the substrates were undoped SI GaAs or Si-doped GaAs (100) direction. For the samples labeled D the source was Si-doped GaAs and the substrates were undoped SI GaAs and Si-doped GaAs. The electrical characteristics were determined by Hall effect measurements (63) using the van der Pauw technique at room and liquid nitrogen temperatures. For `l samples, all the deposited layers were n-type with a residual dop.ng concentration of $5X10^{15}$ to $5X10^{17}$ $cm^{-3}$. The measured room temperature carrier mobilities were in the range of 3000 ±1500 $cm^2/Vs$.

The temperature range of the epitaxial deposition was 750 to 880°C with a nominal temperature difference of 40°C between the source and the substrate The thickness of the deposited epitaxial layers were varying from 2.5 to 70μm.

Knowing the above characteristics from the laboratory where we fabricated the epitaxial layers, it was therefore possible to characterize those samples by the C(V), I(V) and DLTS measurements. The DLTS measurements allowed us to identify deep level traps donor such as EL2 and ELCS1 in samples labeled with R, B, E, AL, AU and AS. In samples labeled with D we have found different donor traps in addition to EL2 and ELCS1.

In the following sections, we discuss the results obtained by the method described in previous chapters. Then we show that the evolution of EL2 concentration is function of the possible off-stoichiometry variation with the deposition temperature (64) in CSVT as it is the case in GaAs grown by vapor phase epitaxy (VPE), metal organic chemical vapor deposition (MOCVD) (65) and liquid-encapsulated Czochralski (LEC) GaAs grown crystal (66).

**5.1 Determination of free carrier concentration and barrier height**

The n-type GaAs samples grown by CSVT have unknown free carrier concentration $N_D$ and barrier height Vb. In order to find them we use the C(V) measurement as described in section 3.1. An example of $N_D$ and Vb found by the C(V) measurement is given in figure 5.1 for C(V) and figure 5.2 a and b for $1/C(V)^2$. All other values for $N_D$ and Vb have been found the same way and the results can be found in appendix I for all samples studied.

The values of $N_D$ for some samples have been found by the Hall effect (63)(67). The Hall effect measurement using the Van der Paw technique gives the average resistivity through the epitaxial layer whereas the $1/C(V)^2$ measurement uses the slope. The latter measurement

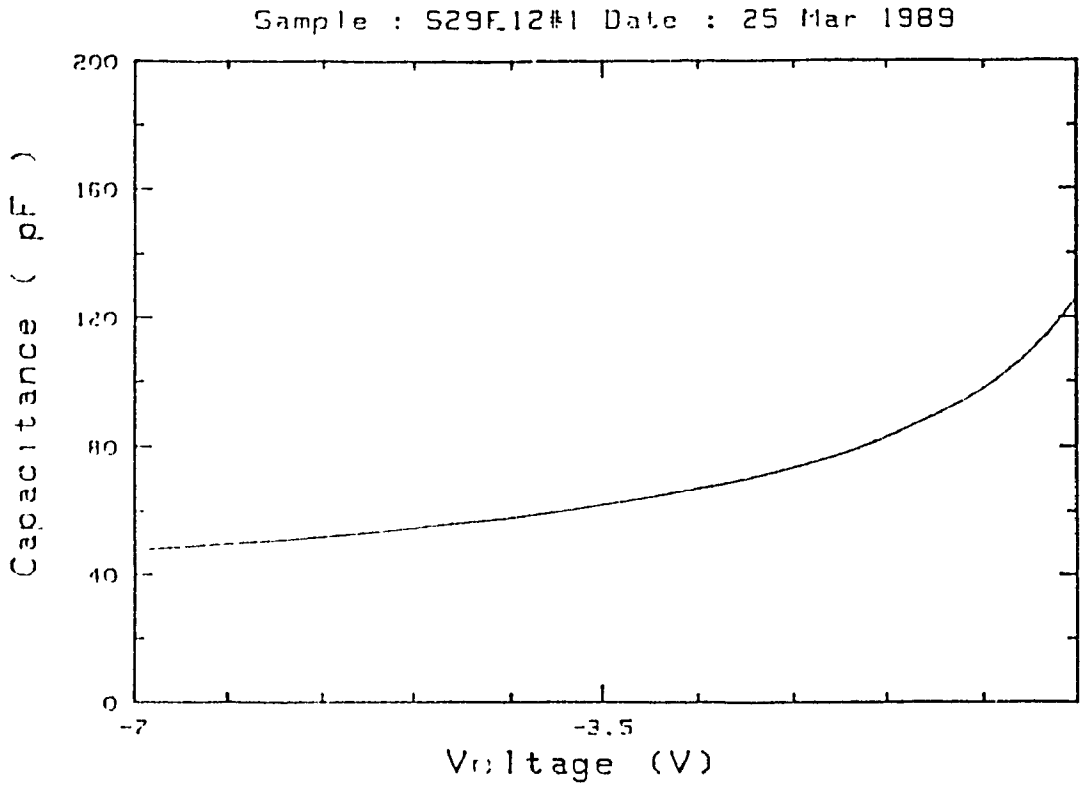


Fig. 5.1 C(V) measurement

(Figures 5.2 a and b) shows the non uniformity of the doping since the slope is not quite linear. There are two apparent straight lines corresponding to two different $N_D$s. Therefore, the Hall effect measurement gives the overall free carrier concentration $N_D$ and can be different from the $1/C(V)^2$ measurement due to the non uniformity of the doping in the GaAs n-type epitaxial layer (68) and the error in diameter of the metal deposited on the epitaxial layer.

The non-uniformity of the doping was discussed extensively in references (68) and (69) for GaAs epitaxial layers grown by CSVT on GaAs substrates. From the charge density, $N_D$, profile of GaAs epitaxies for different thickness, it is shown that the epitaxial layers are not homogeneously doped. Thus the doping concentration $N_D$

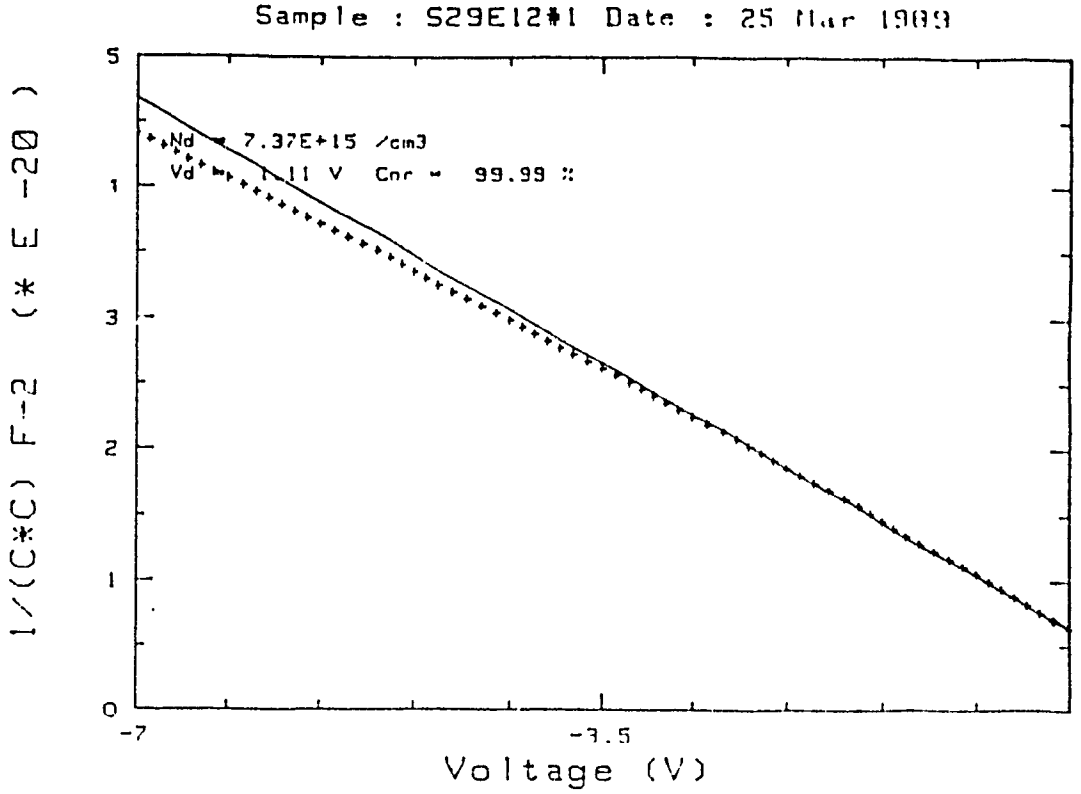


a) (-2V 0V Bias)

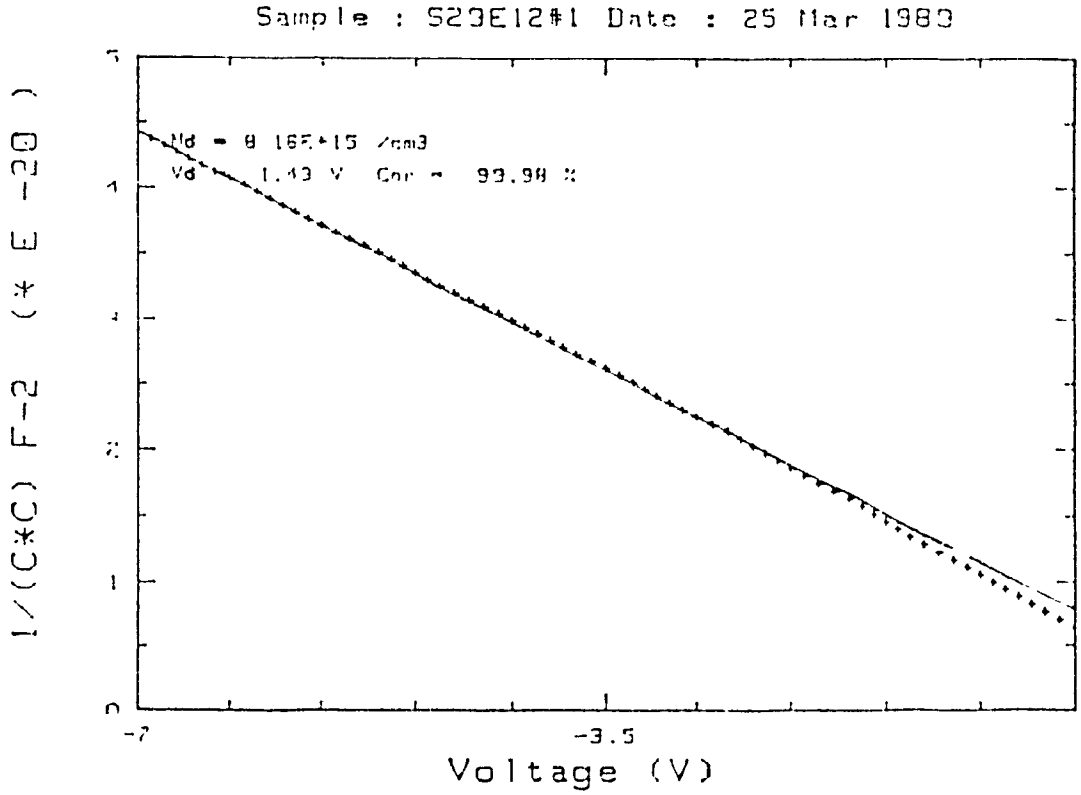


b) (-7 -2V Bias)

Fig. 5.2 $1/C(V)^2$ measurement

varies with the thickness: the doping level increase from the surface of the layer to the interface between the epitaxial layer and the substrate (68).

The accuracy of the diameter of the circle defining the surface area of the metal on the epitaxial layers of the GaAs SC plays an important role in the determination of $N_D$. Referring to equation 3.5, it is seen that $N_D$ depends on the surface area of the junction.

In order to verify the possible range of error in $N_D$, we have taken some samples at random and we measured the diameter of the surface area of the metal with a *Talysurf*. In high resolution, a diamond stylus is used having a tip width of less than 1.25μm and five resolutions of the pen shift control provide a total pen shift equivalent to a change in stylus height of ±0.025mm within ±5% (70). The measured values are given in table 5.1, and tree typical examples of the diameter taken are shown in figure 5.3.

With the help of a microscope and then the *Talysurf* we have noticed that some surface areas where circular and some where elliptical As given in table 5.1, we have calculated the surface area of the elliptical junction ($S=\pi ab$) and we changed it to an effective diameter for a circle ($S=\pi(D/2)^2$) since during the experiment, a diameter of 0.5mm was expected from the masking process which is described in appendix X in section C. Thus we notice from the table that the diameter area are in approximate range from 0.75 to 0.85mm which causes a considerable error in $N_D$.

Originally, we wanted a precise 0.5mm diameter. So we made

a)

5μm
full
scale

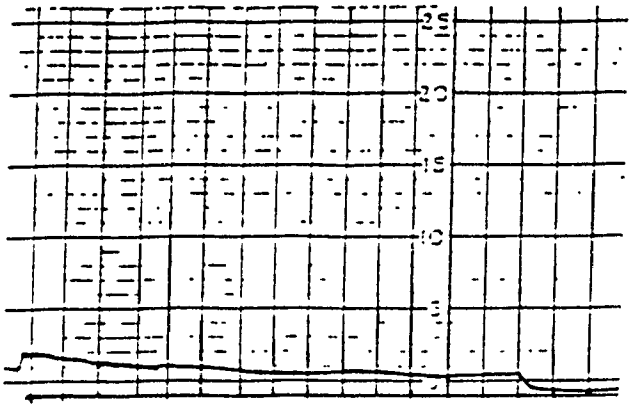

0.05mm/div.

b)

5μm
full
scale

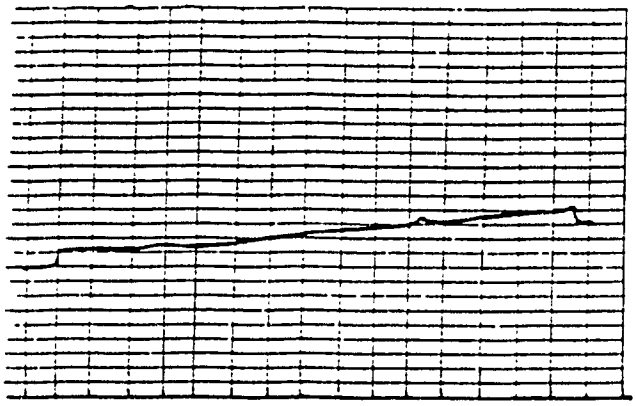

0.05mm/div.

c)

5μm
full
scale

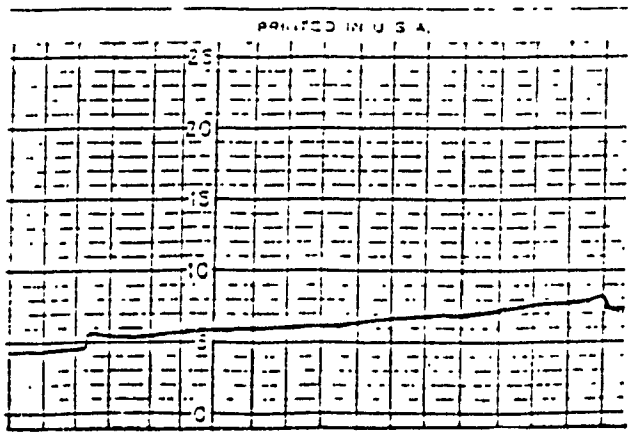

0.05mm/div.

Fig. 5.3 Typical curves from the Talysurf

circles of 20mm of diameter precisely with a compass on *Rubilith*[1] and we reduced them twice five times with a reducing camera in order to obtain the required diameter. For the first set of masks we obtain ellipses since we realized that the camera reduced a bit more on the y axis than on the x axis to which introduced an error in the diameter D.

The second set of masks made where circular and their diameters were found to be around 0.74mm to which can be seen from the table 5.1.

**TABLE 5.1**: Diameter found from the Talysurf.

| No. | S $mm^2$ | Ellipse a(mm) | Ellipse b(mm) | Circle D(mm) | S $mm^2$ | Effective D(mm) |
|---|---|---|---|---|---|---|
| 1 | 0.4959 | 0.820 | 0.770 | | | 0.7946 |
| 2 | 0.4959 | 0.820 | 0.770 | | | 0.7946 |
| 3 | 0.4688 | 0.770 | 0.730 | | | 0.7497 |
| 4 | 0.4898 | 0.810 | 0.770 | | | 0.7897 |
| 5 | 0.4959 | 0.820 | 0.770 | | | 0.7897 |
| 6 | 0.5329 | 0.780 | 0.870 | | | 0.8237 |
| 7 | 0.3675 | 0.600 | 0.780 | | | 0.6841 |
| 9 | | | | 0.740 | 0.4300 | |
| 10 | | | | 0.740 | 0.4300 | |
| 11 | | | | 0.740 | 0.4300 | |
| 12 | | | | 0.850 | 0.5640 | |
| 13 | | | | 0.850 | 0.5640 | |
| 14 | | | | 0.740 | 0.4300 | |

[1] Special paper for photographic process

This time the masks were circular since we reduced the initial circles once five times on the y axis and once five times on the x axis in order to reduce the error considerably. It is noticed that some diameters vary even when we use the same masks for fabricating the diodes. This is because of an improper vertical spacing between the mask and the sample on the *mask aligner* which is not always obvious to the operator. Therefore, an improper spacing can cause a change in D since the ultra violet (UV) light can spread a little under the mask during photo resist polymerization thus increasing the surface area of the junction.

The errors in the diameter and thus the error in $N_D$ are shown in table 5.2. We took a sample (CP26_1) that a nice C(V) characteristic and we measured $N_D$ for different bias. Here the comparison is obvious; for a variation of +6.25% in D (i.e. from 0.8mm as an initial value to 0.85mm), it introduces an error of 27.7% in $N_D$ for bias between (0-2V). For bias between (-2-6V) with +6.25% of variation in D, we have a +29.8% of error in $N_D$. Similarly, for a variation of -6.25% in D, we have an error of -29.6% in $N_D$ for bias of (0-2V), and -51.7% error in $N_D$ for (-2-6V) bias.

Also, another percentage of error in $N_D$ can be added to the above if the slope is taken for larger range of bias (-2-6V) as compared to a lower range (-2-10V). It can be seen from table 5.2 (between # 10 and 13) that there is a 13.46% error between (-2-10V) bias and (-2-6V) bias for the same D. The value for $N_D$ should be more accurate with (-2-10V) bias simply because more points are available for the linear fit. It occurs some times in practice that we cannot go farther than (0-4V) bias since we are limited by the reverse breakdown voltage of the diode

itself where the capacity change drastically. For a low bias (0-2V) (between # 1 and 11) the percentage of error is lower (3.1%) since the carrier concentration does not vary much near the surface (68).

TABLE 5.2: Error found in ND according to a change in diameter D.

| No | Bias(V) | D(mm) | Nd (cm-3) | %err. D | %err. Nd | Between No. | % error |
|---|---|---|---|---|---|---|---|
| 1 | 0 -2 | 0.80 | 2.26E15 | 0.00 | | 1 and 11 | 03.1 |
| 2 | 0 -2 | 0.81 | 2.14E15 | 1.25 | 05.60 | 1 and 2 | 05.60 |
| 3 | 0 -2 | 0.85 | 1.77E15 | 6.25 | 27.68 | 1 and 3 | 27.68 |
| 4 | 0 -2 | 0.90 | 1.70E15 | 12.50 | 33.00 | 1 and 4 | 33.00 |
| 5 | 0 -2 | 0.75 | 2.93E15 | -6.25 | -29.60 | 1 and 5 | -30.00 |
| 6 | -2 -6 | 0.75 | 3.52E15 | -6.25 | -51.70 | | |
| 7 | -2 -6 | 0.90 | 1 41E15 | 12.50 | | 7 and 16 | -25.79 |
| 8 | -2 -6 | 0.85 | 2.08E15 | 6.25 | 29.81 | | |
| 9 | -2 -6 | 0.81 | 2.57E15 | 1.25 | | | |
| 10 | -2 -6 | 0 80 | 2.70E15 | 0.00 | | 10 and 13 | 13.46 |
| 11 | 0 -2 | 0.80 | 2.33E15 | 0.00 | 03.10 | | |
| 12 | -4 -10 | 0.80 | 3 21E15 | 0.00 | | 12 and 13 | 37.00 |
| 13 | -2 -10 | 0.80 | 3.12E15 | 0.00 | 13.46 | | |
| 14 | 0 -2 | 0.90 | 1.46E15 | 12.50 | | | |
| 15 | -4 -10 | 0.90 | 1.95E15 | 12.55 | | | |
| 16 | -2 -10 | 0 90 | 1.90E15 | 12.55 | | | |

Finally, it is observed that the choice of the points for the linear fit may introduce another percentage of error (71). For example, we have taken the slope for bias between (-2--10V) and (-4-10V) and we found 37% of error (between # 12 and 13). It is therefore critical to

choose the proper points for the linear fit in the most linear region that appears to the operator on the screen of the computer.

Therefore, the error in $N_D$ depends mostly on what was discussed above since the C-meter is a reliable piece of equipment. Because of the importance of the C(V) measurement, the C-meter is discussed below.

The basic measurement accuracy of the 4280A C-meter is 0.01%, and measurement resolution is 1fF on the most sensitive range (pF). The measured capacitance is displayed with 5-1/2 digit on high resolution (72). For a small $\Delta C/C$ transient, the capacitance measured may be very small (near 1fF) thus limiting the measurement of the peak S(T). This small measurement in capacitance C can keep from seeing the EL2 trap for example. At this point the C-meter is working on its limit.

The capacitance measurement is achieved by an internal 1MHz sine wave source of 30m Vrms or 10m Vrms to suit the characteristics of the device under test (the measurement range is given in the manufacturer table). A built in DC source whose output can be swept in a staircase manner, and an automatic error correction function to ensure accurate repeatable measurements are used to change the capacitance of an SC diode junction under test. The error correction function "virtually eliminates the effects of error-causing strays and residual inherent in the test leads and tests fixtures used to connect test samples to the unknown terminals" (73). Figure 5.4 shows the simplified capacitance circuit measurement.

The diode is connected inside the cryostat under vacuum to which the cryostat is linked by two coaxial cables to the two terminal pair configuration at the C-meter. This eliminates mutual inductance between test leads because of their insulation and reduce the effect of

environmental noise when measurement requiring pulse biasing (72). With this connection mode, the C-meter measures the capacitance C and the conductance G, of the equivalent unknown parallel circuit of the device connected to the terminals (73).

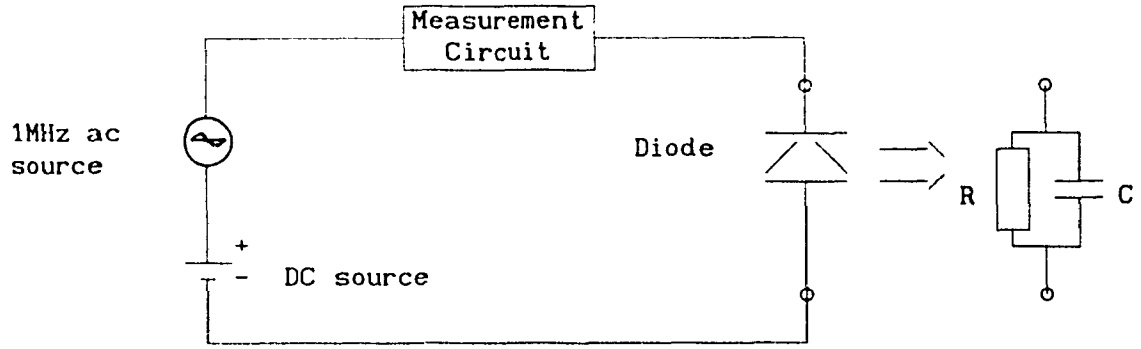


Fig. 5.4 Capacitance circuit measurement

The 1MHz sine wave frequency source is periodically tested with an oscilloscope and a frequency counter. The internal DC source is also verified periodically using the HP3456A multi meter[2] where the procedure is described in the users manual using appropriate tables (74). Finally the manufacturer gives the procedures to follow and tables to perform the C and G standard tests according to specific connection modes. Here the manufacturer specifies that the tests must be performed at 23°C ±5°C with the C-meter warmed up 30 minutes before the test.

Therefore, we can rely on this sophisticated C-meter to find the free carrier concentration $N_D$ after tests performed periodically.

---

[2] The multi meter will be discussed in a further section.

## 5.2 Apparent Activation Energy Ea

In this section, we determine experimentally the thermal ionization energy Ea (or equivalently the apparent activation energy) from the DLTS measurements performed in all our samples. Then we discuss the probable causes of error. In further sections we will discuss the particularity of each activation energy Ea or deep lying trap level.

### 5.2.1 Identification of deep level traps

The ionization energy Ea was found from the DLTS peak measured as described in section 4.2.4 and 4.2.5. An example of DLTS peaks is shown in figure 5 5 . Then the Arrhenius plot described in section 4.3.2 was used. In practice we selected samples where the peak height was high enough in order to determine Ea.

In all the samples except some samples in the series D369 though D378, we found two different peaks which are shown in figure 5.5 where the growth of epitaxial layers made by CSVT was performed using semi-insulating source for all samples and both a semi-insulating and Si-doped substrates. The peak on the left hand side is found at a temperature near 300K for a rate window $\tau_n$ equals to 0 391s and the one on the right hand side is found at a temperature near 335K for the same rate window. These two peaks have been found in all samples with different peak height especially for the peak at 300K as it will be discussed later on.

For the peak on the right hand side, we have drawn twenty seven peaks using the DLTS spectrum program given by the flow chart of figure 4.10. Figure 5.6 shows only 5 peaks for convenience. The sample used was #R16. From these peaks, the temperature were taken for each

maximum peak and corresponding emission rate. The results are shown in table 5.3. Then the Arrhenius plot was used as described by the computer program from the flow chart of figure 4.11. The plot is shown in figure 5.7. Finally, from this plot, the apparent activation energy Ea was found to be equal to 816.07meV and the capture cross section $\sigma_n$ was found to be equal to $3.02 \times 10^{-13} cm^2$. This ionization energy and capture cross section is a particular trap level identified as the EL2 deep level donor electron trap. Our measurement agrees with the published results (65)(75) where EL2 is found to be Ea equals to 820meV and $\sigma_n$ equals to $1.7 \times 10^{-13} cm^2$.

In order to find the uncertainty of our results in Ea, we have taken the same sample (R16) and we have performed six DLTS measurements on it Then we have found six Ea and six $\sigma_n$ using 14 temperature peaks and emission rates each time. Then we averaged up the six Ea and $\sigma_n$ and we calculated the standard deviation (76). The results are given in table 5.4. Thus we found an average Ea equal to 800.2meV with ±18meV of deviation from the mean and with $\sigma_n$ equal to $1.97 \times 10^{-13} cm^2$ with $\pm 1.4 \times 10^{-13} cm^2$.

The uncertainty found in Ea is ±18meV which is low since the total band gap energy Eg for GaAs is equal to 1420meV (77). Furthermore, a variation of a few degrees in temperature does not change much the slope of the line on the Arrhenius plot (i.e no large variation in Ea) but may cause a large variation in $\sigma_n$; since $\sigma_n$ is taken on the y axis of the plot. Thus a slight change in the slope will give rise to a large error in $\sigma_n$ even if the mean of $\sigma_n$ agrees with published results.

In order to support our results for Ea for EL2, we measured Ea for sample B51 with the above method. We found Ea equals to 830meV and $\sigma_n$

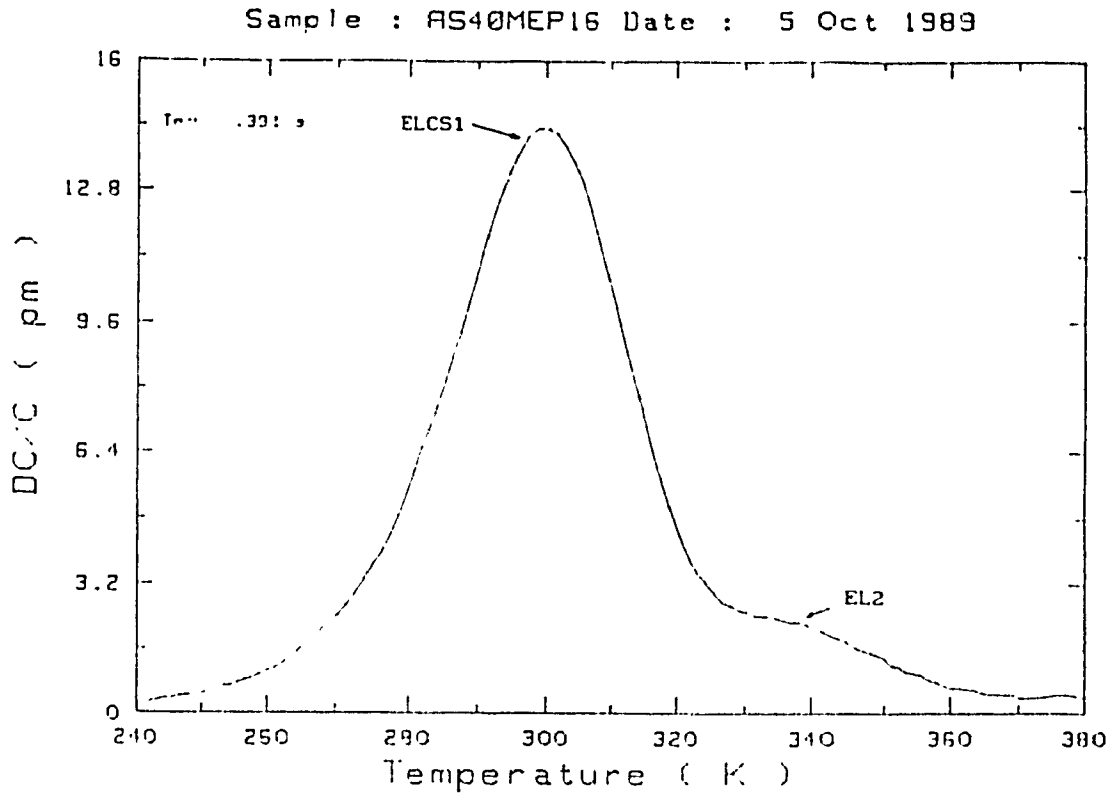


Fig. 5.5 Typical DLTS spectrum

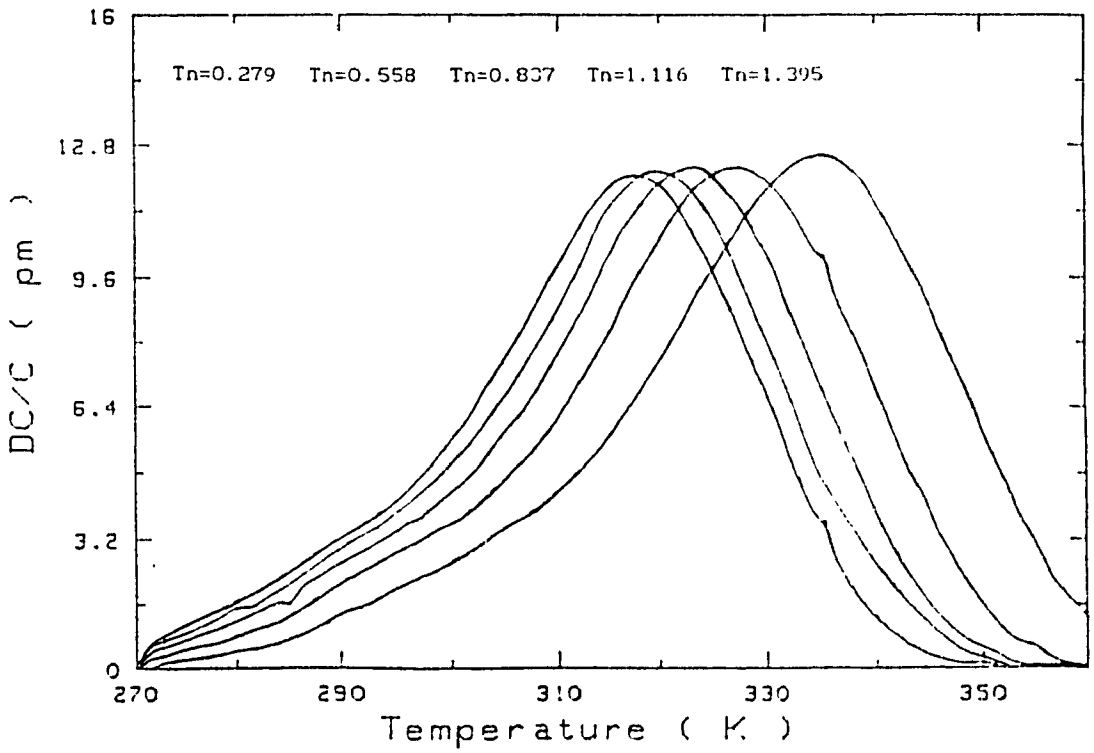


Fig. 5.6 DLTS peaks for different rate window (for EL2)

TABLE 5.3: Temperature with corresponding rate window for fig. 5.7.

| No. | Temperature (K) | rate (s) window | No. | Temperature (K) | rate (s) window |
|---|---|---|---|---|---|
| 1 | 308.05 | 3.5410 | 15 | 319.51 | 1.1160 |
| 2 | 310.98 | 2.6560 | 16 | 326.34 | 0.5130 |
| 3 | 321 46 | 0.8850 | 17 | 333.90 | 0.2660 |
| 4 | 310.73 | 7.7910 | 18 | 325.36 | 0.6700 |
| 5 | 312.68 | 2.2320 | 19 | 322.93 | 0.8730 |
| 6 | 315.12 | 1.6740 | 20 | 327.78 | 0.5020 |
| 7 | 319.51 | 1.1160 | 21 | 332.68 | 0.3350 |
| 8 | 326.34 | 0.5580 | 22 | 339.07 | 0.1670 |
| 9 | 306.34 | 3.9090 | 23 | 319.05 | 1.1730 |
| 10 | 312.68 | 2.3450 | 24 | 321.46 | 0.9380 |
| 11 | 322.19 | 0.7820 | 25 | 323.41 | 0.7040 |
| 12 | 336 59 | 0.2350 | 26 | 327.59 | 0.4690 |
| 13 | 315.61 | 1.5[illegible]30 | 27 | 309.27 | 3.1270 |
| 14 | 322.93 | 0.7970 | 28 | | |

TABLE 5.4: Several measurements of apparent activation energy for EL2

| No. | Ea(meV) | Sigma(cm-2) |
|---|---|---|
| 1 | 782.23 | 8.48E-14 |
| 2 | 796.22 | 1.33E-13 |
| 3 | 818.30 | 3.27E-13 |
| 4 | 824.23 | 4.21E-13 |
| 5 | 797.29 | 1.36E-13 |
| 6 | 782.23 | 8.46E-14 |
| average | 800.20 | 1.97E-13 |

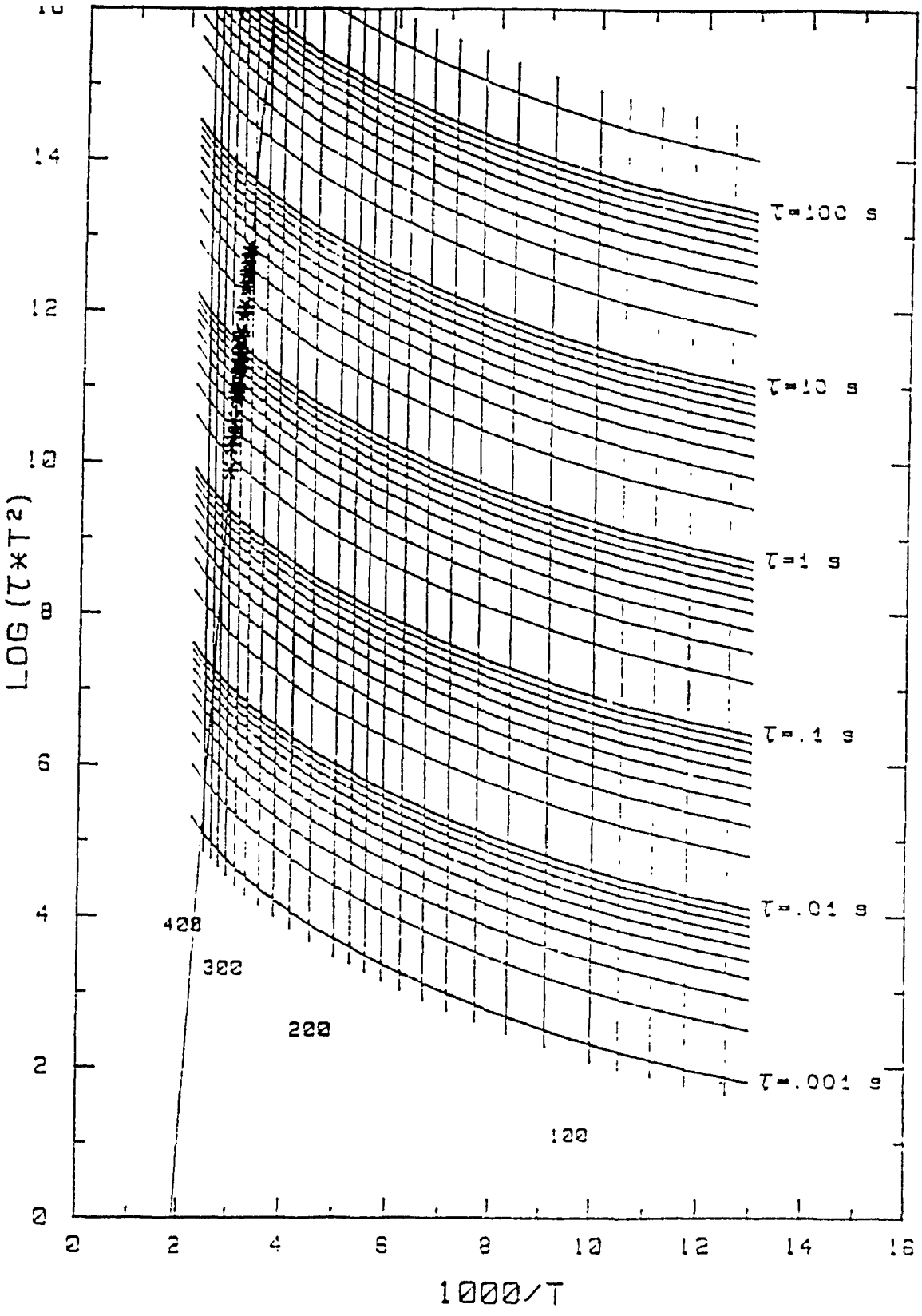


Fig. 5.7 Arrehnius plot allowing to find Ea

equals to $1.9 \times 10^{-13} cm^2$. Furthermore, we took a Bridgman sample where EL2 is expected to be found (78). We performed our DLTS experiments on the sample with our experimental apparatus and we found Ea equals to 804.0meV and $\sigma_n$ equals to $2.46 \times 10^{-13} cm^2$ which agrees with published results.

In some cases the EL2 deep lying trap level is seen in low concentration (low peak height) and for these cases it is rather difficult to measure Ea. An example of EL2 in low concentration (right hand side peak) was shown in figure 5.5. Therefore once we have determine Ea properly, we may recognize the EL2 trap level if the peak is located at 335K for $\tau_n$ being equal to 0.391s. EL2 can also be recognized for each temperature and corresponding $\tau_n$ in figure 5.6 since it has been determined from this plot.

The next trap to be discussed is also found in all samples with the peak temperature near 300K for $\tau_n$ at 0.391s. This is the left hand side peak shown in figure 5.5. We have measured Ea and $\sigma_n$ with the same method as described above. We found an overall average in Ea equal to 730meV ±31meV with $\sigma_n$ equal to $3.5 \times 10^{-13} cm^2$ $\pm 4.2 \times 10^{-13} cm^2$ where the capture cross section may vary considerably for the reasons mentioned above. This deep donor trap is identified as ELCS1 with 730meV and $10^{-13} cm^2$ (79)(80). Our results agree with published results within the limit of error found above.

We have verified this deep donor trap by comparing the DLTS measurement made on samples at USTL Montpellier France and at Concordia University in Montreal. We took eleven samples at random (#AU & ALU) that where characterized in Montpellier and thirteen samples at random that where characterized in Montreal: samples series # S29E, S30R and

R. Then we averaged up each set and we found the results which are shown in table 5.5. These results show that the ionization energies Ea were comparable for different samples where they were characterized at two different laboratories.

**TABLE 5.5**: Comparison for ELCS1 trap found at different laboratories

| Sample # | Ea(meV) | Sigma(cm-2) |
|---|---|---|
| AU & AL | 726.8±34 | 4.38E-13 |
| S29E | 712.3±43 | 5.77E-13 |
| S30R | 710.2±26 | 2.20E-13 |
| R | 715.4±27 | 3.28E-13 |

We have found another particular peak in samples D372 and D373 after annealing and etching them. Eight different measurements have been taken for Ea. We found an average Ea equal to 614.75meV ±43meV with $\sigma_n$ equal[3] to $1.58\times10^{-15}cm^2$. We think that this trap was not found elsewhere in GaAs epitaxial growth by CSVI. Of course more results should be taken to ascertain the validity of this result. This trap can be recognized for a temperature 285K for $\tau_n$ equal to 0.391s

Finally, in samples series D370 we found four donor traps after annealing the samples at 750 °C for 1/2 hour. These are shown in figure 5.8. Using always the same method, we found the ionization energies and capture cross sections. They are given in table 5.6 For these traps found at low temperatures it is not possible to determine

---

[3] Let Ea=0.62eV and $\sigma n=1.6\times10^{-15}$ $cm^2$ for convenience, for this particular trap.

Ea correctly with the cryostat we are usually using in our laboratory. The reason will be given in the next subsection. We can say that the Ea values found are rough approximation for the latter case.

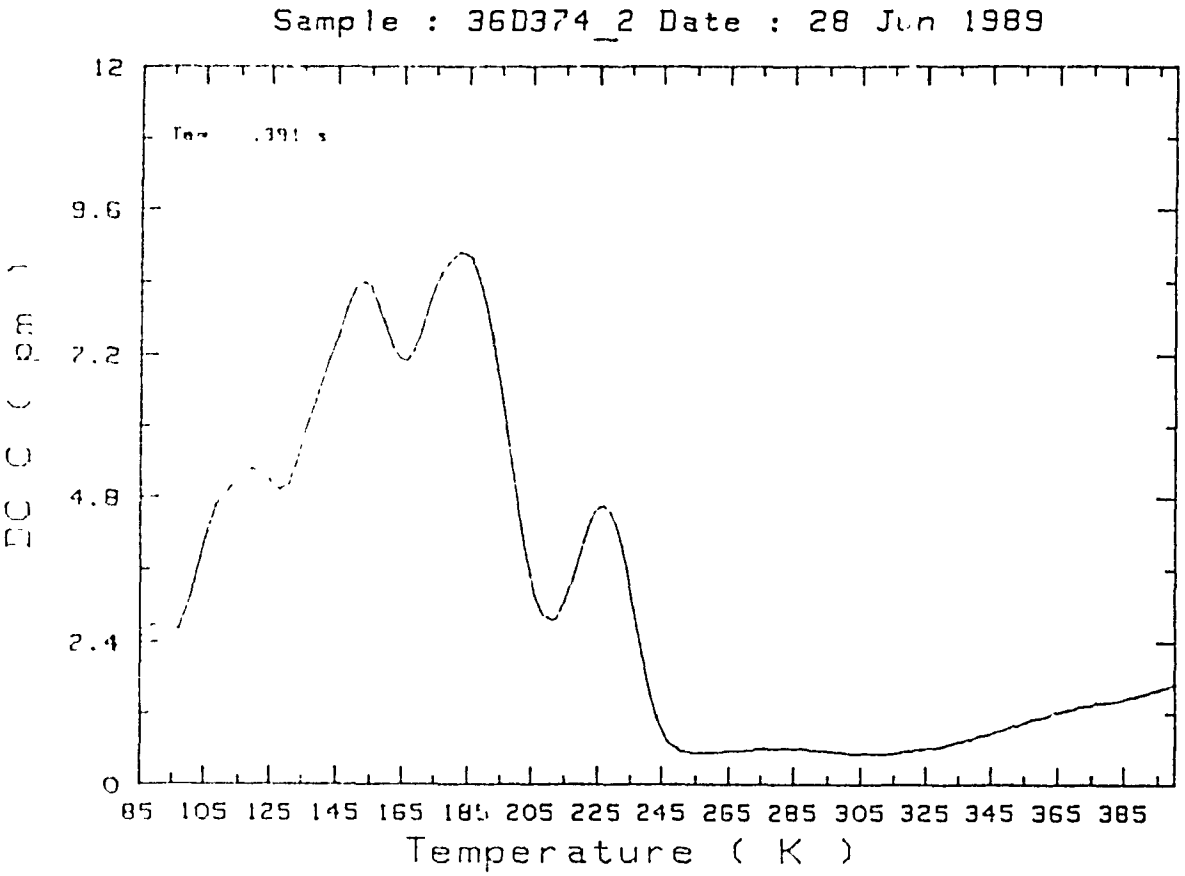


Fig. 5.8 DLTS spectrum for sample D374

TABLE 5.6. Apparent activation energies for peaks shown in fig. 5.8.

| Peak No. | Ea(meV) | Sigma(cm-2) |
|---|---|---|
| 1 | 238.00 | |
| 2 | 327.70 | 4.83E-14 |
| 3 | 387.50 | 4.11E-15 |
| 4 | 517.05 | 1.51E-14 |

5.2.2 Probable causes of error in finding Ea

From one DLTS measurement to another for a given rate window the peak may shift a few degrees in temperature. This shift in temperature may cause errors in finding Ea and $\sigma_n$. Furthermore, the thermal velocity rate ($\Delta T$) is suppose to be constant and slow ($\Delta T \cong 1$ to 2K/min.) for a better averaging for the DLTS peak signal S(T).

From the discussion in the previous section, we know that we can rely on the equipment for the DLTS measurement. Consequently, the validity of our experiment depends on the temperature measurement at the sample which is under vacuum inside the cryostat. The temperature is measured with a platinum resistance which is placed on the sample. Then the temperature is calculated with equation 4.28

To check the validity of our platinum resistance, we have measured its resistance at liquid nitrogen (77K or -196°C), at melting temperature with deionized water (DI) (273K or 0°C), at ambient temperature (298K or 25°C), and at boiling DI water temperature (373k or 100°C ). Thus we have measured the resistance and compared with the manufacturer specifications. Then we have calculated the corresponding temperature using equation 4.28.

It is observed from table 5.7 that the errors in resistance and in temperature are low. Thus the temperature given by the platinum resistance is reliable.

Another point that we have verified was where to put the resistance for maximum reliability in temperature? In order to ascertain the validity of our measurement in temperature depending where the resistance is located, we have put two identical platinum resistances that we have tested before the experiment, and we have put

TABLE 5.7. Error between theoretical and experimental temperature measurements.

| Temperature T1 | | R (ohm) | | % Error | Temp(K) T2 | DT | % Error |
|---|---|---|---|---|---|---|---|
| C | K | Read | Given | in R | Calculated | K | T1 & T2 |
| -196.0 | 77 | 21.62 | 21.00 | 2.95 | 80.79 | 3.79 | -4.40 |
| 00.0 | 273 | 101.00 | 100.00 | 1.00 | 275.59 | 2.58 | -0.94 |
| 25.0 | 298 | 110.68 | 110.00 | 0.62 | 300.47 | 2.47 | -0.82 |
| 100.0 | 373 | 137.00 | 138.50 | 1.10 | 369.09 | 3.95 | +1.08 |

one inside the cryostat tip tail (made of copper) and one on the sample which is placed on the tail inside the cryostat. Then we have performed a DLTS measurement from 80K to 400K and we have measured the values of R1 and R2 at an average spacing at every 3 ohms. The results are shown in table 1 in appendix IX.

The results show that the sample and the cryostat tail are following each other in temperature within an average of 1% of error. This is very important that the sample and the cryostat tail follow to each other in temperature; if it is not the case, a large error in temperature reading will occur thus shifting the DLTS peak in temperature inducing an error in finding Ea. Therefore, whether the platinum resistance is placed on the tip tail of the cryostat or on the sample, the reading in temperature should be correct within 1% of error in the resistance value.

Another problem in using the cryostat is the thermal rate velocity in temperature ($\Delta T$): the cryostats used are cooled down with liquid nitrogen (77K) and warmed up to around 400K so the sample can follow this range of temperature.

The main problem is the high thermal velocity (K/min.) in low temperature. The cryostat used in Montreal has a tendency to warm up to rapidly from around 100k to 260k where the operator has no control over it. An example is shown in figure 5.9a. This is the reason why we cannot assure the validity of Ea found for the four DLTS peaks given in table 5.6, which was discussed in subsection 5.2.1. Therefore the proper measurement of Ea for the peaks found below 260K should be done with a cryostat that has a low thermal rate velocity in low temperature from 77K to 260K.

For temperatures higher than 260K up to 400K, it is up to the operator to control the temperature manually so that the thermal speed be as constant as possible because we want a good averaging of the signal S(T). Figure 5.9a shows a typical example of an average control in thermal speed where $\Delta T$ is around 1.5K/min. In this case Ea can be determined properly. Figure 5.9b shows an example where $\Delta T$ varies from around 1K/min. to 4.4K/min. For the latter case the signal averaging is not correct thus inducing an error in the DLTS peak measurement.

The cryostat used in Montpellier France had the possibility of a low thermal rate velocity in low temperature. In order to keep our $\Delta T$ as constant as possible, we have built a temperature regulator. The circuit is shown in figure IX.1 in appendix IX. This circuit compares the increment in temperature with a linear ramp where we can choose its desired increment in thermal speed. The ramp is generated by a simple integrator circuit (S1). By comparing the two signals, the power supply feeds more or less power to the heating element inside the tail of the cryostat. This circuit worked out very well with the cryostat used in Montpellier. Table IX.2 in appendix IX shows the results in

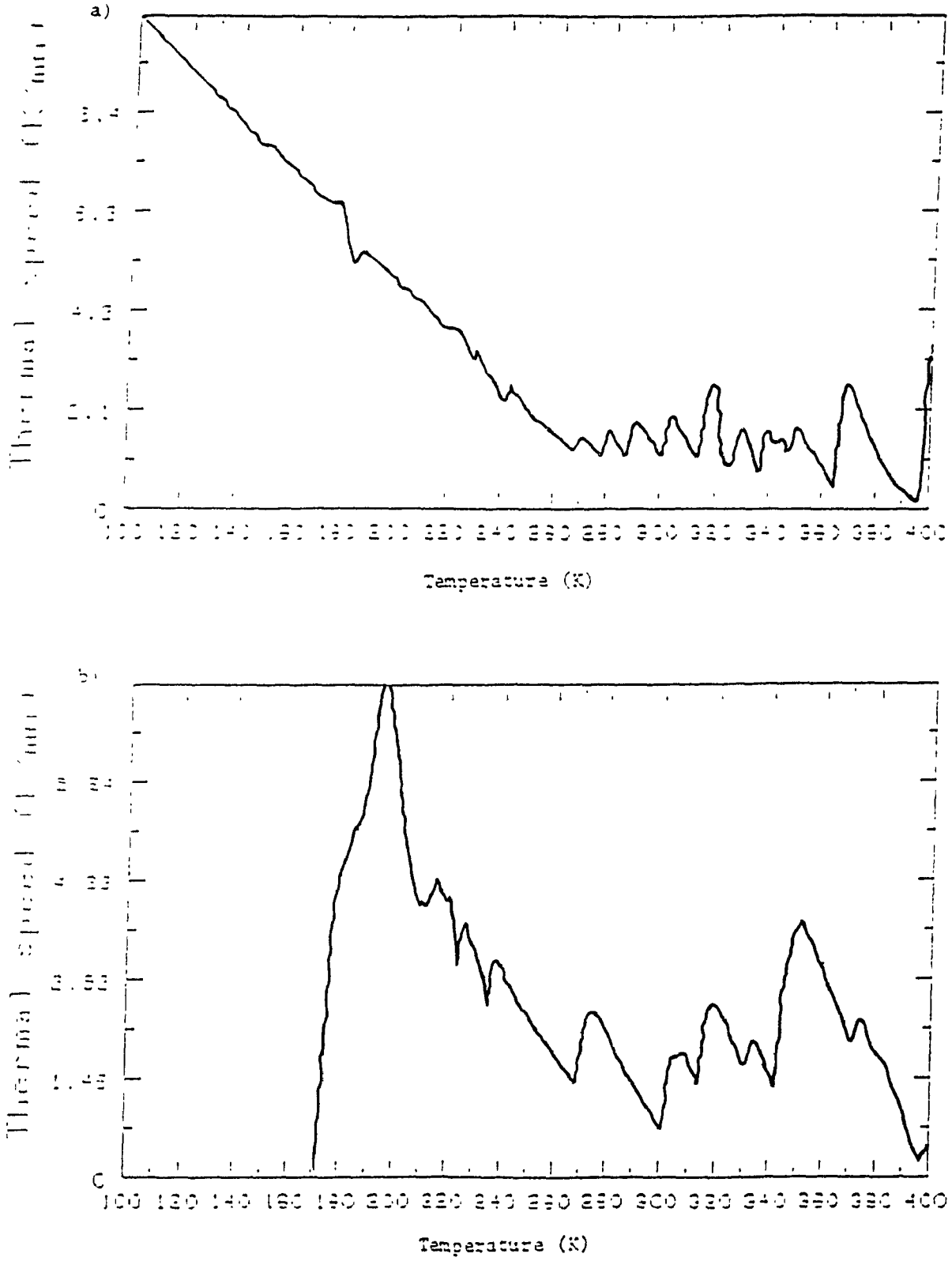


Fig. 5.9 Examples of thermal speed as function of the temperature

ΔT for a DLTS experiment from 80K to 400K. The low variation in ΔT (ΔTaverage = 1.5K/min.) shows that the increment in temperature was fairly constant thus allowing the operator to determine Ea properly for DLTS peaks found at any temperature range.

Unfortunately, this circuit did not function properly with the cryostat used in Montréal because of the high thermal speed change in low temperature. However it could work out for temperatures greater than 260K after a proper adjustment of the potentiometer in the circuit. In order to make it work in low temperature, we suggest to redesign the circuit using a pump that would cool down the cryostat by injecting liquid nitrogen in it if the case may be. This way, ΔT would be constant throughout the whole experiment.

## 5.3 Experimental Results

The determination of deep level trap concentration $N_T$ allows to draw interesting conclusions as it will be seen in further sections. We have determine the value of $N_T$ experimentally using equation 4.30. From the plot of DLTS experiments we have measured the peak height $S(T_M)$. Then we find $C(V_0)$ and $C(V_1)$ from the C(V) plot (figure 5.1) in order to find $W_0$ and $W_1$. Finally $\lambda$ is found from equation 4.17 since Ea has been found previously. Then the value for $N_T$ were calculated for all samples.

Here we show the experimental results for samples R16, B46 and B51 put in tables 5.8, 5.9 and 5.10 respectively. For example, table 5.8 shows the sample number on the upper left hand side rectangle. Then "Tsubs" represents the substrate temperature during the epitaxial layer growth for that particular sample (R16). Then the epitaxial layer

thickness, the free carrier concentration ($N_DH$) and the mobility ($\mu$) are given. Both $N_DH$ and $\mu$ were found from the Hall effect measurements. From the table, we can find in each column:

Ea. The apparent activation energy (eV)

$W_0$: Depth from the junction corresponding to the bias voltage $V_0$ ($\mu$m)

$W_1$ Depth from the junction corresponding to the bias voltage $V_1$ ($\mu$m)

Rs: The series resistance ($\Omega$)

Rsh. The shunt resistance (1*E6) ($\Omega$)

Js The reverse saturation current (1*E-9) ($A/cm^2$)

$N_T$: Deep level trap concentration (1*E14) ($cm^{-3}$)

$N_D$: Concentration of shallow donor (1*E15) ($cm^{-3}$)

n The ideality factor

$\phi_b$ Barrier height determined by I(V) measurement (eV)

$V_b$: Barrier height determined by C(V) measurement (eV)

%er Percentage of error between $V_b$ and $n*\phi_b$.

For example, in table 5.S, in the first row, the values for Rs, Rsh, Js, $N_D$, n, $\phi_b$ and $V_b$ are given from the experimental characterization of a Schottky barrier discussed previously. The results are now put in tables. Thus in the first row and the first column of table 5.S. we may observe the apparent activation energy Ea (0.80eV) where its corresponding deep trap concentration can be found (in the same row). $W_0$ and $W_1$ correspond to the distance from the junction depth where the DLTS have been investigated in order to find $N_T$. For example, in the first row, at $V_0$=-5V and $V_1$=0V we have the

TABLE 5.8: Results for sample R16

| Sample R16 | | | | Tsubs = 560.0 °C | | | | | | | | | |
|---|---|---|---|---|---|---|---|---|---|---|---|---|---|
| Thickness = 41.0 μm | | | | : $N_D H$ = 8 15E15 at/cm$^3$ | | | | | : μ = 4760 cm$^2$/V-s | | | | |
| Ea | $W_0$ | $W_1$ | Rs | Rsn | Js | $N_T$ | $N_D$ | $V_0$ | $V_1$ | n | $\phi_b$ | $V_b$ | %err |
| eV | μm | μm | Ω | Ω | A/cm$^2$ | at/cm$^3$ | at/cm$^3$ | Volt | Volt | | eV | eV | $V_b$ & $n^*\phi_b$ |
| | | | | E6 | E-9 | E14 | E15 | | | | | | |
| .80 | 1.534 | 0.620 | 30.4 | 140. | .626 | 0.417 | 03.69 | -5 | 0 | 1 074 | 0.880 | 1.060 | 12. 1 |
| .72 | 1.534 | 0.620 | | | | 0.631 | 03.69 | -5 | 0 | | | | |
| .80 | 1.767 | 0.911 | | | | 0.516 | 03.69 | -7 | -1 | | | | |
| .72 | 1.767 | 0.911 | | | | 0.572 | 03.69 | -7 | -1 | | | | |
| .80 | 1.767 | 0.911 | | | | 0.485 | 03.69 | -7 | -1 | | | | |
| .72 | 1.767 | 0.911 | | | | 0.608 | 03.69 | -7 | -1 | | | | |
| .80 | 1.985 | 1.029 | 33.1 | 9.64 | .907 | 0.394 | 02.93 | -7 | -1 | 1.095 | 0.847 | 0 950 | 02.4 |
| .72 | 1.985 | 1.029 | | | | 0.461 | 02.93 | -7 | -1 | | | | |
| .80 | 1.985 | 1.029 | | | | 0.390 | 02.93 | -7 | -1 | | | | |
| .72 | 1.985 | 1.029 | | | | 0.447 | 02.93 | -7 | -1 | | | | |
| 80 | 2.200 | 1.166 | 163 | 11.0 | .861 | 0.749 | 0.361 | -2 | 0 | 1.099 | 0.887 | --- | |
| .72 | 2.200 | 1.166 | | | | 0.110 | 0.861 | -2 | 0 | | | | |
| .80 | 3.470 | 2.450 | | | | 0.622 | 1.061 | -7 | -3 | | | | |
| .72 | 3.470 | 2.450 | | | | 0.097 | 1.061 | -7 | -3 | | | | |

TABLE 5.9: Results for sample B46

| Sample B46 | | | | Tsubs = 850.0 °C | | | | | | | | | |
|---|---|---|---|---|---|---|---|---|---|---|---|---|---|
| Thickness = 70.0 μm | | | | $N_D$H = 5.11E16 at/cm$^3$ | | | | | | μ = 4150 cm$^2$/V-s | | | |
| Ea eV | $W_0$ μm | $W_1$ μm | Rs Ω | Rsh Ω E6 | Js A/cm$^2$ E-9 | $N_T$ at/cm$^3$ E14 | $N_D$ at/cm$^3$ E15 | $V_0$ Volt | $V_1$ Volt | n | $\phi_b$ eV | $V_b$ eV | %err $V_b$ & $n^*\rho_b$ |
| 80 | 0.535 | 0.230 | 4.33 | 2.39 | 99.0 | 01.13 | 32.10 | -5 | 0 | 1.316 | 0.757 | --- | |
| 72 | 0.535 | 0.230 | | | | --- | 32.10 | -5 | 0 | | | | |
| 80 | 0.663 | 0.416 | 5.47 | | 34.6 | 01.27 | 27.26 | -7 | -2 | 1.310 | 0.768 | --- | |
| 72 | 0.663 | 0.416 | | | | 08.91 | 27.26 | -7 | -2 | | | | |
| 80 | 0.353 | 0.237 | | | | 0.806 | 73.90 | -1 | 0 | --- | --- | 0.970 | |
| 72 | 0.353 | 0.237 | | | | 12.40 | 73.90 | -1 | 0 | | | | |
| 80 | 1.116 | 1.035 | 6.27 | 13.2 | 1.07 | 2.655 | 40.70 | -1 | 0 | 1.091 | 0.854 | 0.890 | -4.5 |
| 72 | 1.116 | 1.035 | | | | 12.30 | 40.70 | -1 | 0 | | | | |
| 80 | 1.395 | 1.186 | | | | 01.16 | 40.70 | -7 | -2 | | | | |
| 72 | 1.395 | 1.186 | | | | 09.10 | 40.70 | -7 | -2 | | | | |
| 80 | 2.475 | 2.363 | | | | 0.786 | 79.20 | -1 | 0 | 1.083 | 0.846 | 0.850 | -7.2 |
| 72 | 2.475 | 2.363 | | | | 6.420 | 79.20 | -1 | 0 | | | | |
| 80 | 2.737 | 2.475 | | | | 0.551 | 79.20 | -5 | -1 | | | | |
| 72 | 2.737 | 2.475 | | | | 5.180 | 79.20 | -5 | -1 | | | | |
| 80 | 3.365 | 3.410 | | | | --- | 22.00 | -2 | 0 | 1.068 | 0.894 | 0.880 | -7.8 |
| 72 | 3.465 | 3.410 | | | | 4.761 | 22.00 | -2 | 0 | | | | |
| 80 | 3.465 | 3.465 | | | | --- | 22.00 | -7 | -2 | | | | |
| 72 | 3.846 | 3.465 | | | | 4.180 | 22.00 | -7 | -2 | | | | |

**TABLE 5.10: Results for sample BS1**

| Sample BS1 | | | | | Tsubs = 880.0 °C | | | | | | | | |
|---|---|---|---|---|---|---|---|---|---|---|---|---|---|
| Thickness = 44.0 μm | | | | | : $N_D$H = 6.90E16 at/cm$^3$ | | | | | · μ = 3940 cm$^2$ V-s | | | |
| Ea | $W_0$ | $W_1$ | Rs | Rsh | Js | $N_T$ | $N_D$ | $V_0$ | $V_1$ | n | $\phi_b$ | $V_b$ | Xerr |
| eV | μm | μm | Ω | Ω | A/cm$^2$ | at/cm$^3$ | at/cm$^3$ | Volt | Volt | | eV | eV | $V_b$ & |
| | | | | E6 | E-9 | E14 | E15 | | | | | | $n^*\phi_b$ |
| .80 | 0.670 | 0.267 | 3.61 | 10.9 | 53.1 | 0.292 | 18.20 | -5 | 0 | 1.382 | 0.760 | 0.940 | 10.5 |
| .72 | 0.670 | 0.267 | | | | --- | 18.20 | -5 | 0 | | | | |
| .80 | 0.757 | 0.535 | | | | 0.403 | 18.20 | -7 | -2 | | | | |
| .72 | 0.757 | 0.535 | | | | 2.183 | 18.20 | -7 | -2 | | | | |
| .80 | 0.416 | 0.267 | | | | 0.680 | 18.20 | -1 | 0 | | | | |
| .72 | 0.416 | 0.267 | | | | 2.270 | 18.20 | -1 | 0 | | | | |
| .80 | 0.729 | 0.286 | 5.92 | 9.45 | 1.89 | 0.274 | 16.70 | -5 | 0 | 1.314 | 0.786 | 0.910 | 11.9 |
| .72 | 0.729 | 0.286 | | | | --- | 16.70 | -5 | 0 | | | | |
| | | | | | | --- | 13.30 | -1 | 0 | 1.064 | 0.876 | 1.330 | 0.85 |
| | | | | | | --- | 13.30 | -1 | 0 | | | | |
| .80 | 1.433 | 1.147 | | | | 0.420 | 13.30 | -7 | 0 | | | | |
| .72 | 1.433 | 1.147 | | | | 0.229 | 13.30 | -7 | 0 | | | | |
| .80 | 2.706 | 2.382 | 6.84 | 10.7 | 2.09 | 1.130 | 14.50 | -2 | 0 | 1.025 | 0.911 | --- | |
| .72 | 2.706 | 2.382 | | | | --- | 14.50 | -2 | 0 | | | | |
| .80 | | | | | | 1.230 | 14.50 | -7 | -2 | | | | |
| .72 | | | | | | --- | 14.50 | -7 | -2 | | | | |

corresponding depth as $W_0$=1.534μm and $W_1$=0.620μm respectively. Then, in the second row, for Ea=0.72eV, we may find the same distances ($W_0$ and $W_1$) for the same bias since both traps have been found on the same diode. It can be seen that other DLTS measurements have been performed at different bias on the same diode. For instance, for Ea=0.8eV at $V_0$=-7V and $V_1$=-1V for two different DLTS measurements at those bias, we find $N_T$=0.516 E14 $cm^{-3}$ and $N_T$=0.485 E14 $cm^{-3}$ with 6.3% error between the two and similarly for Ea=0.72eV we find $N_T$=0.572 E14 $cm^{-3}$ and $N_T$=0.608 E14 $cm^{-3}$ on the same diode with 6.3% error also. In appendix I, we can find all the detailed values for all the DLTS experiments performed to all samples studied.

Note that, whenever Rs, Rsh, Js, $N_D$, n, $\phi_b$ and $V_b$ are appearing in a new row, this means that the following DLTS measurements have been made on another SKB but on the same epitaxial layer (for R16 in this case). When, a dotted line cuts the table horizontally, this means that an etch of about 1μm was made on the epitaxial layer of that sample. Thus in table 5.8, in the first row below the dotted line we have $V_0$=-2V and $V_1$=0V for a corresponding $W_0$=1.2μm and $W_1$=0.166μm, but we have added 1μm to $W_0$ (2.2μm) and $W_1$ (1.166μm) since we are now investigating at 1μm deeper from the initial surface since we have etched the sample.

In summary, table R16 shows that the basic characteristics of the fabricated diodes were good since n≤1.1 and $\phi_b$≥0.85eV. With this in mind, we observe that as we go deeper from the junction in performing DLTS measurements. We find that EL2 (Ea=0.8eV) seems to remain constant whereas, the ELCS1 (Ea=0.72) tends to vanish. The same phenomena are observed in sample B46 (table 5.9) and sample B51 (table 5.10) but with

more etching steps. In section 5.5 we will show the curves from these data and discuss them.

## 5.4 n, Io, Vb, Rs and Rsh measurements

The values of n, Io, Vb, Rs and Rsh are also given in table I in appendix I. The diodes are usually checked first with the curve tracer but with no accuracy. This is a quick way to check if the fabricated diodes have a junction that can be exploited. The accurate method to find the above results is done by using the I(V) measurement method as describe in section 3.2. A typical example of I(V) measurement method is shown in figure 5.10 for ln(I) as function of the positive voltage applied. The accuracy of the measurement depends on

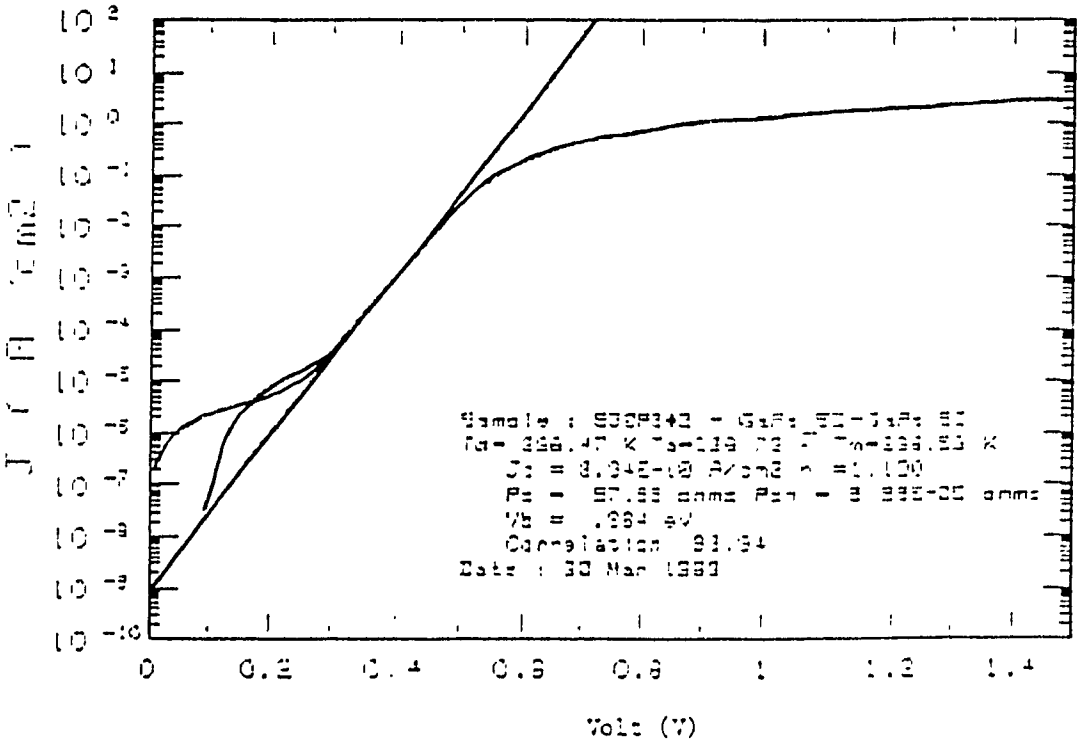


Fig. 5.10 An example of experimental curves of ln(I) vs V

the HP 3455A multi meter accuracy and the resistance R used to find I (see figure 3.6).

The resistance R used have an accuracy of 1% of the nominal value. The multi meter put in ohm-meter mode which reads the value of R chosen by the scanner has an accuracy of 0.0045% of reading +0.004% on high resolution mode (6 digits used) operated at 23°C ±1°C (S2). The multi meter in DC voltmeter mode which assign the voltage values on R has an input resistance Rin greater than $10^{10}$MΩ on 0.1V through 10V range. The accuracy of reading on 10V range on high resolution is ±0.002% of reading +0.0003%. Therefore, we can rely on the multi meter measurement because of its high accuracy performance when it is periodically calibrated. A removable reference module can be sent periodically for calibration (S2) to ensure the accuracy of the apparatus.

Here it can be observed from the tables in appendix I that we have fabricated good Schottky barriers for our analysis purposes since most of our diodes have an ideality factor n between 1.05 and 1.1. The values of Rs and Rsh varies from one sample to the other since we used an approximation method to find them. We require some approximating values for Rs and Rsh in order to have a good idea so as to see if there are in a reasonable expected range since we don't need them for further analysis as far as we are concerned.

5.4.1 Plots of $N_D$ vs $\phi_b$ and Js vs $\phi_b$

From table I.1 in appendix I, it can be seen that $\phi_b$ is not always constant throughout the whole table. This depends partly on the free carrier concentration $N_D$. We recall from section 3.2.1 that the barrier height $\phi_b$ is lower by an amount $\Delta\phi_b$ due to the image force lowering. From equation 3.8, it is seen that $\Delta\phi_b$ is dependent on $N_D$. We note also that $\phi_b$ is also dependent on the work function $\phi_m$. $\phi_m$ should remain constant since we are always using the Al-Pd metalization system on our Schottky barriers thus not altering $\phi_b$ very much.

As discussed in section 5.1, $N_D$ may be different and not uniformly distributed in several samples; thus $\phi_b$ varies. We have plot the free carrier concentration $N_D$ vs $\phi_b$ for samples series D369 through D378 in order to show their dependence. This is shown in figure 5.11.

It is observe that for low $\phi_b$, $N_D$ is large and for $\phi_b$ increasing $N_D$ is decreasing. This means that $\Delta\phi_b$ is increased as $N_D$ is increased, thus decreasing $\phi_b$ where $\phi_b$ is the height of the resultant barrier. This experimental plot is in agreement with the image force lowering theory explained in in appendix V and given in equation 3.8.

The dispersion between the points is about 0.6 decade. This may be caused by the non-uniformity in the doping. If $N_D$ varies for different bias on the same sample $\phi_b$ will vary accordingly. Another probable cause of error is the surface area of the junction. $\phi_b$ is determine from equation 3.7; if there is a small change in S, it will induce a change in $\phi_b$. A third probable cause of error would be due to some kind of contamination left on the sample surface when we where fabricating the diodes. It is very important that the surface be very cleaned. Unfortunately, we don't have a perfect control over it due to

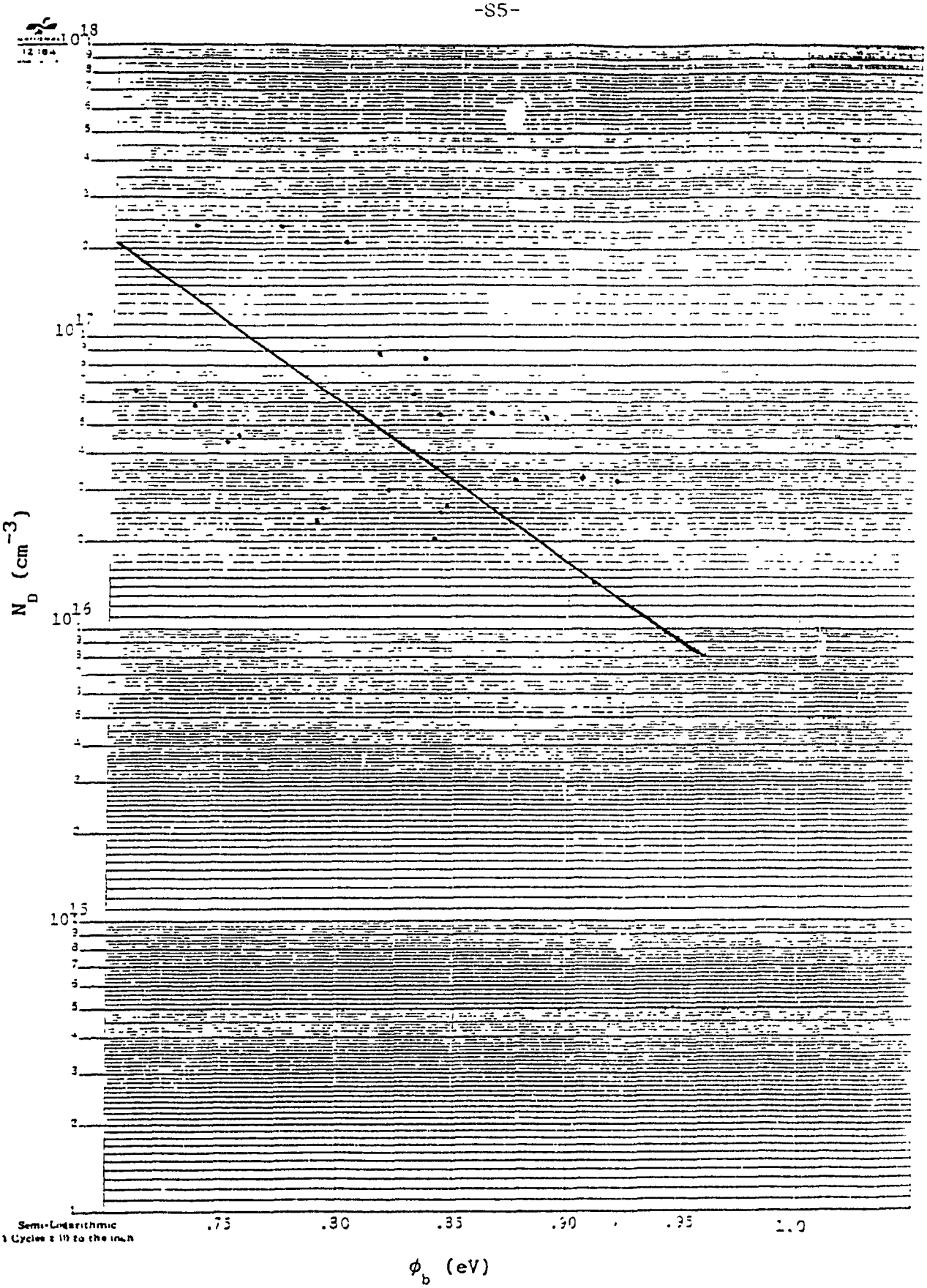


Fig. 5.11 Graph of $N_D$ vs $\phi_b$ for samples D369 through D378

too many parameters variations during the fabrication of Schottky barrier diodes. If there is a layer in between the surface of the sample and the metal due to contamination, a voltage drop may occur across this layer (23)(83), thus lowering the initial value of $\phi_b$ regardless $\Delta\phi_b$. Therefore, if this layer varies in thickness, dispersion of points may occur.

Since $\phi_b$ varies, we have plot in figure 5.12 Js (Js = Io/S) vs $\phi_b$ for the same set of sample in order to verify equation 3.7 experimentally. As $\phi_b$ is increased, Js decreases which verifies this equation (22). Therefore, for each sample used, the characteristic of each diode is slightly different from one to another which is due to the change in $N_D$ and the diode quality fabrication to which we have a good control on n but not as well on $\phi_b$.

To show the dependence on other samples, we have plot $N_D$ vs $\phi_b$ for samples series B39 to B60 as shown in figure 5.13. Due to a low variation in $N_D$ for this set of samples, there is a low variation in $\phi_b$. This leads to $\Delta\phi_b$ mostly constant for this set of sample. This is still in agreement with appendix V but with a slow decreasing slope. The plot of $N_D$ vs $\phi_b$ is also shown in figure 5.14 for samples series R2 through R16. It shows some dependence but with a steeper negative slope within a small range in $\phi_b$. Therefore $N_D$ plays an important role in the determination of $\phi_b$.

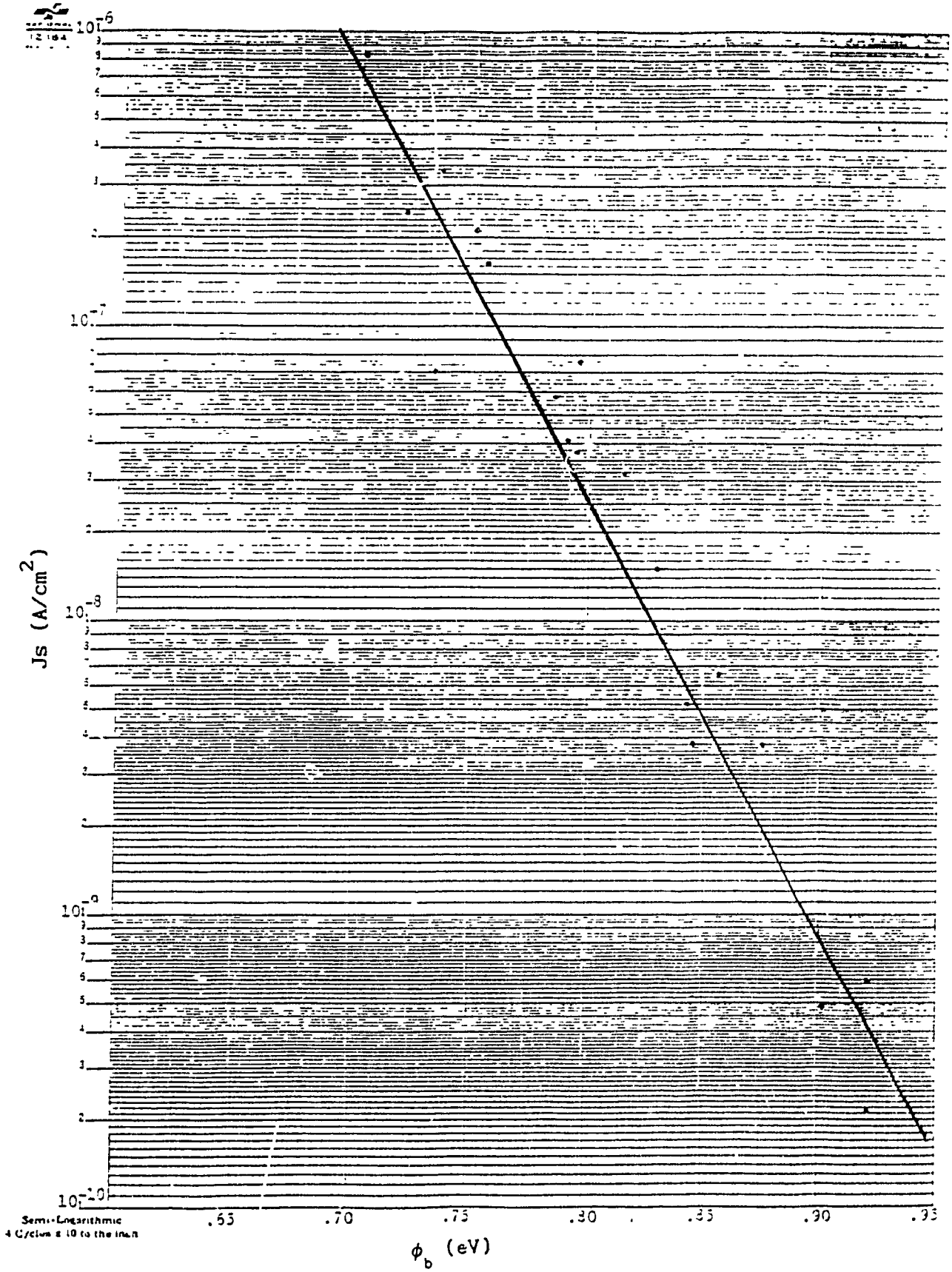


Fig. 5.12 Graph of Js vs $\phi_b$ for samples D369 through D378

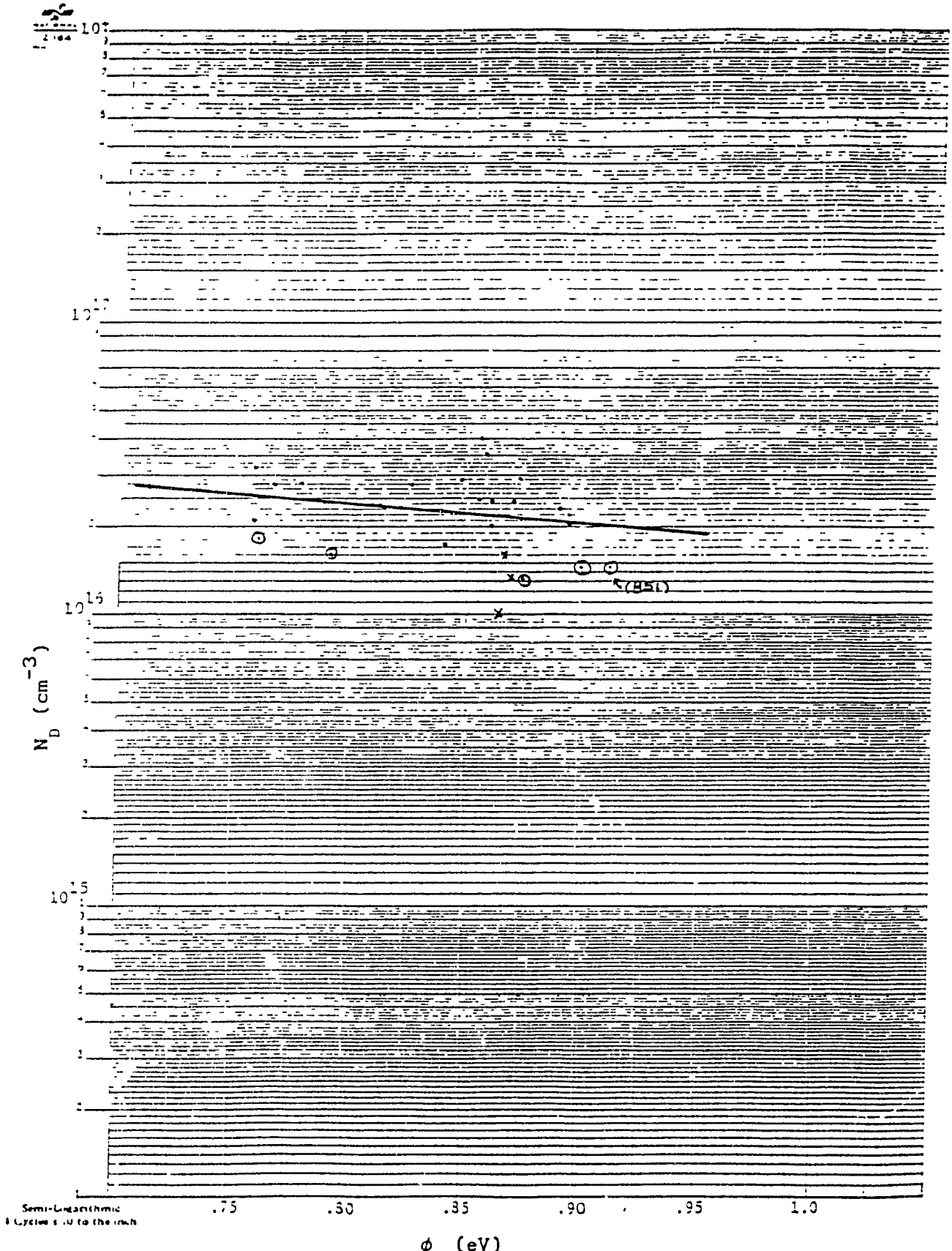


Fig. 5.13 Graph of $N_D$ vs $\phi_b$ for samples B39 through B60

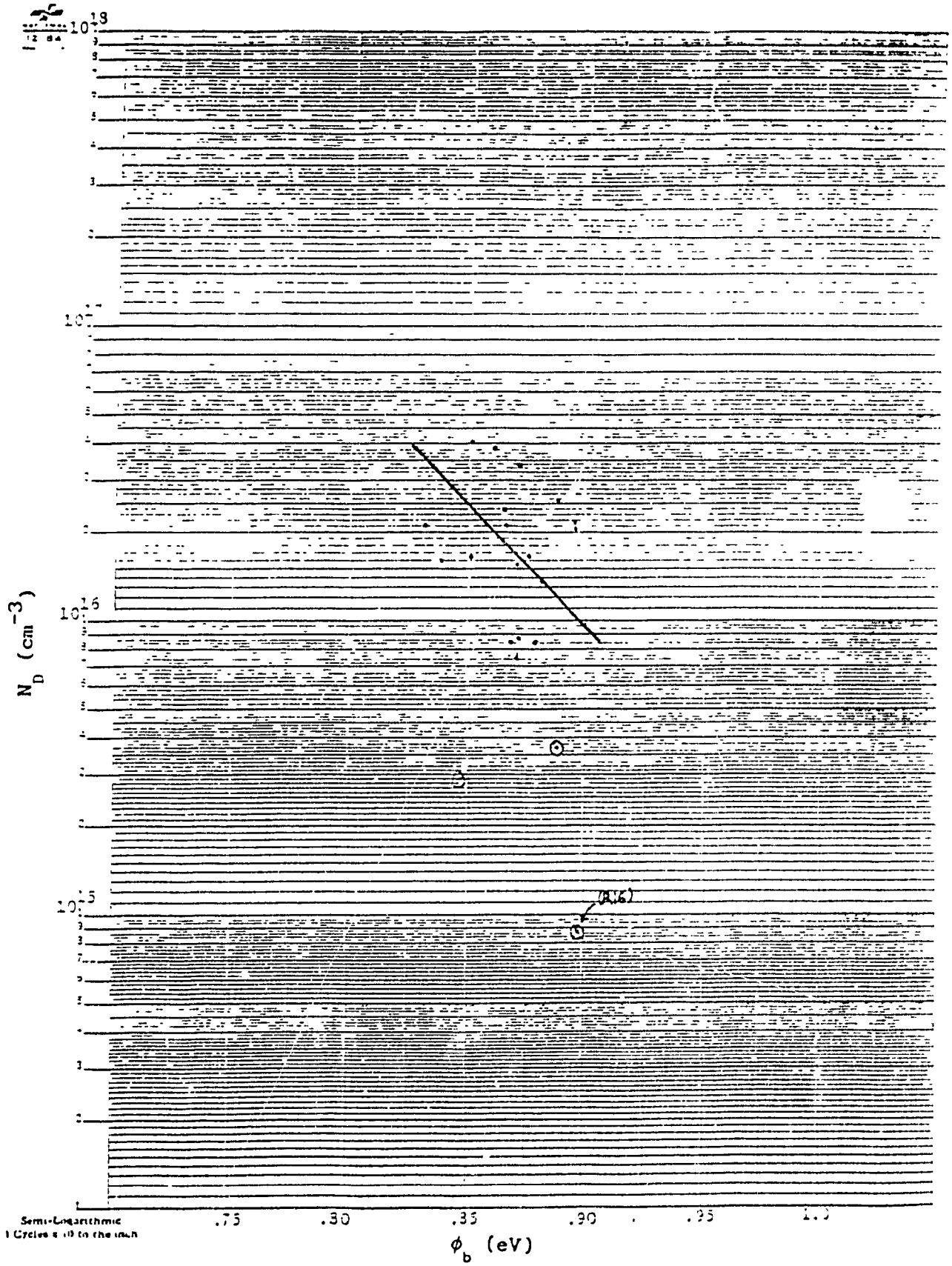


Fig. 5.14 Graph of $N_D$ vs $\phi_b$ for samples R2 through R16

5.4.2 Plots of EL2 vs $\phi_b$ and ELCS1 vs $\phi_b$

It is noticed that the DLTS signal for the mid gap level EL2 seems to be dependent on the Schottky barrier height $\phi_b$ for samples labeled R and B. Thus we have plot the concentration $N_T$ for EL2 vs $\phi_b$. This is shown in figure 5.15. That figure shows that the concentration $N_T$ for EL2 is fairly constant for $\phi_b$ greater than 0.75eV regardless the point dispersions as discussed previously. As suggested by reference (22), for barrier height between 0.62 and 0.82eV, the observe DLTS signal intensity is function of $\phi_b$; consequently the deduced concentration of EL2 level become unreliable. However, in our case, the EL2 deep level donor trap concentration was not affected much by the change in $\phi_b$ as the graph shows, leading to its proper measurement. The few points left on the right hand side bottom where the EL2 is seen at a lower concentration are found in samples R10 and B42. In sub section 5.5.1 we will discuss a proposed model for the EL2 donor trap level that will give us some indication for its change in concentration in the material.

Figure 5.16 shows the curve for $N_T$(ELCS1) vs $\phi_b$ for samples labeled R and B. Note here that we have taken $N_T$(ELCS1) at the surface of the samples only; that is no $N_T$(ELCS1) after an etch are given on the graph. From the results given in table IX.1, it can be seen that after one etch of about one $\mu$m at a time, $N_T$(ELCS1) decreases even if $\phi_b$ is increasing. We have plot $N_T$(ELCS1) vs $\phi_b$ for all other samples and they show similar results as the one shown in figure 5.16. Thus for this trap (figure 5.16), we notice that $N_T$(ELCS1) seems to be dependent on $\phi_b$. This is observed between 0.75 to 0.90eV. Therefore, it seems that the measurement of the trap concentration $N_T$ for ELCS1

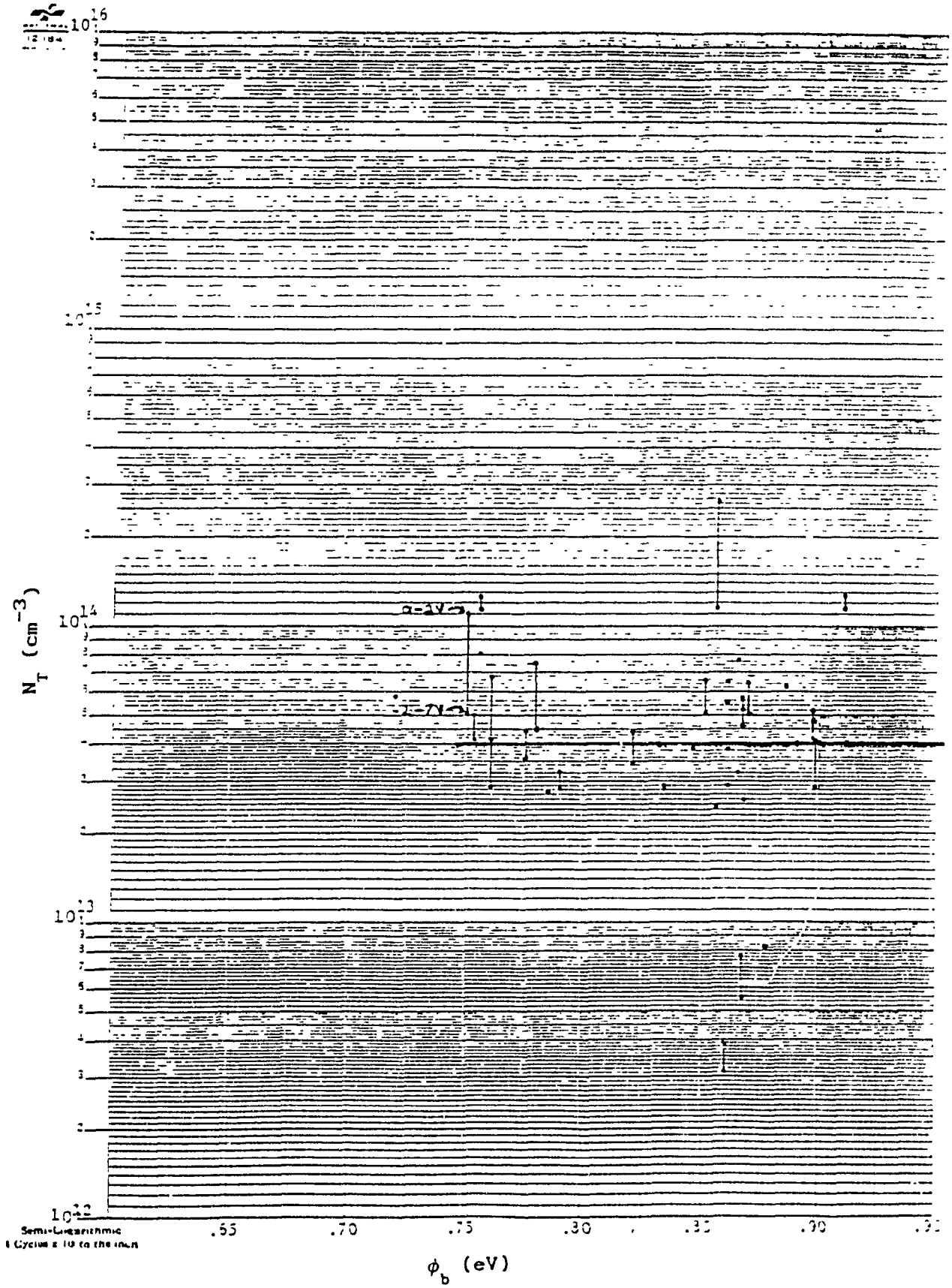


Fig. 5.15 Graph of $N_T$(EL2) vs $\phi_b$ for samples R and B series

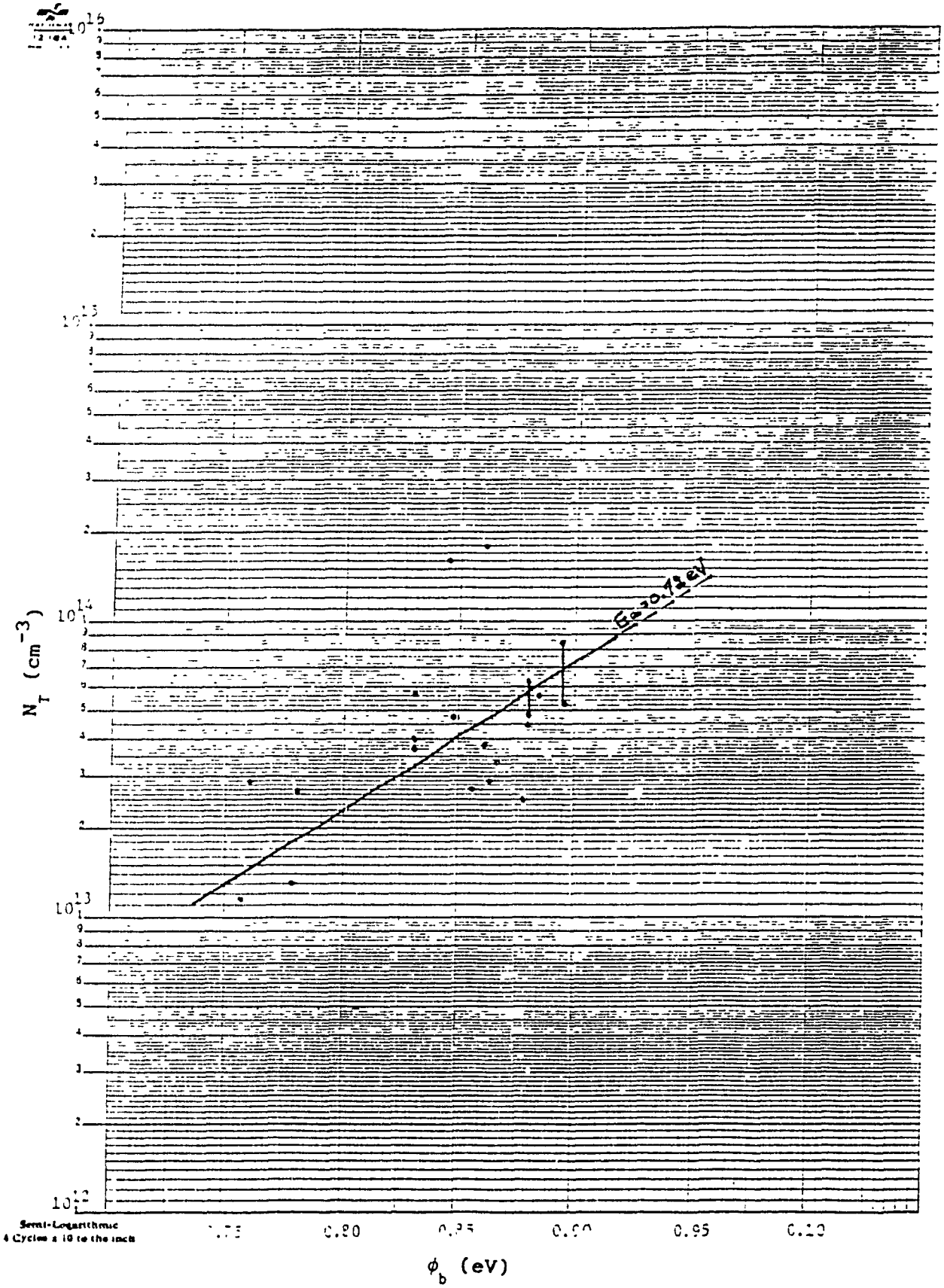


Fig. 5.16 Graph of $N_T$(ELCS1) vs $\phi_b$ for samples R and B series

varies linearly within one decade for $0.75eV<\phi_b<0.90eV$ whereas the measurement of $N_T$ for EL2 seems to be independent of $\phi_b$ as discussed above knowing that $\phi_b$ lies within this range.

5.4.3 Comparison for Vb from C(V) and for $\phi_b$ from I(V) measurement

We have stated in section 3.2.4 that the barrier height determined by the I(V) measurement could be close to one determined from the C(V) measurement if the former is multiplied by the ideality factor n. In order to verify it we have taken the percentage of error for all barrier height involving Vb and $\phi_b$ available in table IX.1.

For eight samples (series AL, AS and AU) available studied in Montpellier France we have compared the barrier heights as follows; for example, for sample (AS40MEP14,4), $\phi_b$=0.785eV, n=1.265, Vb=0.97; therefore Vb'=0.785*1.265=0.993eV . The percentage of error between Vb and Vb' is 2.3%. We have thus calculated each percentage of error for all samples with $\phi_b$ and Vb available and we have made the average. Thus we found that the above statement is true but with a 12.7% of error.

We have checked with fourteen samples in the series D369 through D379 (table 5.11) and, S29E and S30R (table 5.15) studied in Montréal and we have found an average error between Vb and Vb' of 11.3%. The reasons for having Vb and $\phi_b$ different was stated in section 3.2.4.

The reason for correcting $\phi_b$ by a factor n can be seen by the fact that equation 3.7 does not take n into account. References (84) and (85) suggest that n should be included in the expression for the saturation current Io since the effects which cause the deviation from n equal to unity at higher bias voltage are also present at zero bias. Thus equation 3.7 can be rewritten as

$$Io=SA^{*}T^{2}e^{(-\phi b/nkT)} \qquad (5.1)$$

where

$$\phi b' = n\phi b = (nkT/q)\ln(A^{*}ST^{2}/Io) \qquad (5.2)$$

The average 10% of error between Vb and Vb' is probably due to the fact that Vb is taken on the x axis from the $1/C(V)^2$ plot. As discussed previously, if points P1 and P2 are not properly chosen, it may induce a small variation in the slope of the linear fit thus changing the value of Vb (section 3.1.2).

## 5.5 Experimental Observations on EL2 and ELCS1 Traps

In samples R16, B46 and B51, we have studied the as-grown epitaxial layer grown by CSVT, by removing about 1μm layer one step at the time from the surface by chemical etching. The chemical etching solution was made from $H_2SO_4$-$H_2O_2$-$H_2O$ (5:1:1) and was used at 60°C.

Figure 5.17 shows two DLTS spectra of the CSVT epitaxial layers. We have chosen sample R16 (substrate temperature $T_s$ = 860°C) since it represents well the two main traps found in section 5.2.1. In figure 5.17a, we recognize the trap at 300K (ELCS1) and the trap at 335K (EL2) with both the emission rate at 0.39s for Schottky barriers made on the as-grown surface. Figure 5.17b was obtained by the DLTS measurement after a removal of about 1μm from the surface. It is noticed from the figure that the EL2 trap level remains the same even after a chemical etching whereas the other trap level decreases to a negligible amount.

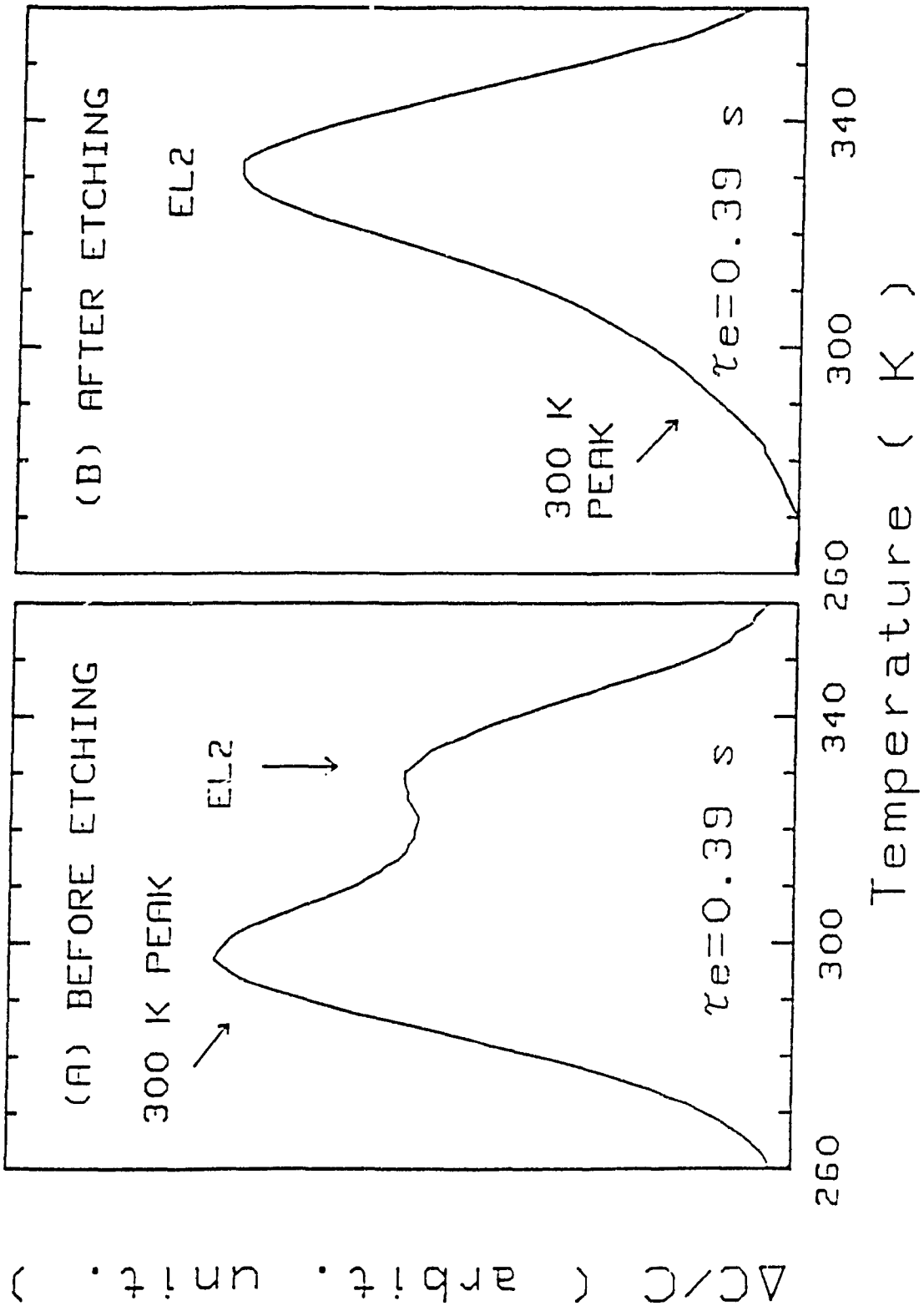


Fig. 5.17 DLTS spectra of the CSVT epitaxial layers.

In order to verify further the depth profile of the concentrations of these two traps, we have plot their concentrations $N_T$ as function of the distance from the junction. Different bias conditions and progressive chemical etching depths were used in the DLTS scans. Figures 5.18, 5.19 and 5.20 show the results for samples R16, B46 ($T_s$=850K) and B51 ($T_s$=880K) respectively. The lines linking the two points corresponding to $W_o$ and $W_1$ represent the zones investigated during the DLTS scan after every chemical etching step. It can be seen for the three cases, that while the EL2 trap concentration remains constant in the bulk, the density of the ELCS1 trap decreases with depth in the epitaxial layer. Further investigations in sample B48 and B50 shows that after a chemical etch of about 5μm to both samples, the trap concentration $N_T$ for ELCS1 is not seen whereas the trap concentration $N_T$ for EL2 is about $3.8X10^{13}$ $cm^{-3}$.

The trap concentration of the DLTS signal for ELCS1 from the above samples studied varies approximately between $2 X 10^{13}$ to $2 X 10^{15} cm^{-3}$. However, it noticed that the ELCS1 diminishes closer to the as-grown surface with increasing deposition temperature. This is shown in figure 5.21 were we have plot the concentration $N_T$ for ELCS1 as function of the substrate temperature.

Figure 5.22 shows the variation of the measured EL2 concentration as function of the substrate temperature. It is observed that the variation of its concentration is approximately between $1.0 X 10^{13}$ to $1.3 X 10^{14} cm^{-3}$. This comparable with those already reported in other epitaxial growth technique such as VPE and OMVPE, where arsenic pressure is taken into account (S6). A monotonic increase of the EL2 concentration from 750 to 850°C deposition temperatures is observed.

Above 850°C a decreasing tendency can be seen.

In order to verify if the values of the shallow donor concentration had an effect on the EL2 trap concentration, we have plot $N_D$ as function of the substrate temperature $\{N_T(T)\}$. This plot is shown in figure 5.23 for samples series labeled with R and B. It is observe that the free carrier concentration $N_D(T)$ is fairly constant regardless sample R16 to which has a low free carrier concentration $N_D$. This leads us to believe, with the help of equation 4.30, that the the trap concentration as function of substrate temperature $N_T(T)$ is not influenced by $N_D(T)$ and should not be influenced by the term in the bracket since it is usually very small (56). Therefore $N_T(T)$ depends on the maximum DLTS peak $S(T_M)$ measured from experimentation.

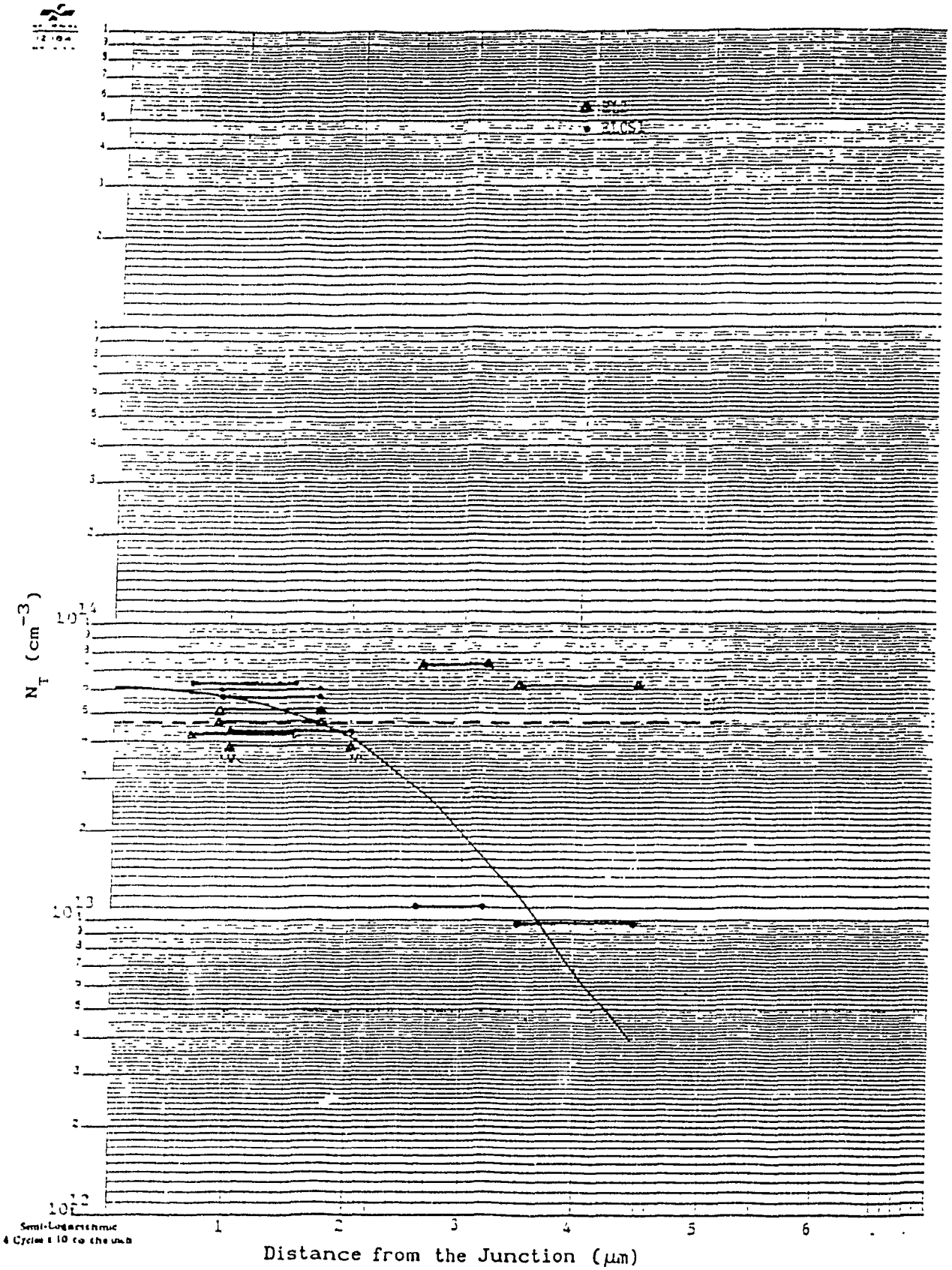


Fig. 5.18 Graph of $N_T$ vs the distance from the junction (sample R16)

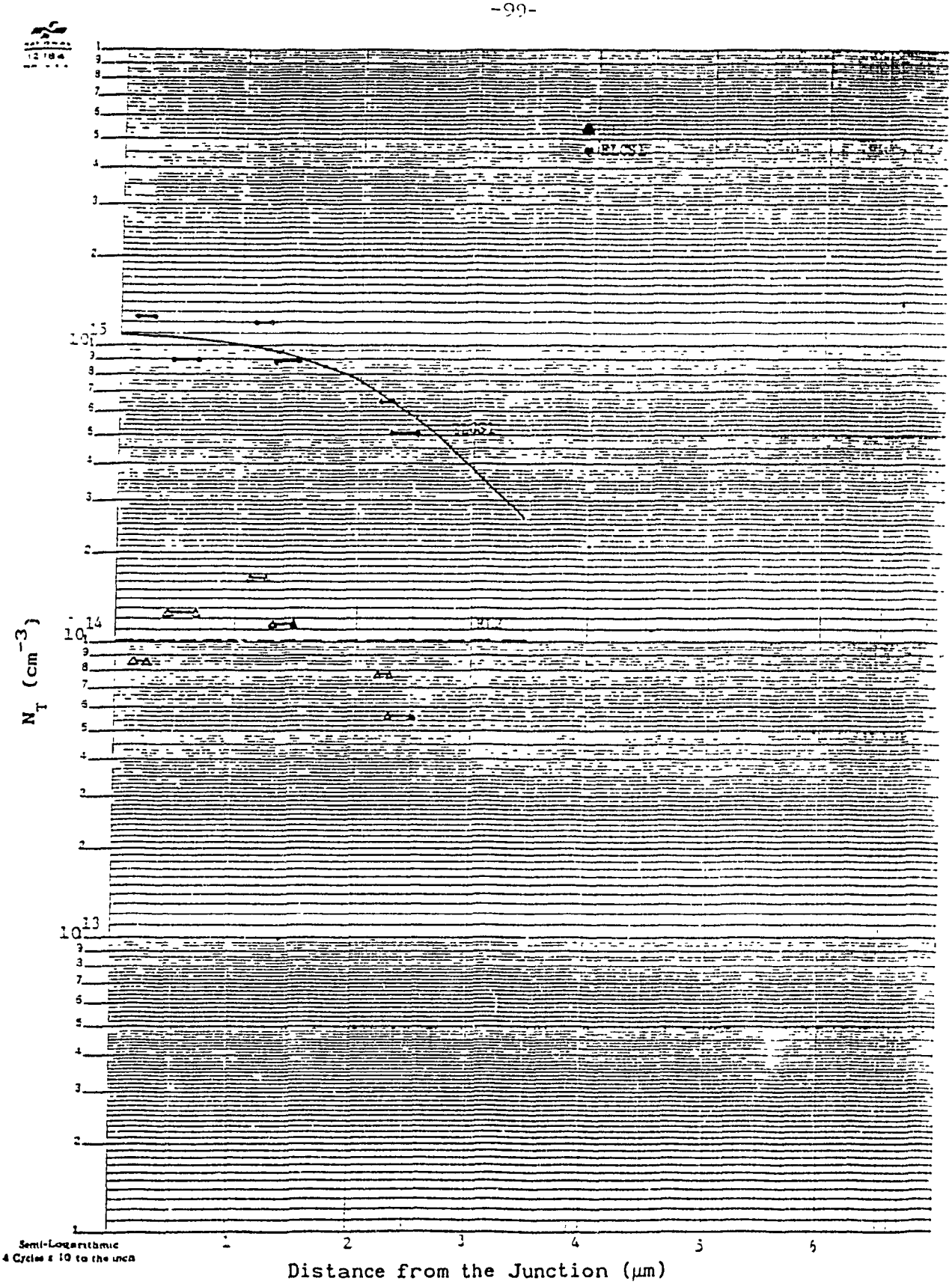


Fig. 5.19 Graph of Nr vs the distance from the junction (sample B46)

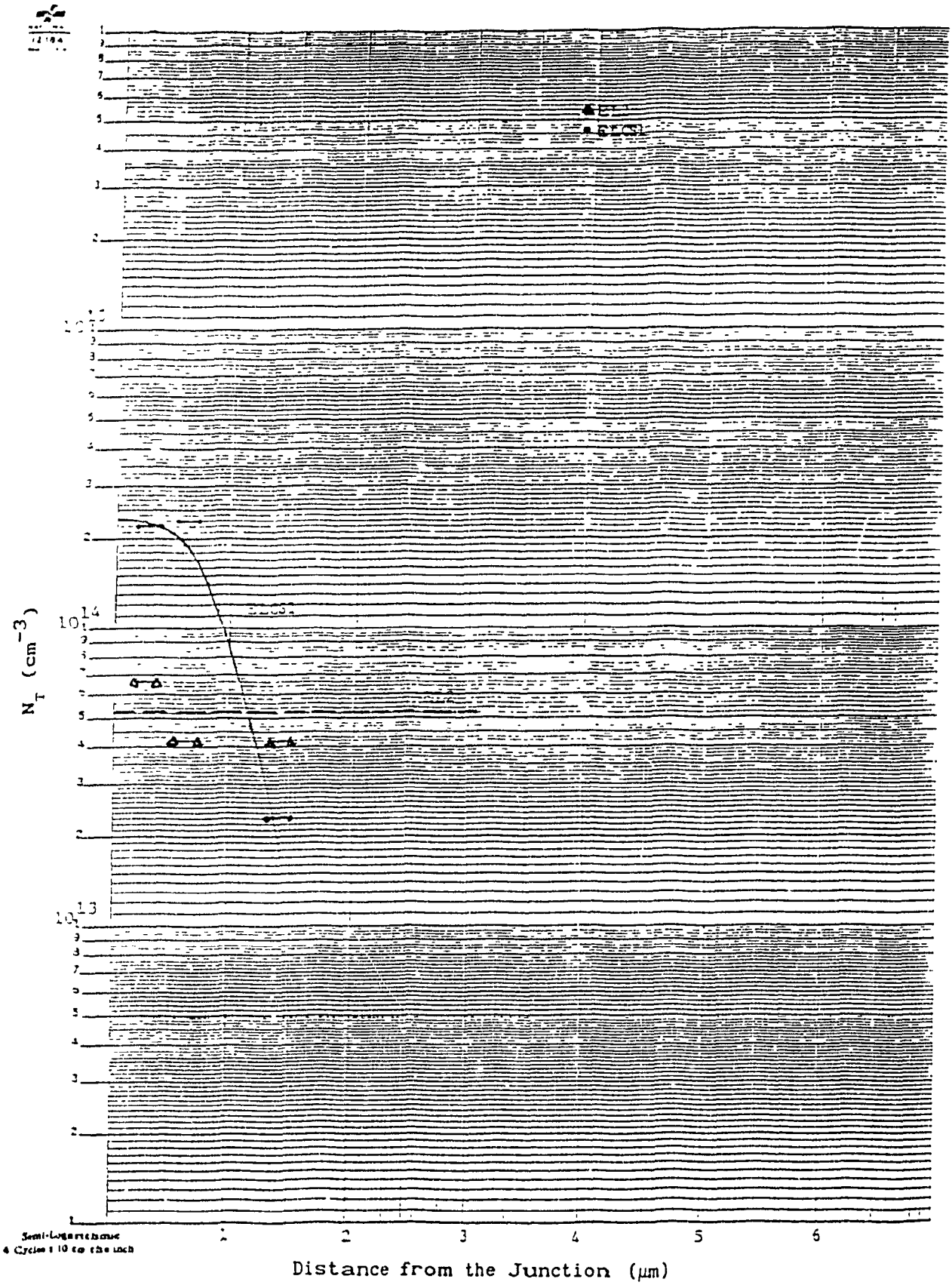


Fig. 5.20 Graph of $N_T$ vs the distance from the junction (sample B51)

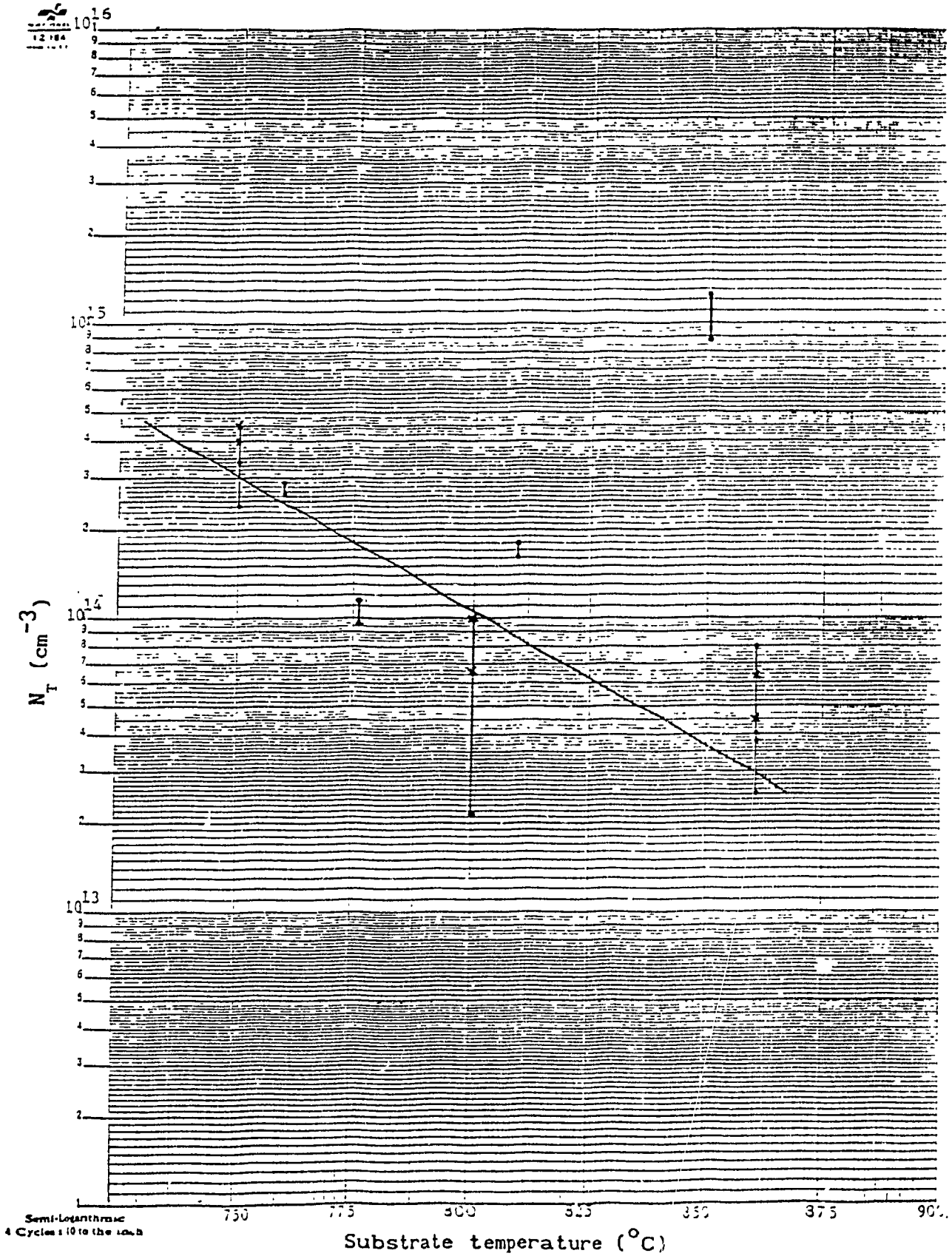


Fig. 5.21 Graph of $N_T$ (ELCS1) vs the substrate temp. (series R & B)

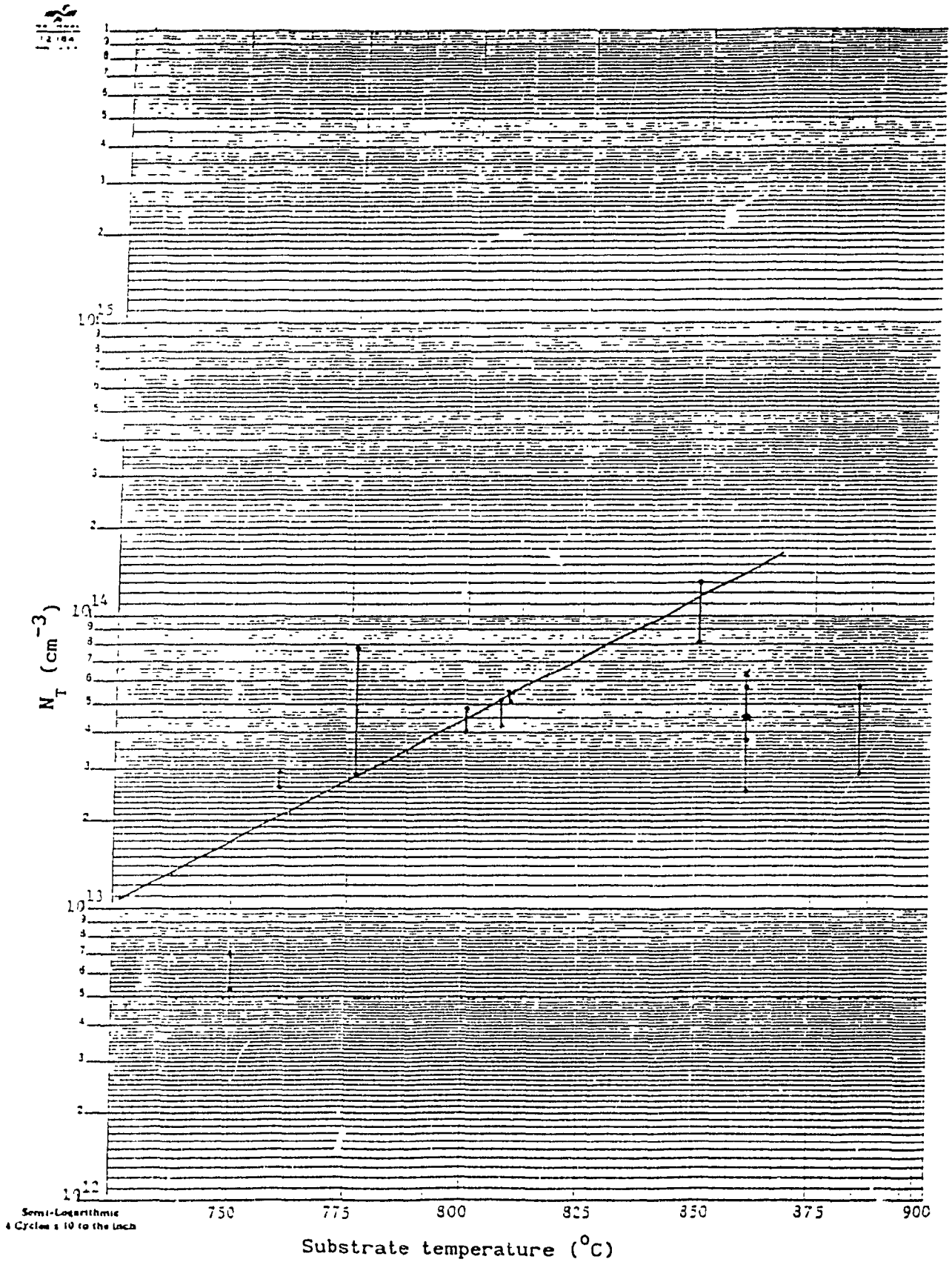


Fig. 5.22 Graph of $N_T$ (EL2) vs the substrate temp. (series R & B)

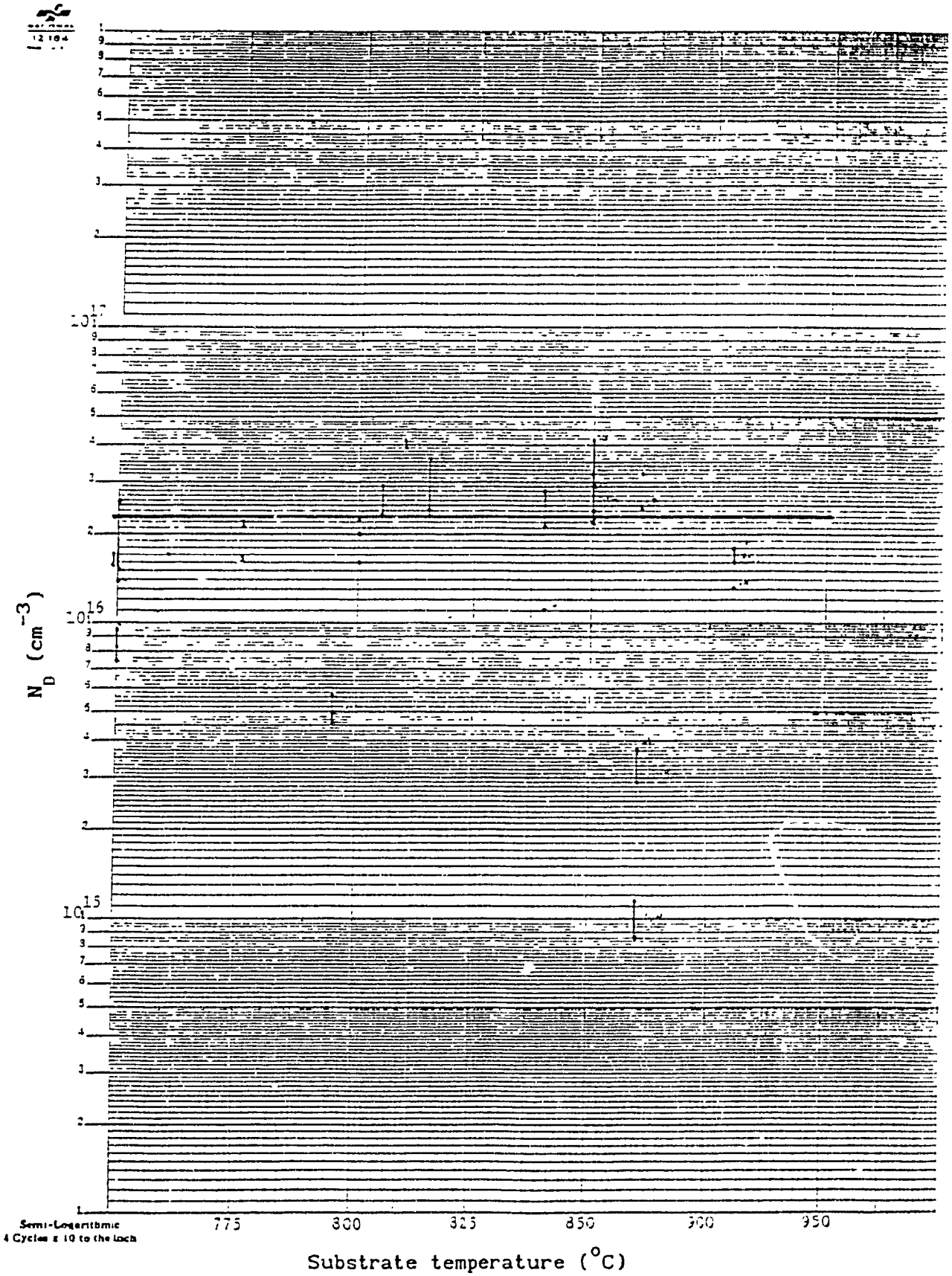


Fig. 5.23 Graph of $N_D$ vs the substrate temp. (series R & B)

5.5.1 Proposed model for EL2 deep donor trap

In order to investigate further the above observations, we discuss first the EL2 model proposed by references (87)(88) and (89), which suggests that EL2 is formed by a complex of gallium vacancies $V_{Ga}$ in As-rich conditions, and anti sites centers formed by the occupation of a gallium vacancy by an arsenic atom of GaAs host lattice leaving behind an arsenic vacancy $V_{As}$. This is represented in figure 5.24 (89). This figure shows the formation of the so called EL2 complex ($As_{Ga}$ + $V_{As}$). Other authors also agree with the origin of the EL2 complex (65)(90)(91)(92) . In figure 5.24a, the gallium vacancy $V_{Ga}$ is shown and in b the complex is represented after the migration of an As atom in $V_{Ga}$.

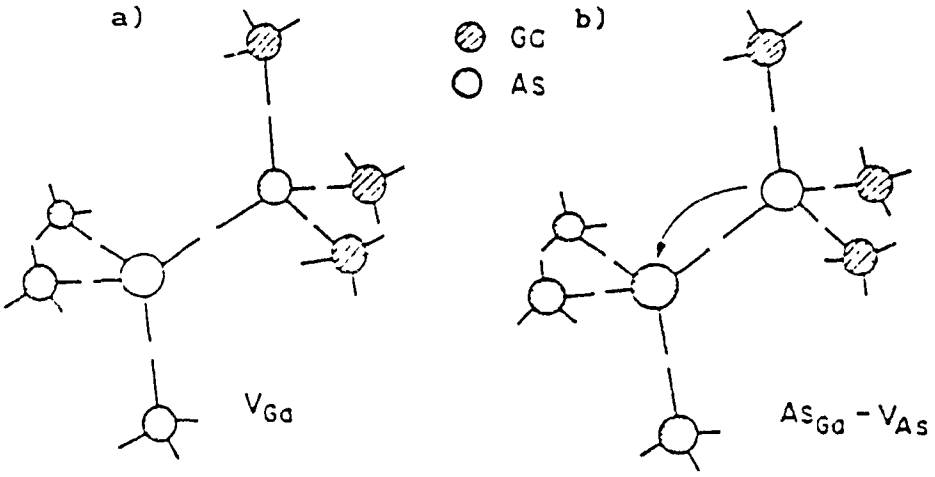


Fig. 5.24 Formation for EL2 complex

The EL2 complex is assumed to be a divalent deep lying donor center and a shallow monovalent donor level (87). This can be explained by the electronic configurations for atoms in the ground state and in the tetrahedral coordination system. For GaAs, the gallium has the configuration; Ga: $[Ar]3d^{10}4s^{2}4p^{1}$ meaning that there are three electrons in the 4s and 4p sub shells whereas arsenic has the

configuration; As: $[Ar]3d^{10}4s^{2}4p^{3}$ showing five electrons on the 4s and 4p sub shells (93). When one atom of Ga and one atom of As are brought together to form GaAs crystal, eight electrons are present on the 4s4p sub shells completing the octet, thus forming the semiconductor's predominantly covalent bonds. As shown in figure 5.25a, if a gallium is removed from its site, thus leaving a gallium vacancy $V_{Ga}$, $V_{Ga}$ will be surrounded by five electrons belonging to the four neighboring arsenic atoms. Now, as shown in figure 5.25b, if a neutral arsenic atom with its five valence electrons occupies the gallium to form an anti site complex, the result may be a site possessing ten electrons. Since eight electrons complete the octet for tetrahedral coordination, two free electrons are left in excess. These excess electrons are thus responsible for the origin of divalent deep trap lying EL2 donor center (87). Note that the arsenic vacancy $V_{As}$ left behind becomes a monovalent donor.

The energy of activation Ea of the EL2 complex has been suggested in the literature (65)(78) to be 25meV and 760meV for the shallow donor ($V_{As}$) and for the deep divalent donor anti site $As_{Ga}$ respectively.

In order to allow the presence of a general shallow donor of variable concentration, silicon doping is introduced during GaAs crystal growth (87). It has been shown previously that silicon (Si) is an amphoteric impurity in GaAs (94) but because of our stoichiometric conditions (As-rich condition), it is reasonable to assume that the silicon acts as a shallow donor on the gallium sub lattice $Si_{Ga}$ (94) (95). The presence of silicon as a shallow donor has an activation energy Ea equal to 0.002eV (21). Note here that Si can be introduced involuntary due to the presence of Si in the system, or purposely added

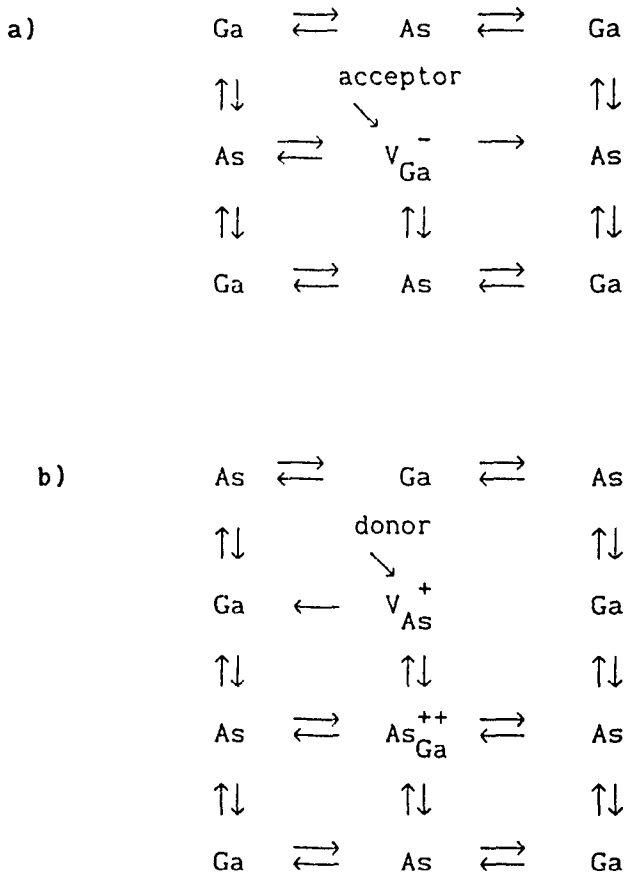


**Fig. 5.25 Representation of EL2 formation**
**a) Gallium vacancy**
**b) Arsenic vacancy and arsenic in site Gallium**

for adjustable concentrations.

Now, by varying the Si shallow donor concentration impurity in GaAs, the material may be considered as n-type, semi-insulating or semi-conducting (21)(S7) by compensation of the deep acceptor present in the GaAs crystal. This can be explained with the help of the diagram shown in figure 5.26.

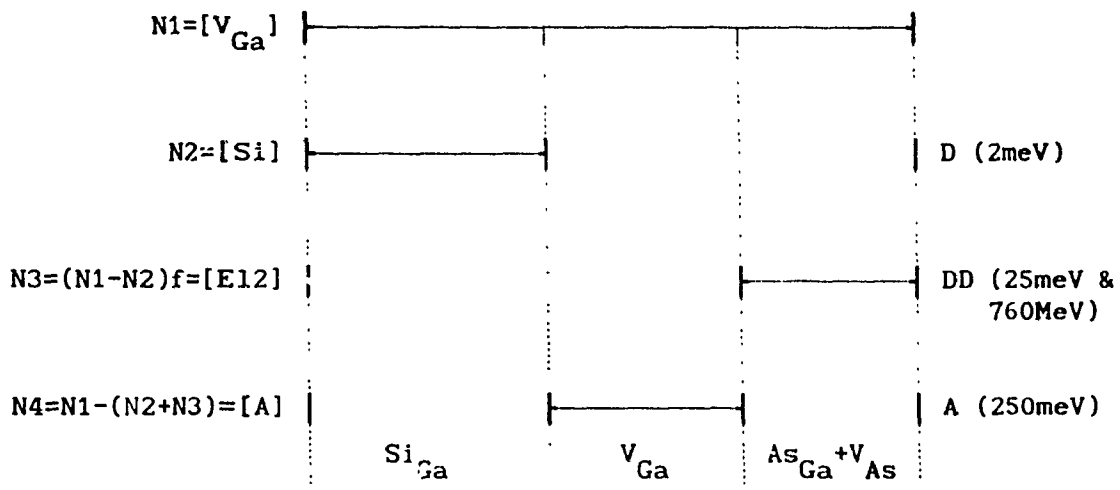


Fig 5.26 Diagram for compensation in GaAs crystal

The above figure suggests that N1 is the total concentration of Gallium vacancy $V_{Ga}$. The total $V_{Ga}$ concentration is due to the fact that the crystal is grown in As-rich conditions (off-stoichiometric condition: As/Ga ratio grater but close to one)[4]. For example, it has been shown previously that the existing phase extent in GaAs containing approximately 2.22 X $10^{22}$ atoms/$cm^{-3}$ (96), of the limiting composition of the arsenic-rich side of its $Ga_{49.999}$ $As_{50.001}$ (off-stoichiometry) correspond to N1=3 X $10^{17}$ atoms/$cm^{3}$ corresponding to a maximum $V_{Ga}$ (21) (87). Then, N2 is the concentration of Si shallow donor introduced in the crystal. N3 is the concentration of the EL2 in the crystal and is formed with the gallium vacancy concentration available (N1-N2) for the formation of anti sites ($As_{Ga}$) assuming that a fraction f of these unfilled gallium vacancies become occupied by arsenic atoms resulting in $V_{As}$. The fraction f was calculated with the thermodynamics

[4] Pure stoichiometry if As/Ga = 1

expressions found in references (5)(62) and (87), and was given as 0.15. Finally, N4 represents the concentration of gallium vacancy ($V_{Ga}$) which are left unoccupied by either silicon or arsenic atoms. Therefore, the deep acceptor concentration [A] available to compensate the donors present in As-rich GaAs crystal is given by N4.

With the help of the above figure, we can explain the behavior of EL2 by varying the stoichiometry with the temperature of a GaAs crystal during its growth or by doping it with Si. For instance, according to the above diagram, if we assume that the concentration of Si remains constant (N2 constant), and during the post growth of the crystal, the As/Ga ratio has increased, more gallium vacancies $V_{Ga}$ are formed. Since there is more $V_{Ga}$, more arsenic can take place in these, thus increasing the probability of an As in Ga site ($As_{Ga}$) with an arsenic vacancy $V_{As}$. Therefore, it follows for this case, that the EL2 deep donor trap in the bulk will increase in concentration since ($As_{Ga}$ + $V_{As}$) will increase in concentration.

Now, if we vary the concentration of silicon, it is possible to obtain a semi-isolating GaAs crystal. According to the diagram, by introducing Si as donor impurity, it will influenced the EL2 donor trap concentration. If both EL2 (N3) and Si (N2) as donors are in concentration near to the deep acceptor $V_{Ga}$ it will compensate to give an SI material (S7). The calculation of the Fermi level in order to show whether if it is n-type, SI-type or semi-conducting type where shown in references (62) and (S7) by using the Schottkly curves. Note here that the silicon concentration influences the EL2 concentration the following way: if more Si are introduced in the GaAs crystal, more gallium vacancies will probably be occupied by Si thus forming an anti

site $Si_{Ga}$. This phenomenon will possibly live less gallium vacancies $V_{Ga}$, there will be less $As_{Ga}$ for the formation of EL2 leading to its lower concentration (21)(87).

From our results obtained, we recall that in sample R16 for example, we were able to see the EL2 clearly after a DLTS scan. This is because the shallow donor concentration $N_D$ found was around 3 to 4 X $10^{15}$ $cm^{-3}$ compared to as 3 to 4 X $10^{16}cm^{-3}$ for the other samples. In most of the graphs shown before, we notice that the points plotted for sample R16 are obviously lower in concentration. These points are often apart from the others. It was shown by references (65) and (87) that for high concentration of shallow donor $N_D$, the EL2 is in very low concentration and for $N_D$ low, the EL2 concentration is seen to be higher which seems to agree with our results.

5.5.2 Application of the EL2 Model to CSVT epitaxial growth

By experimental evidences, the thermodynamic considerations indicate that the CSVT deposited epitaxial layers are normally As-rich since the partial vapor pressure of As containing species is higher than partial vapor pressure of $Ga_2O$ (5)(62)(87). Thus because of the arsenic rich condition, the EL2 originates from gallium vacancies $V_{Ga}$ in the crystal (65)(88). The theoretical solidus curves, calculated for simple atomic disorder, indicate an increasing phase extension (As/Ga ratio) with increasing temperature between about 770°C and 1130°C (97). It has been shown that the concentration of the EL2 trap increases with the increase As/Ga ratio in the vapor phase during the growth (65)(86)(97) for LEC, VPE and MOCVD experiments. This suggest that the evolution of EL2 concentration is function of the

off-stoichiometry variation with the deposition temperature as was shown in figure 5.22 with our CSVT system.

In order to analyze further the results obtained above, we have plot the theoretical EL2 concentration (N3) as function of the off-stoichiometry induced gallium vacancy density (N1) by using N3= (N1-N2)f described from the diagram of figure 5.26. The result is shown in figure 5.27. Here we have assumed the silicon concentration constant (N2 = 5.8 X $10^{16}cm^{-3}$) for undoped layers based on previous results (5)(62) and the fraction f of available gallium vacancies contributing to the formation of the EL2 complex was assumed to be 0.0015. The value of f was equal to 0.15 originally from previous results (21)(27), but was decreased to 0.0015 since in the case of vapor phase growth at about 700°C in contrast to melt growth at 1238°C, the EL2 concentrations exhibit a 2 to 3 order magnitude decrease (86). Thus, by varying the off-stoichiometry induced gallium vacancy concentration (N1) from 6 x $10^{16}$ to 1.1 X $10^{17}cm^{-3}$, we find that figure 5.27 is comparable to the DLTS measured EL2 concentrations as function of the deposition temperature in figure 5.22 (64). Figure 5.22 has been replotted with the same scale as in figure 5.27. This can be seen in figure 5.28. The comparison is now obvious between figures 5.27 and 5.28.

The origin of the decrease of the EL2 concentrations for temperature above 850°C in figure 5.22 is still unknown. However, it might be related to a surface decomposition of the epitaxial layer during the growth at these elevated temperatures.

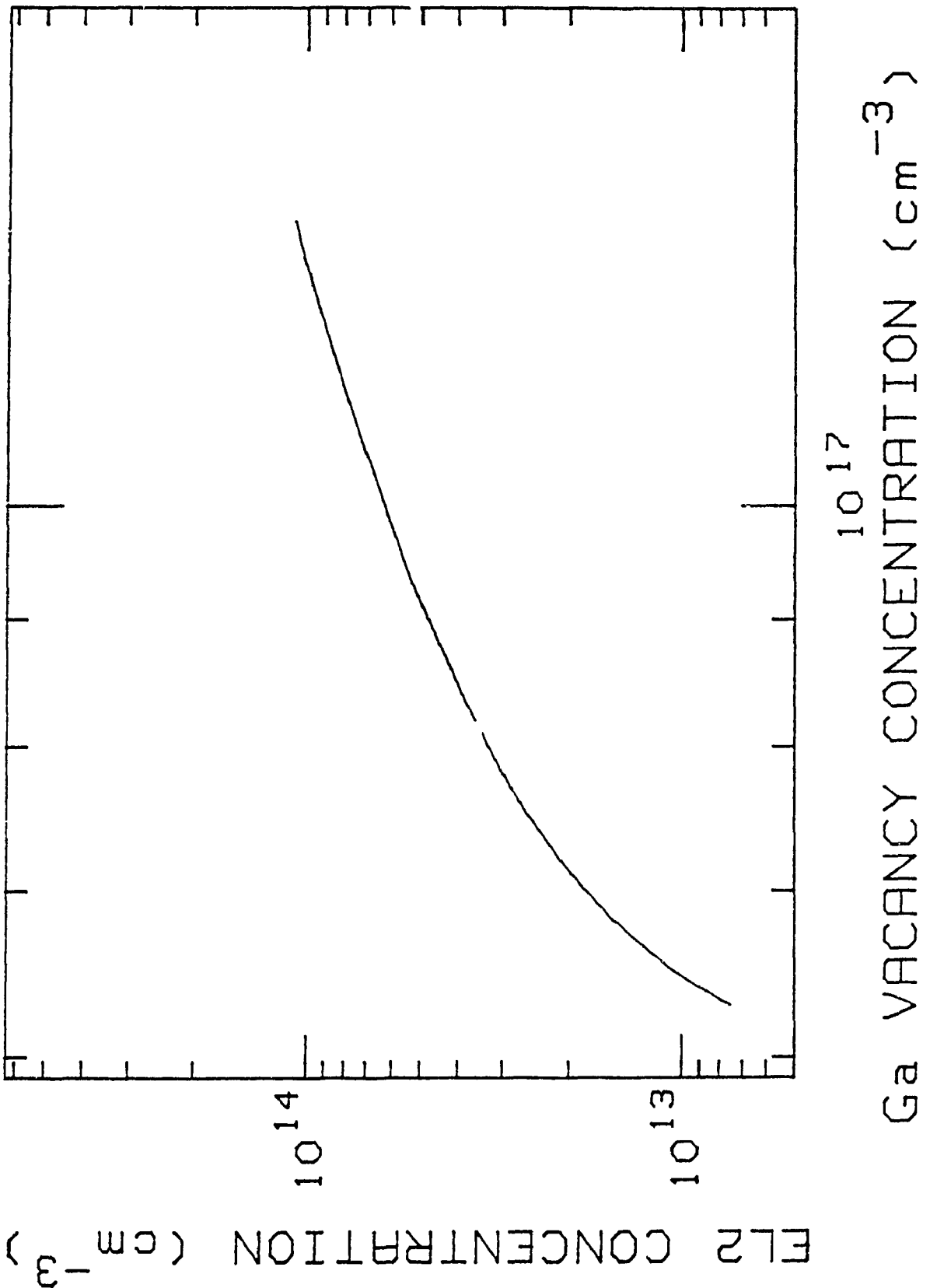


Fig. 5.27 $N_T$ (EL2) vs $V_{Ga}$ concentration

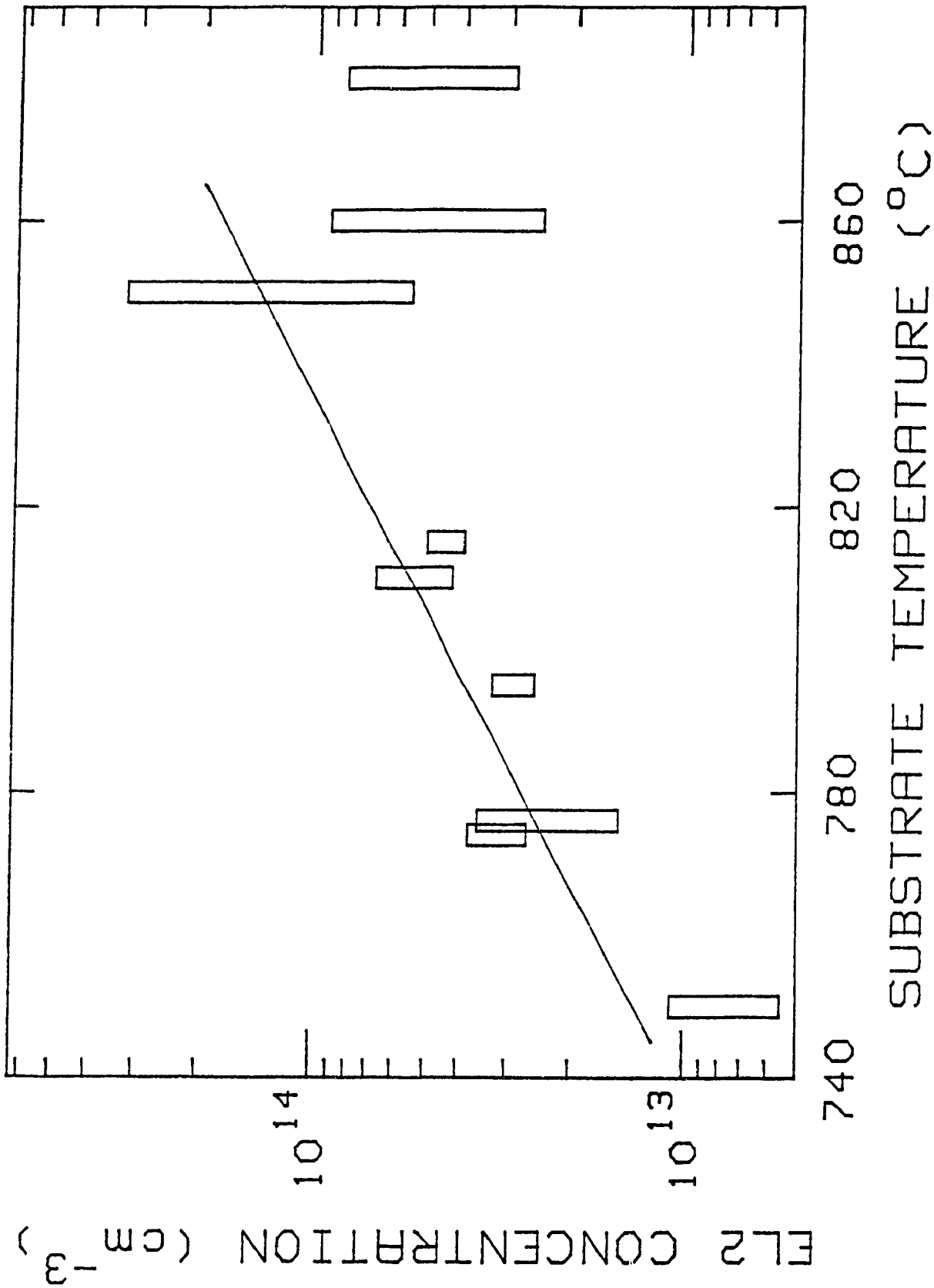


Fig. 5.28 $N_T$ (EL2) vs substrate temperature

5.5.3 The 300K trap ELCS1

As shown in figures 5.18 to 5.20 , we have observed that the ELCS1 trap is not characteristic to the bulk; this trap was shown near the surface only. The source and substrate used were both SI wafers. While reference (79) suggested that ELCS1 trap is a bulk defect[5] we have shown that the ELCS1 traps in GaAs samples grown by CSVT were seen near the surface only (64). After chemical etching of a few μm in depth from the surface, the ELCS1 (300K) trap has a tendency to vanish while EL2 remain constant throughout the bulk. These 300K levels have been found mainly in wafer submitted to a half and hour heat treatment in the reactor after epitaxial layer growth. As a result the surface structure of these layers might be altered (66). These can be due to out diffusion of impurities or arsenic itself. Therefore, these responsible decompositions of these effect surface layers might be responsible for the 300K (ELCS1) peak.

[5] The samples analyzed in reference (79) were fabricated using the CSVT set-up at Concordia University in Montreal.

# 6.0 CONCLUSIONS

This report has shown a thorough analysis on the DLTS method for the characterization of deep level traps in GaAs epitaxial layers grown by CSVT. The basic definitions on GaAs crystalline structure were given as an introduction to the other chapters. Then the derivation of capacitance-voltage characteristics of a Schottky barrier was given in order to find the shallow donor concentration $N_D$. Furthermore, the DLTS method required the capacitance of a diode under reverse bias for the measurement of deep level traps.

The current-voltage characteristics of a Schottky barrier was given also because of the importance for finding the ideality factor and the barrier height. These two parameters were important to identify since they indicated if the diode can operate properly. The ideality factor n between 1 and 1.1 indicated the thermionic current over the barrier and the barrier height $\phi_b$ greater than 8.2eV allowed to see the EL2 trap level with confidence.

For a thorough understanding of the DLTS method, the general equation of occupation of defect state was given in order to understand Schottky barriers taking deep levels into account. Thus the capacitance transient using a Schottky barrier was derived. This allowed one to the explanation of the DLTS measurements leading to the so called DLTS peaks. This was applied in practice using a capacitance meter, a multi meter and a pulse generator all controlled by the HP-300 computer. Then, once the DLTS peaks were found, the activation energy Ea was determined with the Arrhenius plot $\ln(\tau_n T^2)$ as function of $1000/T$.

Therefore, the experimental procedure to find all parameters by using the DLTS method required first to find the shallow donor concentration $N_D$ by the C(V) method. Then the DLTS peaks were found according to the DLTS measurement procedures. From those peaks, the energies of activation were found. Then the trap concentration $N_T$ was found after the transition region region $\lambda$ was determined and the widths $W_0$ and $W_1$ that were easily calculated from simple formulas derived in the text.

The above analysis allowed the determination of the shallow donor concentration $N_D$ and the barrier height $\phi_b$ of Schottky barriers in order to find the activation energy Ea and the carrier concentration $N_T$ of deep level traps for several samples under investigation.

It has been observed first that the shallow donor concentration $N_D$ was found sometimes with and approximate 30% errordue to the surface area of the metal junction of a Schottky barrier and the choice of the points for the linear fit for the slope of $1/C(V)^2$. These errors were taken into account during our experiments. Then $\phi_b$ and n were found. $\phi_b$ was found experimentally to be greater than 0.75eV in all the samples for a proper measurement of EL2. n was also found in the limit required. The values of Vb found with the C(V) measurement and $\phi_b$ used with the I(V) measurement were compared by multiplying the latter by n. An average 10% error was found. The equipment used for the measurement of $N_D$ and $\phi_b$ were discussed and were found to be accurate according to the manufacturer when properly calibrated periodically.

The activation energy Ea was determined on several samples. A peak at 300K and a peak at 335K labeled ELCS1 and EL2 respectively for the same emission rate ($\tau_n$=0.391) were found in all samples to be

0.73eV for ELCS1 and 0.8eV for EL2 to which both agree with the literature. These peaks were found when the source was SI whether the substrate was SI or Si-doped. When the source was Si-doped, other peaks with other energies of activation were observed. The probable causes of error in finding Ea was discussed. It has been found that 1% of error in the temperature could be induced due to the platinum resistance. Another cause of error in temperature could be caused by an unconstant increase in the thermal velocity for warming up the cryostat. For a proper measurement of the DLTS peak, the thermal speed was set up at a constant $\Delta T$ equal to 1.5K/min.

Finally, the EL2 and ELCS1 traps were analyzed in GaAs epitaxial layers grown by CSVT. It has been shown that the evolution of EL2 concentration was function of the possible off stoichiometry variation with the deposition temperature according to the proposed model discussed. It has been shown also that EL2 is constant throughout the bulk. Then it has been found that ELCS1 was a trap found near the surface of the epitaxial layers grown by CSVT.

## REFERENCES


1. Karp, S., and S. Roosild, "DARPA, SDI and GaAs", Computer, October 1986, pp. 17-19.

2. Cooper, J.A. Jr.,"Limitation On The Performance of Field-Effect Devices For Logic Amplifications", Proceedings of the IEEE, Vol. 69, No. 2, February 1981, pp.226-231.

3. Lang, S.I., B.M. Welch, R. Szucca, P.M. Asbeck, C-P. Lee, C.G. Kirkpatrick, F.S. Lee, G.R. Kaelin, and R.C. Eden, "High speed GaAs Integrater Circuits", Proceedings of the IEEE, Vol. 70, No. 1, January 1982, pp.35-45.

4. Hirayama, M., M. Togoshi, N. Kato, M. Suzuki, Y. Matsuoka and, Y. Kawasaki, "A GaAs 16-Kbit Static RAM Using Dislocation-Free Crystal" Transaction of Electro Devices, Vol. ED-33, No. 1, January 1986, pp. 104-110.

5. Côté, D., J.P. Drolet, B.A. Lombos, J.I. Dickson, "Epitaxy Of GaAs By The Close-Spaced Vapor Transport Technique",Journal of Electrochemical Society: Solid State Science and Technology, Vol. 133, No. 9, September 1986, pp. 1925-1934.

6. Lang, D.V., "Deep-Level Transient Spectroscopy: A New Method To Characterize Traps In Semiconductors", Journal of Applied Phisics, Vol. 45, No. 7, July 1974, pp. 3023-3032.

7. Streetman, B.G., Solid Stade Electronic Devices 2nd ed., (New Jersy: Prentice Hall Inc., 1980), P.3.

8. Sze, S.M., Physics of Semiconductors Devices 2nd ed., (New York: John Wiley & Sons Ltd., 1981), pp.8-9.

9. Leonard,W.F., and T.L. Martin, Electronic Structure And Transport Properties of Crystals, (New York: Robert E. Krieger Publishing Co., 1980), p.289.

10. Bube, R.H., Electronic Properties Of Crystalline Solids, (New York: Academic Press, 1974), pp. 305-306.

11. Lanno, M., and J. Bourgoin, Point Defect In Semiconductors I, (New York: Springer Series in Solid-State Science, Vol. 22,1981), p. 1.

12. Schneider, J. "The Role Of Point Defect In GaAs", Semi-Insulating III-V Materials Evian 1982, pp. 144-153.

13. Lanno, p. 2.

14. Leonard, p. 290.

15 Murr, L.E., Solid State Electronics, (New York: Marcel Dekker, Inc., 1978), pp. 78-80.

16. Grimmeiss, H.G., "Deep-Level Impurities In Semiconductors", Annual Review Material Science, 1977, pp. 341-376.

17. Miller, G.L., D.V. Lang, and L.C. Kimberling, "Capacitance Transient Spectroscopy", Annual Review Material Science, 1977, pp. 377-448.

18. Streetman, pp. 28-49.

19. Sze, p. 21.

20. Vapaille, A., and A Castagné, Dispositif Et Circuit Integres Semiconducteurs, (Paris: Dunod, 1987), p. 15.

21. Lombos B.A., N. Yemenidjian, and M. Averous, "Compensation by Deep-Levels In Semi-Insulating GaAs", Canadian Journal of Physics, Vol. 60, No. 1, 1982, pp. 35-40.

22. Ma, Q.Y., M.T. Schmidt, X. Wu, H.L. Evans, and E.S. Yang, "Effect Of Schottky Barriers Height On EL2 Measurement By Deep-Level Transient Spectroscopy", Journal of Applied Phisics, Vol. 64, No. 5, September 1988, pp. 2469-2472.

23. Sharma, B.L., Metal-Semiconductor Schottky Barrier Junction And Their Applications, (New York: Plenum Press, 1984), pp. 46-48.

24. Sze, p. 300.

25. Sze, pp. 805-806.

26. Sharma, pp. 3-6.

27. Sze, pp. 246-249.

28. Sharma, p. 31.

29. Sharma, p. 34.

30. Sharma, p. 20.

31. Burden, R.L., et al, Numerical Analysis, (Boston: Prindle Weber & Schmidt, 1981), pp. 320-323.

32. Nguyen, P.H., B. Lepley, A. Nadeau, and S. Ravelet, "Computer Techniques For Solving Metal-Semiconductor Barrier Height", Proceedings of the IEEE, Vol. 122, No. 11, November 1975, pp. 1192-1199.

33. Streetman p. 190.

34. Sharma, pp. 6-8.

35. Sharma, pp. 27-29.

36. Streetman, pp. 142-147.

37. Sharma, p. 199.

38. Srivastava, A.K., B.M. Arora, and S. Guha, "Measurement or Richardson Constant Of GaAs Schottky Barriers", Solid State Electronics Vol. 24, pp. 185-191.

39. Sharma, pp. 16-17.

40. Sze, pp. 250-254.

41. Bourit, C., J.C. Georges and, S. Ravelet, "Computer Technique For Solving Schottky Barrier From Dark Foward Current-Voltage Characteristics", IEE Proceedings, Vol. 127 Pt, I, No. 5, October 1980, pp. 250-253.

42. Sze, p. 279.

43. Sharma, pp. 21-22

44. Sze, pp. 304-307.

45. D'Asaro, l.A., S. Nakahara, and Y. Okinaka, "Electroless Gold Plating On III-V Compound Crystals", Journal of Electrochemical Society: Electrochemical Science and Technology, Vol. 127, No. 9, September 1980, pp. 1935-1941.

46. Bourgoin, J., M. Lanno, Point Defects In Semiconductors II, (New York: Springer Series in Solid-State Science, Vol. 35,1983), pp. 155-169.

47. Sah, C.T., R.N. Noyce, and W. Shockley, "Carrier Generation And Recombination In p-n Junction Characteristics", Proceedings of the IRE, Vol. 45, 1957, pp. 1228-1243.

48. Sze, p. 36.

49. Bourgoin, p. 158.

50. Bois, D., Deep Level and Optical Spectroscopy in "Electronic Structure of Crystal Defects and Disordered System" Aussois Sept. 1980 (Paris: Les editions de Physique, 1981), pp. 337-440.

51. Bourgoin, p. 155.

52. Bourgoin, pp. 163-164.

53. Bourgoin, p. 157.

54. Blackmore, J.S., and S. Rahimi, Semiconductors And Semimetals Semi-insolating GaAs, (New York: Academic Press Inc., Vol. 20, 1984), pp. 294-296.

55. Bourgoin, pp. 159-162.

56. Bourgoin, p. 168.

57. Streetman, pp. 75-77.

58. Bourgoin, pp. 164-167.

59. Weast, R., et al.,CRC Handbook Of Chemistry And Physics 65th ed.,(Florida: CRC Press, Inc., 1984-1985), p. A-84.

60. Bourgoin, pp. 177-181.

61. HP. 4280A 1MHz C-Meter/C-V Plotter, Operating And Service Manual, (Tokyo: Hewlett-Packard, Ltd., 1983)

62. Lombos, B.A, D. Côté, J.P. Dodelet, M.F. Lawrence, and J.I. Dickson, "Thermodynamic Equilibrium Displacement Controlled Epitaxial Growth of GaAs", Journal of Crystal Growth, Vol.79, 1986, pp. 455-462.

63. Pauw van der, L.J., "A Method Of Measuring Specific Resistivity and Hall Effect Of Discs Of Arbitrary Shape", Phillips Research Reports, Vol. 13, No. 1, February 1958, pp. 1-9.

64. Lombos, B.A., T. Bretagnon, A. Jean, R. Le Van Mao, S. Bourassa, and J.P. Dodelet, "EL2 Trends In As-Rich GaAs Grown By Close-Space Vapor Transport", Journal of Applied Physics, Vol 67, No. 4, February 1990, pp. 1879-1883.

65. Lagoski, J., H.C. Gatos, J.m. Parsey, K. Wada, M. Kaminska, and W. Walukiewicz, "Origin Of The 0.82-eV Electron Trap In GaAs And Its annihilation by Shallow donors", Applied Physics Letters, Vol. 40, No. 4, February 1982, pp. 342-344.

66. Chichibu, S , N. Ohkubo, and S. Matasumoto, "Effects Of Controlled As Pressure Annealing On Deep Levels Of Liquid-Encapsulated Czchralski GaAs Single Crystal", Journal of Applied Physics, Vol. 64, No. 8, October 1988, pp. 3987-3993.

67. Blight, S.R., R.E. Nicholls, S.P.S. Shangha, P.B. Kirby, L. Teale, S.P. Hiscock and C.p. Stewart, "Automated Hall Profiling System For Characterization Of Semiconductors At Room And Liquid Nitrogen Temperatures", IOP Puplishing Limited, 1988, pp. 470-479.

68. Koskiade,E., E.Verney, J.P. Dodelet, M.F. Lawrence, B.A. Lombos and R. Philippe, "Charge Density Profiles Of Closed Spaced Vapor Transport GaAs Epitaxial Layers", Journal of Electrochemical Society: Solid-State Science and Technology, Vol. 135, No. 10, October 1988, pp. 2634-2640.

69. Koskiahde,E., D. Cossement, R. Paynter, J.P. Dodelet, A. Jean, and B.A. Lombos, "Doping Of GaAs Epitaxial Layers Grown On (100) GaAs By Close-Spaced Vapor Transport", Canadian Journal of Physics, Vol. 67, 1989, pp. 251-257.

70. Talysurf 4, Operator's Handbook, (Rank Precision Industries Ltd.).

71. Goodman, A.M., "Metal-Semiconductor Barrier Height Measurement By The Differential Capacitance Method-One Carrier System", Journal of Applied Phisics, Vol. 34, No. 2, February 1963, pp. 329-338.

72. HP. 4280A 1MHz C-Meter/C-V Plotter, pp. 1-1, 1-2.

73. HP. 4280A 1MHz C-Meter/C-V Plotter, pp. 3-34, 3-35.

74. HP. 4280A 1MHz C-Meter/C-V Plotter, p. 4-15

75. Martin, G.M., A, Mitoneau, A. Mircea, "Electron Traps In Bulk And Epitaxial GaAs Crystals", Electrinics Letters, Vol. 13, No. 7, March 1977, pp. 191-192.

76. Walpole, R.E., and R.H. Myers, Probability And Statistics For Engineers And Scientists 2nd ed., (New York: Macmillan Publishing Co. Inc., 1978), pp.161 & 165.

77. Sze, p. 849.

78. Walukiewicz, W., J. Lagowski, and H.C. Gatos, "Shallow Donor Associated With The Main Eiectron Trap (EL2) In Melt-Grown GaAs", Applied Physics Letters, Vol. 43, No. 1, July 1983, pp. 112-114.

79. Massé, G., M.F. Lawrence, and J.M. Lacroix, "Dominant Donor Trap In n-Type Epitaxial GaAs Grown By CSVT", Journal of Physics Chemical Solids, Vol. 49, No. 11, 1988, pp. 1349-1353.

80. Massé, G., J.M. Lacroix, and M.F. Lawrence, "Deep-Level Transient Spectroscopy Study Of n-Type GaAs Epitaxial Layers Grown By Close-Spaced Vapor Transport", Journal of Applied Physics, Vol. 65., February 1989, pp. 1126-1129.

81. Sedra, A.S., and K.C. Smith, Micro-Electronics Circuits, (New York: CBS College Publishing, 1982), pp. 74-75.

82. HP. 3455A Digital Voltmeter, Operating And Service Manual, (Colorado: Hewlett-Packard Company, 1976), pp. 1-1 & 1-2.

83. Hasegawa, F., M. Onomura, C. Mogi, and Y. Nannichi, "Reduction Of Schottky Barrier Heights By Surface Oxidation Of GaAs And Its Influence On DLTS Signals For The Midgap Level EL2", Solid State Electronics Vol. 31., No. 2, 1988, pp. 223-228.

84. Tyagi, M.S., and S.N. Arora, "Metal Zinc Selenide Schottky Barriers", Physics State Solid, Vol. 32, 1975, pp. 165-172.

85. Hackman, R., and P. Hanop, "Temperature Dependence Of The Schottky Barrier Height In Gallium Arsenide", Solid State Communication Vol. 11, 1972, pp. 669-672.

86. Gatos, H.C., and J. Lagowski, "EL2 And Related Defects In GaAs --Challanges And Pitfalls", Material Research Society, Vol. 46, 1985, pp. 153-167.

87. Lombos, B.A., M.F. Lawrence, J.P. Dodelet, D. Côté, and M. Averous, "Vacancy Doping Of GaAs", Physics State Solid, Vol. 96, 1986, pp. 663-674.

88. Lagowski, J., M. Kaminska, J.M. Parsey, H.C. Gatos and, W. Walukiewicz, "Microscopic Model Of The EL2 Level In GaAs", Institute Physics Comference Series, No. 65: Chapter 1, 1982, pp. 41-48.

89. Baraff, G.A., and M. Schulter, "Bistability And Metostability Of Vga In GaAs", Proc. ICDS 14: Material Science Forum, Vol. 10-12, 1986, pp. 293-298.

90. Miller, M.D., G.H. Olsen, and M. Ettenberg, "The Effect Of GaAs-Phase Stoichiometry On Deep Levels In Vapor-Grown GaAs", Applied Physics Letters, Vol. 31, No. 8, October 1977, pp. 538-540.

91. Fang, Z.Q., T.E. Schlesinger, and A.G. Milnes, "Evidence For EL6 (Ec - 0.35eV) Acting As A Dominant Recombination Center In n-Type Horizontal Bridgman GaAs", Journal of Applied Physics, Vol. 61, No. 11, June 1987, pp. 5047-5050.

92. Cho, H.Y., E. Kyu, and S.K. Min, " A Relation Between EL2 (Ec - 0.81eV) And EL6 (Ec - 0.35eV) In Annealed HB-GaAs By Hydrogen Plasma Exposure", Journal of Applied Physics, Vol. 66, No. 7, October 1989, pp. 3038-3041.

93. Streetman, pp. 48-49.

94. Teramoto, I., "Calculation Of Distribution Equilibrium Of Amphoteric Silicon In Gallium Arsenide", Journal of Chemical Solids, Vol. 33, 1972, pp. 2089-2099.

95. Hurle, D.T.J., "The Site Distribution Of Amphoteric Dopants In Multiply-Doped GaAs", Journal of Crystal Growth, Vol. 50, 1980, pp. 638-643.

96. Streetman, p. 10.

97. Lagowski, J., and H.C. Gatos, "Nonstoichiometric Defects In GaAs And The EL2 Band", 13th International Conference in Semiconductors Proceedings, (Publication of the Metallurgical Soc. of AIME, 1984), pp. 73-85.

## Appendix I: List of Symbols and Results for all Samples

### I.1 List of symbols

A : Arbitrary constant

$A^*$ : Rickardson constant ($Acm^{-2}K^{-2}$)

As : Arsenide atom

$As_{Ga}$ : Arsenide in gallium site

$\alpha$ : Arbitrary constant

$\beta$ : Arbitrary constant

C : Capacitance (F)

**C** : Arbitrary constant

Cj : Junction capacitance of the diode (F)

$C_n$ : Coefficient capture for electrons ($cm^3/s$)

$C_p$ : Coefficient capture for holes ($cm^3/s$)

C(t) : Capacitance as function of time

C(V) : Capacitance-Voltage measurement method

CB : Conduction band

D : Diameter (cm)

DLTS : Deep Level Transient Spectroscopy

$\Delta C/C$ : Normalize value of C(t)

$\Delta\phi_b$ : Variation in $\phi_b$ due to image force lowering (eV)

$\Delta H_n$ : Enthalpy

$\Delta S_n$ : Entropy

$\Delta t$ : Pulse width (sec.)

Ea : Apparent activation energy (eV)

$E_D$ : Gibbs free energy of transition (eV)

Ec : Energy level at the conduction band (eV)

Ei : Ionization energy level (eV)

Efs : Fermi level (SC) (eV)

Eg : Band gap (eV)

ET : Energy level of a trap (eV)

Ev : Energy level at the valence band (eV)

eV : Electron volt

$e_n$ : Emission rate for electron ($sec^{-1}$)

%er : Percentage of error between Vb and $n^*\phi b$

$e_p$ : Emission rate for hole ($sec^{-1}$)

$\epsilon s$ : Semiconductor permitivity (F/cm)

$\varepsilon(x)$ : Electric field at any point x in the SC (V/cm)

$\phi b$ : Barrier height determined by the I(V) measurement (eV)

$\phi m$ : Work function of the metal (eV)

$\phi n$ : Energy difference between Ec and Efs (ev)

$\phi s$ : Work function of the semiconductor (eV)

G : Conductance ($1/\Omega$)

Ga : Gallium

Gsh : Conductance shunt ($1/\Omega$)

$g^*$ : Degenerency factor

I : Current (A)

Imes : Current flowing out of the non-ideal diode (A)

Itheo : Current flowing out of the ideal diode (A)

I(V) : Current-voltage measurement method

Io : Reverse saturation current (A)

Js : Reverse saturation current density ($A/cm^2$)

K : Kelvin (K)

k : Boltzmann constant (J/K)

Kn : Capture rate for electron ($Ccm^3/s$)

$K_p$ : Capture rate for hole

$\lambda$ : Transition region (cm)

$m_n^*$ : Electron mass effective (kg)

$m_p^*$ : Hole mass effective

$\mu_n$ : Electron moblity ($cm^2/V\text{-}s$)

$\mu_p$ : Hole mobility

$N_A$ : Shallow acceptor impurity density ($cm^{-3}$)

Nc : Effective density of states in conduction band ($cm^{-3}$)

$N_D$ : Shallow donor impurity density ($cm^{-3}$)

$N_{DH}$ : Shallow donor impurity density found by Hall measurement ($cm^{-3}$)

$N_T$ : Deep level trap concentration ($cm^{-3}$)

Nv : Effective density of states in the valence band ($cm^{-3}$)

n : Ideality factor

*n* : Concentration of electrons in the conduction band ($cm^{-3}$)

$n_T(t)$ : Fraction of $N_T$ ($cm^{-3}$)

$n_{T_f}(t)$: Fraction of $N_T$ for trap filling ($cm^{-3}$)

$n_{T_e}(t)$: Fraction of $N_T$ for trap emptying ($cm^{-3}$)

q : Magnitude of electronic charge (C)

R : Resistance ($\Omega$)

Rs : Series resistance ($\Omega$)

Rsh : Shunt resistance ($\Omega$)

S : Junction area ($cm^2$)

SC : Semiconductor

Si : Silicon atom

SKB : Schottky barrier

$S(T_M)$ : Maximum height of the exprimental DLTS peak

$\sigma_n$ : Capture cross section for electron ($cm^2$)

$\sigma_p$ : Capture cross section for hole

T : Temperature (K)

$T_M$ : Maximum temperature (K)

Tsub : Substrate temperature (K)

t : Time (second)

$t_n$ : Rate window (second)

V : External voltage applied (V)

$V_{As}$ : Arsenic vacancy

Vb : Barrier height determined by the C(V) measurement method (eV)

Vi : Contact potential (eV)

$V_{Ga}$ : Gallium vacancy

Vmes : Measured voltage at the non-ideal diode (V)

Vtheo : Voltage of the ideal diode (V)

$\langle V_{thn} \rangle$: Average thermal velocity of an electron (cm/s)

$\langle V_{thp} \rangle$: Average thermal velocity of a hole

W : Space charge region width at voltage V applied (cm)

Wo : Space charge region width at voltage Vo applied

Ω : Ohm (Ω)

X.2 Results for all samples

The results of our experimental data are given in the followng table. In the table, "Tsubs" represents the substrate temperature during the epitaxial layer growth for a particular sample. Then the epitaxial layer thickness, the free carrier concentration ($N_D$H) and the mobility ($\mu$) are given. Both $N_D$H and $\mu$ were found from the Hall effect measurements. Thus from the table, we can find in each column:

Ea: The apparent activation energy (eV)

$W_0$: Depth from the junction corresponding to the bias voltage $V_0$ ($\mu$m)

$W_1$: Depth from the junction corresponding to the bias voltage $V_1$ ($\mu$m)

Rs: The series resistance ($\Omega$)

Rsh: The shunt resistance (1*E6) ($\Omega$)

Js: The reverse saturation current (1*E-9) ($A/cm^2$)

$N_T$: Deep level trap concentration (1*E14) ($cm^{-3}$)

$N_D$: Concentration of shallow donor (1*E15) ($cm^{-3}$)

n: The ideality factor

$\phi_b$: Barrier height determined by I(V) measurement (eV)

$V_b$: Barrier height determined by C(V) measurement (eV)

%er: Percentage of error between $V_b$ and $n*\phi_b$.

TABLE I.1: Results for all samples studied

| Ea | $W_0$ | $W_1$ | Rs | Rsh | Js | $N_T$ | $N_D$ | $V_0$ | $V_1$ | n | $\phi_b$ | $V_b$ | %err |
|---|---|---|---|---|---|---|---|---|---|---|---|---|---|
| eV | μm | μm | Ω | Ω | $A/cm^2$ | $at/cm^3$ | $at/cm^3$ | Volt | Volt | | eV | eV | $V_b$ & |
| | | | | E6 | E-9 | E14 | E15 | | | | | | $n*\phi_b$ |
| Sample D369 | | | Tsubs = 820.0 °C | | | | | | | | | | |
| Thickness = 8.0 μm | | | :$N_D$H = | | | at/$cm^3$ | | :μ = | | $cm^2$/V-s | | | |
| .52 | 0.416 | 0.269 | 5.43 | 3.95 | 69.8 | 05.59 | 13.30 | -.75 | 0 | 1.008 | 0.792 | 0.860 | 07.7 |
| .72 | 0.416 | 0.269 | | | | 13.10 | 13.30 | -.75 | 0 | | | | |
| .24 | 0.925 | 0.583 | | | | 07.72 | 13.30 | -7 | -2 | | | | |
| .33 | 0.925 | 0.583 | | | | 08.71 | 13.30 | -7 | -2 | | | | |
| .39 | 0.925 | 0.583 | | | | 07.78 | 13.30 | -7 | -2 | | | | |
| .52 | 0.925 | 0.583 | | | | 03.37 | 13.30 | -7 | -2 | | | | |
| .72 | 0.925 | 0.583 | | | | 18.60 | 13.30 | -7 | -2 | | | | |
| .24 | 1.416 | 1.225 | 9.96 | 13.4 | 0.54 | 09.46 | 23.50 | -2 | -0 | 1.032 | 0.790 | 0.850 | 04.3 |
| .33 | 1.416 | 1.225 | | | | 10.50 | 23.50 | -2 | -0 | | | | |
| .39 | 1.416 | 1.225 | | | | 09.71 | 23.50 | -2 | -0 | | | | |
| .52 | 1.416 | 1.225 | | | | 04.66 | 23.50 | -2 | -0 | | | | |
| .72 | 1.416 | 1.225 | | | | 17.80 | 23.50 | -2 | -0 | | | | |
| .24 | 1.557 | 1.416 | 8.25 | 2.82 | 37.2 | 09.97 | 25.90 | -5 | -2 | 1.006 | 0.793 | 0.990 | 24.1 |
| .33 | 1.557 | 1.416 | | | | 10.70 | 25.90 | -5 | -2 | | | | |
| .39 | 1.557 | 1.416 | | | | 09.84 | 25.90 | -5 | -2 | | | | |
| .52 | 1.557 | 1.416 | | | | 04.85 | 25.90 | -5 | -2 | | | | |
| .72 | 1.557 | 1.416 | | | | 15.37 | 25.90 | -5 | -2 | | | | |

TABLE I.1 (Continued)

| Ea | $W_0$ | $W_1$ | Rs | Rsh | Js | $N_T$ | $N_D$ | $V_O$ | $V_1$ | n | $\phi_b$ | $V_b$ | %err |
|---|---|---|---|---|---|---|---|---|---|---|---|---|---|
| eV | μm | μm | Ω | Ω | $A/cm^2$ | $at/cm^3$ | $at/cm^3$ | Volt | Volt | | eV | eV | V & $n*\phi_b$ |
| | | | | E6 | E-9 | E14 | E15 | | | | | | |
| Sample D371_1 | | | | Tsubs = 810.0 °C | | | | 1 etch of 1μm | | | | | |
| Thickness = 8.1 μm | | | | : $N_DH$ = | | | at/$cm^3$ | | : μ = | | $cm^2$/V-s | | |
| .24 | 1.308 | 1.167 | 5.15 | 0.11 | 211. | 05.43 | 43.90 | -2 | 0 | 1.016 | 0.750 | 0.840 | 10.2 |
| .33 | 1.308 | 1.167 | | | | 05.96 | 43.90 | -2 | 0 | | | | |
| .39 | 1.308 | 1.167 | | | | 05.71 | 43.90 | -2 | 0 | | | | |
| .72 | 1.308 | 1.167 | 66.4 | 2.45 | 163. | 18.90 | 43.90 | -2 | 0 | 2.151 | 0.755 | --- | |
| .24 | 1.438 | 1.308 | 4.96 | 2.37 | 57.8 | 04.86 | 46.00 | -5 | -2 | 1.034 | 0.784 | 0.800 | -1.3 |
| .33 | 1.438 | 1.308 | | | | 04.85 | 46.00 | -5 | -2 | | | | |
| .39 | 1.438 | 1.308 | | | | 04.96 | 46.00 | -5 | -2 | | | | |
| .72 | 1.438 | 1.308 | | | | 14.60 | 46.00 | -5 | -2 | | | | |
| Sample D372 | | | | Tsubs = 760.0 °C | | | | | | | | | |
| Thickness = 2.5 μm | | | | : $N_DH$ = 3.23E17 at/$cm^3$ | | | | | : μ = 1480 $cm^2$/V-s | | | | |
| .39 | 0.341 | 0.185 | 1.12 | 0.51 | 3.77 | 11.50 | 36.60 | -2 | 0 | 1.120 | 0.845 | 0.900 | -4.9 |
| .62 | 0.341 | 0.185 | | | | 123.0 | 36.00 | -2 | 0 | | | | |
| .39 | 0.438 | 0.341 | | | | 07.13 | 36.00 | -4 | -2 | | | | |
| .62 | 0.438 | 0.341 | | | | 112.0 | 36.00 | -4 | -2 | | | | |
| .39 | 0.371 | 0.181 | 54.1 | 2.86 | 5.08 | 10.60 | 35.40 | -2 | 0 | 1.043 | 0.844 | 0.850 | -3.4 |
| .62 | 0.371 | 0.181 | | | | 114.0 | 35.40 | -2 | 0 | | | | |
| .39 | 0.452 | 0.371 | | | | 10.70 | 36.90 | -4 | -2 | | | | |
| .62 | 0.452 | 0.371 | | | | 151.0 | 36.90 | -4 | -2 | | | | |
| .39 | 0.231 | 0.137 | 27.7 | 3.78 | 0.15 | 11.90 | 63.90 | -1.5 | 0 | 1.144 | 0.830 | 0.850 | -10. |
| .62 | 0.231 | 0.137 | 28.9 | 4.89 | 5.34 | 151.0 | 63.90 | -1.5 | 0 | 1.086 | 0.857 | --- | |

TABLE I.1 (Continued)

| Ea | $W_0$ | $W_1$ | Rs | Rsh | Js | $N_T$ | $N_D$ | $V_0$ | $V_1$ | n | $\phi_b$ | $V_b$ | %err |
|---|---|---|---|---|---|---|---|---|---|---|---|---|---|
| eV | μm | μm | Ω | Ω | $A/cm^2$ | $at/cm^3$ | $at/cm^3$ | Volt | Volt | | eV | eV | $V_b$ & $n*\phi_b$ |
| | | | | E6 | E-9 | E14 | E15 | | | | | | |
| Sample D372e#1 | | | Tsubs = 760.0 °C | | | | 1 etch of 1μm | | | | | | |
| Thickness = 2.5 μm | | | $:N_DH$ = 3.23E17 $at/cm^3$ | | | | :μ = 1480 $cm^2/V$-s | | | | | | |
| .62 | 1.128 | 1.077 | 68.6 | 2.26 | 124. | 57.30 | 243.0 | -1.5 | 0 | 1.175 | 0.772 | --- | |
| .62 | 1.128 | 1.077 | | | | 55.50 | 243.0 | -1.5 | -.08 | | | | |
| .62 | 1.278 | 1.077 | 48.3 | | 4.96 | 09.85 | 243.0 | -0.5 | -0 | 1.360 | 0.739 | 1.260 | 25.3 |
| Sample D373#2 | | | Tsubs = 810.0 °C | | | | | | | | | | |
| Thickness = 9.3 μm | | | $:N_DH$ = 1.53E17 $at/cm^3$ | | | | :μ = 2300 $cm^2/V$-s | | | | | | |
| .62 | 0.452 | 0.179 | 25.2 | | 1.47 | 05.93 | 43.20 | -5 | 0 | 1.094 | 0.878 | 0.970 | 01.0 |
| .39 | 0.452 | 0.179 | | | | | 43.20 | -5 | 0 | | | | |
| Sample D374e#2 | | | Tsubs = 760.0 °C | | | | 1 etch of 1μm | | | | | | |
| Thickness = 3.5 μm | | | $:N_DH$ = 4.77E17 $at/cm^3$ | | | | :μ = 1640 $cm^2/V$-s | | | | | | |
| 62 | 1.116 | 1.073 | 34.2 | 3.81 | 15.6 | 22.20 | 274.0 | -1.5 | 0 | 1.073 | 0.839 | 1.020 | 13.3 |
| 62 | 1.116 | 1.073 | | | | 20.30 | 274.0 | -1.5 | -.08 | | | | |
| .62 | 1.091 | 1.073 | 52.5 | 2.57 | 27.5 | 23.00 | 274.0 | -0.5 | -.08 | 1.095 | 0.824 | --- | |
| Sample D374Re_2 | | | Tsubs = 760.0 °C | | | | 1 etch of 1 μm | | | | | | |
| Thickness = 3.5 μm | | | $:N_DH$ = 4.77E17 $at/cm^3$ | | | | :μ = 1640 $cm^2/V$-s | | | | | | |
| 62 | 1.139 | 1.067 | 24.7 | 2.99 | 32.9 | 11.00 | 325.0 | -1 | 0 | 1.097 | 0.817 | 0.950 | 06.0 |

TABLE I.1 (Continued)

| Ea | $W_0$ | $W_1$ | Rs | Rsh | Js | $N_T$ | $N_D$ | $V_0$ | $V_1$ | n | $\phi_b$ | $V_b$ | %err |
|---|---|---|---|---|---|---|---|---|---|---|---|---|---|
| eV | μm | μm | Ω | Ω | $A/cm^2$ | $at/cm^3$ | $at/cm^3$ | Volt | Volt | | eV | eV | $V_b$ & $n*\phi_b$ |
| | | | | E6 | E-9 | E14 | E15 | | | | | | |
| Sample D374R_2 | | | Tsubs = 760.0 °C | | | | | | | | | | |
| Thickness = 3.5 μm | | | : $N_DH$ = 4.77E17 $at/cm^3$ | | | | | : μ = 1640 $cm^2/V-s$ | | | | | |
| .24 | 1.422 | 1.023 | 59.5 | 12.6 | .668 | 3.920 | 32.60 | -1 | 0 | 1.092 | 0.921 | --- | |
| .33 | 1.422 | 1.023 | 56.3 | | | 4.100 | 32.60 | -1 | 0 | 3.364 | 0.582 | --- | |
| .39 | 1.422 | 1.023 | | | | 3.700 | 32.60 | -1 | 0 | | | | |
| Sample D374 | | | Tsubs = 760.0 °C | | | | | | | | | | |
| Thickness = 3.5 μm | | | : $N_DH$ = 4.77E17 $at/cm^3$ | | | | | : μ = 1640 $cm^2/V-s$ | | | | | |
| 24 | 0.555 | 0.468 | 24.1 | 22.4 | .215 | 21.10 | 35.30 | -2 | 0 | 1.100 | 0.920 | --- | |
| .33 | 0.555 | 0.468 | | | | 29.16 | 35.30 | -2 | 0 | | | | |
| .39 | 0.555 | 0.468 | | | | 29.11 | 35.30 | -2 | 0 | | | | |
| .52 | 0.555 | 0.468 | | | | 12.20 | 35.30 | -2 | 0 | | | | |
| .24 | 0.641 | 0.555 | | | | 26.20 | 74.60 | -7 | -2 | | | | |
| .33 | 0.641 | 0.555 | | | | 42.40 | 74.60 | -7 | -2 | | | | |
| .39 | 0.641 | 0.555 | | | | 43.80 | 74.60 | -7 | -2 | | | | |
| .52 | 0.641 | 0.555 | | | | 30.20 | 74.60 | -7 | -2 | | | | |
| Sample D374_1 | | | Tsubs = 760.0 °C | | | | | | | | | | |
| Thickness = 3.5 μm | | | : $N_DH$ = 4.77E17 $at/cm^3$ | | | | | : μ = 1640 $cm^2/V-s$ | | | | | |
| .24 | 0.550 | 0.507 | 25.3 | 14.2 | .467 | 25.70 | 33.60 | -1 | 0 | 1.062 | 0.906 | --- | |
| .33 | 0.550 | 0.507 | | | | 28.00 | 33.60 | -1 | 0 | | | | |
| .39 | 0.550 | 0.507 | | | | 26.90 | 33.60 | -1 | 0 | | | | |
| .52 | 0.550 | 0.507 | | | | 11.00 | 33.60 | -1 | 0 | | | | |

TABLE I.1 (Continued)

| Ea | $W_0$ | $W_1$ | Rs | Rsh | Js | $N_T$ | $N_D$ | $V_0$ | $V_1$ | n | $\phi_b$ | $V_b$ | %err |
|---|---|---|---|---|---|---|---|---|---|---|---|---|---|
| eV | μm | μm | Ω | Ω | $A/cm^2$ | $at/cm^3$ | $at/cm^3$ | Volt | Volt | | eV | eV | $V_b$ & $n*\phi_b$ |
| | | | | E6 | E-9 | E14 | E15 | | | | | | |
| Sample D374_2 | | | Tsubs = 760.0 °C | | | | | | | | | | |
| Thickness = 3.5 μm | | | : $N_D$H = 4.77E17 $at/cm^3$ | | | | | | : μ = 1640 $cm^2$/V-s | | | | |
| .24 | 0.620 | 0.550 | 29.3 | 5.52 | 4.33 | 30.07 | 54.80 | -4 | -1 | 1.095 | 0.871 | --- | |
| .33 | 0.620 | 0.550 | | | | 50.20 | 54.80 | -4 | -1 | | | | |
| .39 | 0.620 | 0.550 | | | | 54.40 | 54.80 | -4 | -1 | | | | |
| .52 | 0.620 | 0.550 | | | | 29.50 | 54.80 | -4 | -1 | | | | |
| Sample D374_1a | | | Tsubs = 760.0 °C | | | | | | | | | | |
| Thickness = 3.5 μm | | | : $N_D$H = 4.77E17 $at/cm^3$ | | | | | | : μ = 1640 $cm^2$/V-s | | | | |
| .24 | 0.445 | 0.408 | 24.9 | 5.45 | 2.40 | 23.90 | 52.80 | -1 | 0 | 1.053 | 0.887 | --- | |
| .33 | 0.445 | 0.408 | 29.4 | 5.54 | 4.33 | 27.90 | 52.80 | -1 | 0 | 1.095 | 0.871 | --- | |
| .39 | 0.445 | 0.408 | | | | 27.20 | 52.80 | -1 | 0 | | | | |
| .52 | 0.445 | 0.408 | | | | 13.70 | 52.80 | -1 | 0 | | | | |
| .24 | 0.498 | 0.445 | | | | 39.90 | 89.40 | -4 | -2 | | | | |
| .33 | 0.498 | 0.445 | | | | 72.10 | 89.40 | -4 | -2 | | | | |
| .39 | 0.498 | 0.445 | | | | 76.60 | 89.40 | -4 | -2 | | | | |
| .52 | 0.498 | 0.445 | | | | 48.20 | 89.40 | -4 | -2 | | | | |

TABLE I.1 (Continued)

| Ea | $W_0$ | $W_1$ | Rs | Rsh | Js | $N_T$ | $N_D$ | $V_O$ | $V_1$ | n | $\phi_b$ | $V_b$ | %err |
|---|---|---|---|---|---|---|---|---|---|---|---|---|---|
| eV | μm | μm | Ω | Ω | $A/cm^2$ | $at/cm^3$ | $at/cm^3$ | Volt | Volt | | eV | eV | $V_b$ & $n*\phi_b$ |
| | | | | E6 | E-9 | E14 | E15 | | | | | | |
| Sample D375 | | | | Tsubs = 810.0 °C | | | | | | | | | |
| Thickness = 10.0 μm | | | | : $N_D$H = 1.87E18 $at/cm^3$ | | | | | : μ = | | $cm^2$/V-s | | |
| .24 | 1.316 | 0.063 | 41.6 | 3.28 | 44.2 | 1.910 | 22.80 | -2 | 0 | 1.281 | 0.810 | --- | |
| .33 | 1.316 | 0.063 | | | | 2.990 | 22.80 | -2 | 0 | | | | |
| .39 | 1.316 | 0.063 | | | | 3.800 | 22.80 | -2 | 0 | | | | |
| .52 | 1.316 | 0.063 | | | | 3.610 | 22.80 | -2 | 0 | | | | |
| Sample D377#1 | | | | Tsubs = 780.0 °C | | | | | | | | | |
| Thickness = 3.7 μm | | | | : $N_D$H = 04.0E17 $at/cm^3$ | | | | | : μ = 1770 $cm^2$/V-s | | | | |
| .72 | 0.278 | 0.119 | 24.6 | 3.13 | 7.41 | 35.90 | 89.70 | -4 | 0 | 1.036 | 0.836 | 1.010 | 16.0 |
| .39 | 0.278 | 0.119 | | | | | 64.20 | -4 | 0 | | | | |
| .72 | 1.589 | 1.540 | 23.3 | 2.97 | .178 | 12.60 | 52.10 | -2 | 0 | 1.086 | 0.816 | 0.920 | 3.81 |
| .39 | 1.589 | 1.540 | | | | | 52.10 | -2 | 0 | | | | |
| Sample D378_1 | | | | Tsubs = 780.0 °C | | | | | 1 etch of 1 μm | | | | |
| Thickness = 3.8 μm | | | | : $N_D$H = | | | $at/cm^3$ | | : μ = | | $cm^2$/V-s | | |
| .62 | 0.256 | 0.146 | 5.39 | 5.48 | 345. | 14.60 | 58.40 | -2 | 0 | 1.021 | 0.736 | 0.880 | 17.1 |
| .62 | 0.371 | 0.256 | 5.50 | .181 | 843. | 11.40 | 64.20 | -5 | -2 | 1.075 | 0.709 | 0.880 | 15.3 |

TABLE I.1 (Continued)

| Ea eV | $W_0$ μm | $W_1$ μm | Rs Ω | Rsh Ω E6 | Js $A/cm^2$ E-9 | $N_T$ $at/cm^3$ E14 | $N_D$ $at/cm^3$ E15 | $V_0$ Volt | $V_1$ Volt | n | $\phi_b$ eV | $V_b$ eV | %err $V_b$ & $n^*\phi_b$ |
|---|---|---|---|---|---|---|---|---|---|---|---|---|---|
| Sample D379#2 | | | | Tsubs = 780.0 °C | | | | | | | | | |
| Thickness = 4.2 μm | | | | :$N_DH$ = 2.20E17 $at/cm^3$ | | | | | :μ = 1500 $cm^2/V\text{-}s$ | | | | |
| .24 | 0.857 | 0.729 | 48.6 | | .121 | 13.30 | 29.80 | -4 | -0 | 1.571 | 0.822 | --- | |
| .33 | 0.857 | 0.729 | | | | 25.20 | 29.80 | -4 | 0 | | | | |
| .39 | 0.857 | 0.729 | | | | 07.08 | 29.80 | -4 | 0 | | | | |
| .52 | 0.857 | 0.729 | | | | 03.57 | 29.80 | -4 | 0 | | | | |
| Sample R2 | | | | Tsubs = 776.0 °C | | | | | 1 etch of 1μm | | | | |
| Thickness = 10.0 μm | | | | :$N_DH$ = 5.67E16 $at/cm^3$ | | | | | :μ = 3680 $cm^2/V\text{-}s$ | | | | |
| .80 | 1.833 | 1.276 | 46.4 | 38.7 | .407 | 0.284 | 16.50 | -7 | 0 | 1.072 | 0.874 | 0.960 | 02.5 |
| .72 | 1.833 | 1.276 | | | | 1.040 | 16.50 | -7 | 0 | | | | |
| .80 | 1.833 | 1.279 | 37.1 | 4.77 | .245 | 0.286 | 16.10 | -7 | 0 | 1.099 | 0.832 | 0.960 | 05.0 |
| .72 | 1.833 | 1.279 | | | | 0.957 | 16.10 | -7 | 0 | | | | |
| 80 | 1.833 | 1.419 | | | | 0.290 | 16.10 | -7 | -1 | | | | |
| .72 | 1.833 | 1.419 | | | | 1.070 | 16.10 | -7 | -1 | | | | |
| | | | 48.7 | 9.51 | 1.13 | | 16.50 | | | 1.087 | 0.850 | 0.970 | 05.0 |
| Sample R3 | | | | Tsubs = 776.0 °C | | | | | | | | | |
| Thickness = 10.0 μm | | | | :$N_DH$ = 4.35E16 $at/cm^3$ | | | | | :μ = 3660 $cm^2/V\text{-}s$ | | | | |
| .80 | 0.738 | 0.521 | | | | 0.399 | 21.11 | -3 | 0 | 1.200 | 0.830 | --- | |
| .72 | 0.738 | 0.521 | | | | 2.020 | 21.11 | -3 | 0 | | | | |

TABLE I.1 (Continued)

| Ea | $W_0$ | $W_1$ | Rs | Rsh | Js | $N_T$ | $N_D$ | $V_0$ | $V_1$ | n | $\phi_b$ | $V_b$ | %err |
|---|---|---|---|---|---|---|---|---|---|---|---|---|---|
| eV | μm | μm | Ω | Ω | $A/cm^2$ | $at/cm^3$ | $at/cm^3$ | Volt | Volt | | eV | eV | $V_b$ & $n*\phi_b$ |
| | | | | E6 | E-9 | E14 | E15 | | | | | | |
| Sample R5 | | | | | Tsubs = 774.0 °C | | | | | | | | |
| Thickness = 09.0 μm | | | | | : $N_DH$ = 5.20E16 $at/cm^3$ | | | | | : μ = 3390 $cm^2/V-s$ | | | |
| | | | | | .480 | | 13.50 | -7 | 0 | 1.138 | 0.870 | 1.010 | 02.1 |
| | | | | | .344 | | 25.73 | -7 | 0 | 1.170 | 0.881 | 1.240 | 20.3 |
| | | | | | | | 23.90 | -7 | 0 | 1.147 | 0.864 | 1.030 | 03.9 |
| Sample R6 | | | | | Tsubs = 810.0 °C | | | | | | | | |
| Thickness = 13.0 μm | | | | | : $N_DH$ = 3.83E16 $at/cm^3$ | | | | | : μ = 4080 $cm^2/V-s$ | | | |
| .80 | 0.572 | 0.193 | 31.2 | | 1.08 | 0.548 | 38.80 | -7 | 0 | 1.082 | 0.860 | 0.910 | 02.2 |
| .72 | 0.572 | 0.193 | | | | 1.820 | 38.80 | -7 | 0 | | | | |
| .80 | 0.286 | 0.193 | | | | --- | 38.80 | -1 | 0 | | | | |
| .72 | 0.286 | 0.193 | | | | 2.230 | 38.80 | -1 | 0 | | | | |
| .80 | 0.572 | 0.353 | | | | 0.548 | 38.80 | -7 | -2 | | | | |
| .72 | 0.572 | 0.353 | | | | 1.828 | 38.80 | -7 | -2 | | | | |
| .80 | 0.521 | 0.182 | 40.8 | 17.1 | .721 | 0.511 | 40.10 | -7 | 0 | 1.091 | 0.846 | 0.920 | 00.3 |
| .72 | 0.521 | 0.182 | | | | 1.641 | 40.10 | -7 | 0 | | | | |

TABLE I.1 (Continued)

| Ea | $W_0$ | $W_1$ | Rs | Rsh | Js | $N_T$ | $N_D$ | $V_0$ | $V_1$ | n | $\phi_b$ | $V_b$ | %err |
|---|---|---|---|---|---|---|---|---|---|---|---|---|---|
| eV | μm | μm | Ω | Ω | $A/cm^2$ | $at/cm^3$ | $at/cm^3$ | Volt | Volt | | eV | eV | $V_b$ & $n*\phi_b$ |
| | | | | E6 | E-9 | E14 | E15 | | | | | | |
| Sample R8 | | | | Tsubs = 860.0 °C | | | 1 etch of 1μm | | | | | | |
| Thickness = 30.0 μm | | | | : $N_D$H = 6.66E16 $at/cm^3$ | | | : μ = 3850 $cm^2$/V-s | | | | | | |
| .80 | 1.595 | 1.282 | 13.4 | 86.9 | .701 | 0.570 | 33.80 | -7 | -1 | 1.080 | 0.868 | 0.890 | 05.1 |
| .72 | 1.595 | 1.282 | | | | 0.400 | 33.80 | -7 | -1 | | | | |
| .80 | 1.595 | 1.282 | | | | 0.526 | 33.80 | -7 | -1 | | | | |
| .72 | 1.595 | 1.282 | | | | 0.400 | 33.80 | -7 | -1 | | | | |
| .80 | 1.282 | 1.194 | | | | 0.452 | 38.80 | -1 | 0 | | | | |
| .80 | 1.282 | 1.194 | | | | 0.799 | 38.80 | -1 | 0 | | | | |
| Sample R10 | | | | Tsubs = 750.0 °C | | | 1 etch of ≈ 1μm | | | | | | |
| Thickness = 06.0 μm | | | | : $N_D$H = 2.90E16 $at/cm^3$ | | | : μ = 3680 $cm^2$/V-s | | | | | | |
| .80 | 2.051 | 1.329 | 256. | 174. | .640 | 0.071 | 08.39 | -7 | 0 | 1.089 | 0.877 | 1.300 | 35.0 |
| .72 | 2.051 | 1.329 | | | | --- | 08.39 | -7 | 0 | | | | |
| .80 | 1.772 | 1.303 | | | | 0.052 | 07.41 | -2 | 0 | 1.089 | 0.867 | 1.000 | 05.9 |
| .72 | 1.772 | 1.303 | | | | 0.529 | 07.41 | -2 | 0 | | | | |
| .80 | 2.760 | 1.772 | | | | 0.089 | 09.63 | -7 | -2 | | | | |
| .72 | 2.760 | 1.772 | | | | 0.835 | 09.63 | -7 | -2 | | | | |
| | | | 205. | 10.8 | .430 | | | | | 1.080 | 0.879 | --- | |
| | | | 203. | 14.5 | .350 | | | | | 1.079 | 0.781 | 0.980 | 04.3 |
| | | | 256. | 14.6 | .402 | | | | | 1.089 | 0.867 | 1.000 | 05.9 |

TABLE I.1 (Continued)

| Ea | $W_0$ | $W_1$ | Rs | Rsh | Js | $N_T$ | $N_D$ | $V_0$ | $V_1$ | n | $\phi_b$ | $V_b$ | %err |
|---|---|---|---|---|---|---|---|---|---|---|---|---|---|
| eV | μm | μm | Ω | Ω | $A/cm^2$ | $at/cm^3$ | $at/cm^3$ | Volt | Volt | | eV | eV | $V_b$ & $n*\phi_b$ |
| | | | | E6 | E-9 | E14 | E15 | | | | | | |
| Sample R16 | | | | Tsubs = 860.0 °C | | | | | | | | | |
| Thickness = 41.0 μm | | | | : $N_D H$ = 8.15E15 $at/cm^3$ | | | | | : $\mu$ = 4760 $cm^2/V-s$ | | | | |
| .80 | 1.534 | 0.620 | 30.4 | 140. | .626 | 0.417 | 03.69 | -5 | 0 | 1.074 | 0.880 | 1.060 | 12.1 |
| .72 | 1.534 | 0.620 | | | | 0.631 | 03.69 | -5 | 0 | | | | |
| .80 | 1.767 | 0.911 | | | | 0.516 | 03.69 | -7 | -1 | | | | |
| .72 | 1.767 | 0.911 | | | | 0.572 | 03.69 | -7 | -1 | | | | |
| .80 | 1.767 | 0.911 | | | | 0.485 | 03.69 | -7 | -1 | | | | |
| .72 | 1.767 | 0.911 | | | | 0.608 | 03.69 | -7 | -1 | | | | |
| .80 | 1.985 | 1.029 | 33.1 | 9.64 | .907 | 0.394 | 02.93 | -7 | -1 | 1.095 | 0.847 | 0.950 | 02.4 |
| .72 | 1.985 | 1.029 | | | | 0.461 | 02.93 | -7 | -1 | | | | |
| .80 | 1.985 | 1.029 | | | | 0.390 | 02.93 | -7 | -1 | | | | |
| .72 | 1.985 | 1.029 | | | | 0.447 | 02.93 | -7 | -1 | | | | |
| .80 | 2.200 | 1.166 | 163. | 11.0 | .861 | 0.749 | 0.861 | -2 | 0 | 1.099 | 0.887 | --- | |
| .72 | 2.200 | 1.166 | | | | 0.110 | 0.861 | -2 | 0 | | | | |
| .80 | 3.470 | 2.450 | | | | 0.622 | 1.061 | -7 | -3 | | | | |
| .72 | 3.470 | 2.450 | | | | 0.097 | 1.061 | -7 | -3 | | | | |

TABLE I.1 (Continued)

| Ea | $W_0$ | $W_1$ | Rs | Rsh | Js | $N_T$ | $N_D$ | $V_0$ | $V_1$ | n | $\phi_b$ | $V_b$ | %err |
|---|---|---|---|---|---|---|---|---|---|---|---|---|---|
| eV | μm | μm | Ω | Ω | $A/cm^2$ | $at/cm^3$ | $at/cm^3$ | Volt | Volt | | eV | eV | $V_b$ & $n*\phi_b$ |
| | | | | E6 | E-9 | E14 | E15 | | | | | | |
| Sample B39 | | | | Tsubs = 805.0 °C | | | | | | | | | |
| Thickness = 21.0 μm | | | | : $N_DH$ = 7.53E16 $at/cm^3$ | | | | | | : μ = 3460 $cm^2/V-s$ | | | |
| | | | | 139. | .381 | --- | 29.10 | -5 | 0 | 1.087 | 0.872 | 1.030 | 8.66 |
| | | | | 4.69 | 3.63 | --- | 23.30 | -4 | 0 | 1.089 | 0.821 | 0.870 | 02.3 |
| Sample B41 | | | | Tsubs = 800.0 °C | | | | | | | | | |
| Thickness = 30.0 μm | | | | : $N_DH$ = 7.00E16 $at/cm^3$ | | | | | | : μ = 3530 $cm^2/V-s$ | | | |
| .72 | 0.729 | 0.223 | 6.93 | 11.7 | .750 | 0.660 | 22.40 | -7 | 0 | 1.070 | 0.830 | --- | |
| Sample B42 | | | | Tsubs = 800.0 °C | | | | | | | | | |
| Thickness = 20.5 μm | | | | : $N_DH$ = 4.30E16 $at/cm^3$ | | | | | | : μ = 3825 $cm^2/V-s$ | | | |
| 80 | 7.050 | 5.560 | 28.8 | 9.38 | 1.14 | 0.041 | 19.90 | -7 | 0 | 1.087 | 0.860 | 0.930 | -.52 |
| .72 | 7.050 | 5.560 | | | | 0.215 | 19.90 | -7 | 0 | | | | |
| 80 | 7.050 | 5.560 | | | | 0.049 | 19.90 | -7 | 0 | | | | |
| 72 | 7.050 | 5.560 | | | | 0.215 | 19.90 | -7 | 0 | | | | |

TABLE I.1 (Continued)

| Ea | $W_0$ | $W_1$ | Rs | Rsh | Js | $N_T$ | $N_D$ | $V_0$ | $V_1$ | n | $\phi_b$ | $V_b$ | %err |
|---|---|---|---|---|---|---|---|---|---|---|---|---|---|
| eV | μm | μm | Ω | Ω | $A/cm^2$ | $at/cm^3$ | $at/cm^3$ | Volt | Volt | | eV | eV | $V_b$ & $n*\phi_b$ |
| | | | | E6 | E-9 | E14 | E15 | | | | | | |
| Sample B46 | | | | Tsubs = 850.0 °C | | | | | | | | | |
| Thickness = 70.0 μm | | | | $:N_DH$ = 5.11E16 $at/cm^3$ | | | | | $:\mu$ = 4150 $cm^2/V-s$ | | | | |
| .80 | 0.535 | 0.230 | 4.33 | 2.39 | 99.0 | 01.13 | 32.10 | -5 | 0 | 1.316 | 0.757 | --- | |
| .72 | 0.535 | 0.230 | | | | --- | 32.10 | -5 | 0 | | | | |
| .80 | 0.663 | 0.416 | 5.47 | | 34.6 | 01.27 | 27.26 | -7 | -2 | 1.310 | 0.768 | --- | |
| .72 | 0.663 | 0.416 | | | | 08.91 | 27.26 | -7 | -2 | | | | |
| .80 | 0.353 | 0.237 | | | | 0.806 | 73.90 | -1 | 0 | --- | --- | 0.970 | |
| .72 | 0.353 | 0.237 | | | | 12.40 | 73.90 | -1 | 0 | | | | |
| .80 | 1.116 | 1.035 | 6.27 | 13.2 | 1.07 | 2.655 | 40.70 | -1 | 0 | 1.091 | 0.854 | 0.890 | -4.5 |
| .72 | 1.116 | 1.035 | | | | 12.30 | 40.70 | -1 | 0 | | | | |
| .80 | 1.395 | 1.186 | | | | 01.16 | 40.70 | -7 | -2 | | | | |
| .72 | 1.395 | 1.186 | | | | 09.10 | 40.70 | -7 | -2 | | | | |
| .80 | 2.475 | 2.363 | | | | 0.786 | 79.20 | -1 | 0 | 1.083 | 0.846 | 0.850 | -7.2 |
| .72 | 2.475 | 2.363 | | | | 6.420 | 79.20 | -1 | 0 | | | | |
| 80 | 2.737 | 2.475 | | | | 0.551 | 79.20 | -5 | -1 | | | | |
| .72 | 2.737 | 2.475 | | | | 5.180 | 79.20 | -5 | -1 | | | | |
| .80 | 3.365 | 3.410 | | | | --- | 22.00 | -2 | 0 | 1.068 | 0.894 | 0 880 | -7.8 |
| .72 | 3.465 | 3.410 | | | | 4.761 | 22.00 | -2 | 0 | | | | |
| .80 | 3.465 | 3.465 | | | | --- | 22.00 | -7 | -2 | | | | |
| .72 | 3.846 | 3.465 | | | | 4.180 | 22.00 | -7 | -2 | | | | |

TABLE 1.1 (Continued)

| Ea | $W_0$ | $W_1$ | Rs | Rsh | Js | $N_T$ | $N_D$ | $V_0$ | $V_1$ | n | $\phi_b$ | $V_b$ | %err |
|---|---|---|---|---|---|---|---|---|---|---|---|---|---|
| eV | μm | μm | Ω | Ω | $A/cm^2$ | $at/cm^3$ | $at/cm^3$ | Volt | Volt | | eV | eV | $V_b$ & $n*\phi_b$ |
| | | | | E6 | E-9 | E14 | E15 | | | | | | |
| Sample B47 | | | Tsubs = 840.0 °C | | | | | 1 etch of 1μm | | | | | |
| Thickness = 32 0 μm | | | : $N_DH$ = 1.07E17 $at/cm^3$ | | | | | : μ = 3290 $cm^2/V-s$ | | | | | |
| | | | 5.09 | 6.58 | 2.81 | --- | 78.40 | -5 | 0 | 1.094 | 0.824 | 0.880 | 02.4 |
| | | | 5.32 | 2.94 | 25.3 | --- | 78.30 | -7 | 0 | 1.162 | 0.777 | 0.830 | 08.1 |
| | | | 7.90 | 2.65 | 40.0 | --- | 71.60 | -7 | 0 | 1.108 | 0.757 | 0.840 | 00.2 |
| Sample B48 | | | Tsubs = 860.0 °C | | | | | Etch 4.8μm | | | | | |
| Thickness = 50 0 μm | | | : $N_DH$ = 2.76E16 $at/cm^3$ | | | | | : μ = 4260 $cm^2/V-s$ | | | | | |
| .80 | 5.463 | 5.077 | 8.15 | 15.9 | .990 | 0.385 | 24.60 | -7 | 0 | 1.084 | 0.860 | 0.940 | 0.83 |
| .80 | 5.494 | 5.156 | 8.09 | 6.85 | .698 | 0.247 | 24.70 | -7 | -1 | 1.073 | 0.854 | 0.970 | 5.80 |
| Sample B50 | | | Tsubs = 815.0 °C | | | | | Etch 4.8μm | | | | | |
| Thickness = 18 0 μm | | | : $N_DH$ = 7.11E16 $at/cm^3$ | | | | | : μ = 4290 $cm^2/V-s$ | | | | | |
| 80 | 5 355 | 5.033 | 16 5 | 14.5 | 1.07 | 0.388 | 22.80 | -4 | 0 | 1.062 | 0.830 | 0.880 | 06.9 |
| | | | 18 0 | 28.0 | .686 | --- | 24.20 | -7 | 0 | 1.074 | 0.868 | 0.990 | 06.2 |
| | | | 16.9 | 5.14 | 1.26 | --- | 36.30 | -7 | 0 | 1.089 | 0.853 | 0.890 | 04.2 |

TABLE I.1 (Continued)

| Ea | $W_0$ | $W_1$ | Rs | Rsh | Js | $N_T$ | $N_D$ | $V_0$ | $V_1$ | n | $\phi_b$ | $V_b$ | %err |
|---|---|---|---|---|---|---|---|---|---|---|---|---|---|
| eV | μm | μm | Ω | Ω | $A/cm^2$ | $at/cm^3$ | $at/cm^3$ | Volt | Volt | | eV | eV | $V_b$ & $n*\phi_b$ |
| | | | | E6 | E-9 | E14 | E15 | | | | | | |
| Sample B51 | | | | Tsubs = 880.0 °C | | | | | | | | | |
| Thickness = 44.0 μm | | | | : $N_DH$ = 6.90E16 $at/cm^3$ | | | | | : μ = 3940 $cm^2/V-s$ | | | | |
| .80 | 0.670 | 0.267 | 3.61 | 10.9 | 53.1 | 0.292 | 18.20 | -5 | 0 | 1.382 | 0.760 | 0.940 | 10.5 |
| .72 | 0.670 | 0.267 | | | | --- | 18.20 | -5 | 0 | | | | |
| .80 | 0.757 | 0.535 | | | | 0.403 | 18.20 | -7 | -2 | | | | |
| .72 | 0.757 | 0.535 | | | | 2.183 | 18.20 | -7 | -2 | | | | |
| .80 | 0.416 | 0.267 | | | | 0.680 | 18.20 | -1 | 0 | | | | |
| .72 | 0.416 | 0.267 | | | | 2.270 | 18.20 | -1 | 0 | | | | |
| .80 | 0.729 | 0.286 | 5.92 | 9.45 | 1.89 | 0.274 | 16.70 | -5 | 0 | 1.314 | 0.786 | 0.910 | 11.9 |
| .72 | 0.729 | 0.286 | | | | --- | 16.70 | -5 | 0 | | | | |
| | | | | | | --- | 13.30 | -1 | 0 | 1.064 | 0.876 | 1.330 | 0.85 |
| | | | | | | --- | 13.30 | -1 | 0 | | | | |
| .80 | 1.433 | 1.147 | | | | 0.420 | 13.30 | -7 | 0 | | | | |
| .72 | 1.433 | 1.147 | | | | 0.229 | 13.30 | -7 | 0 | | | | |
| .80 | 2.706 | 2.382 | 6.84 | 10.7 | 2.09 | 1.130 | 14.50 | -2 | 0 | 1.025 | 0.911 | --- | |
| .72 | 2.706 | 2.382 | | | | --- | 14.50 | -2 | 0 | | | | |
| .80 | | | | | | 1.230 | 14.50 | -7 | -2 | | | | |
| .72 | | | | | | --- | 14.50 | -7 | -2 | | | | |

TABLE I.1 (Continued)

| Ea | $W_0$ | $W_1$ | Rs | Rsh | Js | $N_T$ | $N_D$ | $V_0$ | $V_1$ | n | $\phi_b$ | $V_b$ | %err |
|---|---|---|---|---|---|---|---|---|---|---|---|---|---|
| eV | μm | μm | Ω | Ω | $A/cm^2$ | $at/cm^3$ | $at/cm^3$ | Volt | Volt | | eV | eV | $V_b$ & $n*\phi_b$ |
| | | | | E6 | E-9 | E14 | E15 | | | | | | |
| Sample B52 | | | Tsubs = 760.0 °C | | | | | | | | | | |
| Thickness = 07.0 μm | | | : $N_DH$ = 7.79E16 $at/cm^3$ | | | : μ = 3580 $cm^2/V-s$ | | | | | | | |
| 80 | | | 41.8 | 6.69 | 2.08 | 0.294 | 17.10 | -2 | 0 | 1.130 | 0.862 | 0.910 | 6.57 |
| .72 | | | | | | 1.950 | 17.10 | -2 | 0 | | | | |
| .80 | | | | | | 0.273 | 19.50 | -7 | -3 | | | | |
| .72 | | | | | | 1.653 | 19.50 | -7 | -3 | | | | |
| Sample B57 | | | Tsubs = 840.0 °C | | | | | | | | | | |
| Thickness = 26.0 μm | | | : $N_DH$ = 8.98E16 $at/cm^3$ | | | : μ = 3000 $cm^2/V-s$ | | | | | | | |
| .80 | 0.932 | 0.397 | 7.18 | 3.46 | 1.23 | 0.337 | 10.70 | -5 | 0 | 1.109 | 0.864 | 0.910 | 5.03 |
| .72 | 0.932 | 0.397 | | | | 1.660 | 10.70 | -5 | 0 | | | | |
| Sample B58 | | | Tsubs = 750.0 °C | | | | | | | | | | |
| Thickness = 06 0 μm | | | : $N_DH$ = 5.35E16 $at/cm^3$ | | | : μ = 3300 $cm^2/V-s$ | | | | | | | |
| 72 | 1 296 | 0 341 | 91.2 | 35.3 | .504 | 0.448 | 13.40 | -7 | 0 | 1.088 | 0.870 | 0.910 | 04.0 |
| .72 | 1.296 | 0.511 | | | | 0.445 | 13.40 | -7 | -1 | | | | |
| .72 | 0.972 | 0.341 | | | | 0.403 | 11.70 | -3 | 0 | | | | |
| Sample B60 | | | Tsubs = 800.0 °C | | | 1 etch of ≈ 1 μm | | | | | | | |
| Thickness = 15 0 μm | | | : $N_DH$ = 6.07E16 $at/cm^3$ | | | : μ = 3080 $cm^2/V-s$ | | | | | | | |
| .80 | 1.643 | 1.092 | 36.2 | 11.3 | 1.68 | 0.254 | 16.30 | -7 | 0 | 1.091 | 0.867 | 0.980 | 3.61 |
| .72 | 1.643 | 1.092 | | | | 0.989 | 16.30 | -7 | 0 | | | | |

TABLE I.1 (Continued)

| Ea | $W_0$ | $W_1$ | Rs | Rsh | Js | $N_T$ | $N_D$ | $V_0$ | $V_1$ | n | $\phi_b$ | $V_b$ | %err |
|---|---|---|---|---|---|---|---|---|---|---|---|---|---|
| eV | μm | μm | Ω | Ω | $A/cm^2$ | $at/cm^3$ | $at/cm^3$ | Volt | Volt | | eV | eV | $V_b$ & $n*\phi_b$ |
| | | | | E6 | E-9 | E14 | E15 | | | | | | |
| Sample AS40MEP14.4 | | | | Tsubs = 750.0 °C | | | | | | | | | |
| Thickness = 14.4μm | | | | :$N_D$H = | | | $at/cm^3$ | | :μ = | | $cm^2$/V-s | | |
| .72 | 1.268 | 0.675 | 24.2 | 27.3 | 11.8 | 2.944 | 04.60 | -2 | 0 | 1.265 | 0.785 | 0.970 | 02.3 |
| .72 | 1.827 | 1.268 | | | | 2.810 | | -5 | -2 | | | | |
| .72 | 1.827 | 0.675 | | | | 3.263 | | -5 | -0 | | | | |
| .72 | 1.664 | 1.028 | | | | 3.110 | | -4 | -1 | | | | |
| Sample AS10MEP3.3 | | | | Tsubs = 750.0 °C | | | | | | | | | |
| Thickness = 3.3μm | | | | :$N_D$H = | | | $at/cm^3$ | | :μ = | | $cm^2$/V-s | | |
| .72 | 1.165 | 0.681 | 26.1 | 14.2 | 19.0 | 2.070 | 08.50 | -6 | -2 | 1.350 | 0.777 | 1.000 | 04.8 |
| .72 | 1.109 | 0.420 | | | | 2.180 | | -5 | 0 | | | | |
| .72 | 1.109 | 0.716 | | | | 1.343 | | -5 | -3 | | | | |
| Sample AS20M49C.2 | | | | Tsubs = 750.0 °C | | | | | | | | | |
| Thickness = | | | | :$N_D$H = | | | $at/cm^3$ | | :μ = | | $cm^2$/V-s | | |
| .72 | 1.493 | 0.612 | 66.5 | 6.49 | 17.8 | 2.620 | 04.40 | -5 | 0 | 1.166 | 0.783 | 1.420 | 14 2 |
| .72 | 1.493 | 1.093 | | | | 2.260 | | -5 | -2 | | | | |
| Sample ALU7M139_2 | | | | Tsubs = 750.0 °C | | | | | | | | | |
| Thickness = | | | | :$N_D$H = | | | $at/cm^3$ | | :μ = | | $cm^2$/V-s | | |
| .72 | 0.829 | 0.565 | 23.1 | 408. | 3.87 | 7.780 | 29.00 | -5 | 0 | 1.380 | 0.830 | 1.000 | 12.5 |
| .72 | 0.496 | 0.388 | | | | 2.270 | | -4 | -2 | | | | |

TABLE I.1 (Continued)

| Ea | $W_0$ | $W_1$ | Rs | Rsh | Js | $N_T$ | $N_D$ | $V_0$ | $V_1$ | n | $\phi_b$ | $V_b$ | %err |
|---|---|---|---|---|---|---|---|---|---|---|---|---|---|
| eV | μm | μm | Ω | Ω | $A/cm^2$ | $at/cm^3$ | $at/cm^3$ | Volt | Volt | | eV | eV | $V_b$ & $n*\phi_b$ |
| | | | | E6 | E-9 | E14 | E15 | | | | | | |
| Sample ALU8MIN.2 | | | | Tsubs = 750.0 °C | | | | | | | | | |
| Thickness = | | | | : $N_D$H = | | at/$cm^3$ | | : μ = | | $cm^2$/V-s | | | |
| .72 | 1.042 | 0.690 | | | | 0.149 | 09.30 | -5 | -1 | | | | |
| .72 | 0.690 | 0.489 | | | | 0.679 | 06.40 | -1 | 0 | | | | |
| Sample AU20M18.2 | | | | Tsubs = 750.0 °C | | | | | | | | | |
| Thickness = | | | | : $N_D$H = | | at/$cm^3$ | | : μ = | | $cm^2$/V-s | | | |
| .72 | 0.907 | 0 580 | 63.8 | 3.66 | 15.4 | 1.770 | 03.30 | -2 | 0 | 1.138 | 0.840 | 1.020 | 06.7 |
| .72 | 1.318 | 0.580 | | | | 1.920 | 06.30 | -6 | 0 | | | | |
| Sample AL20M18.2 | | | | Tsubs = 750.0 °C | | | | | | | | | |
| Thickness = | | | | : $N_D$H = | | at/$cm^3$ | | : μ = | | $cm^2$/V-s | | | |
| 72 | 0.695 | 0.372 | 198. | 10.0 | 370. | 7.380 | 10.00 | -2 | 0 | 1.897 | 0.787 | --- | |
| 72 | 1.011 | 0 372 | | | | 7.160 | 12.00 | -6 | 0 | 1.897 | 7.280 | 1.160 | 16.0 |
| Sample AU20M18.2 | | | | Tsubs = 750.0 °C | | | | | | | | | |
| Thickness = | | | | : $N_D$H = | | at/$cm^3$ | | : μ = | | $cm^2$/V-s | | | |
| .72 | 0.789 | 0.169 | 47.1 | 17.0 | 285. | 5.770 | 08.10 | -2 | 0 | 1.062 | 0.757 | 0.990 | 23.0 |
| 72 | 0.987 | 0.169 | | | | 4.760 | 09.10 | -6 | 0 | | | | |

TABLE I.1 (Continued)

| Ea | $W_0$ | $W_1$ | Rs | Rsh | Js | $N_T$ | $N_D$ | $V_0$ | $V_1$ | n | $\phi_b$ | $V_b$ | %err |
|---|---|---|---|---|---|---|---|---|---|---|---|---|---|
| eV | μm | μm | Ω | Ω | $A/cm^2$ | $at/cm^3$ | $at/cm^3$ | Volt | Volt | | eV | eV | $V_b$ & $n*\phi_b$ |
| | | | | E6 | E-9 | E14 | E15 | | | | | | |

| Sample 2AS2CM18,2 | | | Tsubs = 750.0 °C | | | | | | | | | | |
|---|---|---|---|---|---|---|---|---|---|---|---|---|---|
| Thickness = | | | | :$N_D$H = | | at/$cm^3$ | | | :μ = | $cm^2$/V-s | | | |
| .72 | 0.489 | 0.435 | | | | 03.03 | 13.00 | -2 | 0 | | | | |
| .72 | 1.078 | 0.489 | | | | 03.09 | 13.00 | -5 | -2 | | | | |
| .72 | 1.078 | 0.435 | | | | 03.17 | 13.00 | -5 | 0 | | | | |
| .72 | 1.078 | 4.899 | | | | 03.06 | 13.00 | -5 | -2 | | | | |

| Sample AU8MIN | | | Tsubs = 750.0 °C | | | | | | | | | | |
|---|---|---|---|---|---|---|---|---|---|---|---|---|---|
| Thickness = | | | | :$N_D$H = | | at/$cm^3$ | | | :μ = | $cm^2$/V-s | | | |
| .72 | | | 28.6 | 3.85 | 336. | 0.521 | 09.31 | -2 | 0 | 1.500 | 0.738 | 2.260 | |

| Sample 2AS2CM18,2 | | | Tsubs = 750.0 °C | | | | | | | | | | |
|---|---|---|---|---|---|---|---|---|---|---|---|---|---|
| Thickness = | | | | .$N_D$H = | | at/$cm^3$ | | | :μ = | $cm^2$/V-s | | | |
| .72 | 0.586 | 0.408 | | | | 08.84 | 26.00 | -1 | 0 | | | | |
| .72 | 0.946 | 0.408 | | | | 09.96 | 26.00 | -5 | 0 | | | | |
| .72 | 0.748 | 0.408 | | | | 09.87 | 26.00 | -3 | 0 | | | | |
| .72 | 0.946 | 0.834 | | | | 07.48 | 26.00 | -5 | -4 | | | | |
| .72 | 0.834 | 0.701 | | | | 11.10 | 26.00 | -4 | -2 | | | | |

TABLE I.1 (Continued)

| Ea | $W_0$ | $W_1$ | Rs | Rsh | Js | $N_T$ | $N_D$ | $V_0$ | $V_1$ | n | $\phi_b$ | $V_b$ | %err |
|---|---|---|---|---|---|---|---|---|---|---|---|---|---|
| eV | μm | μm | Ω | Ω | $A/cm^2$ | $at/cm^3$ | $at/cm^3$ | Volt | Volt | | eV | eV | $V_b$ & $n*\phi_b$ |
| | | | | E6 | E-9 | E14 | E15 | | | | | | |
| Sample EPI6MIN.1 | | | Tsubs = 750.0 °C | | | | | | | | | | |
| Thickness = | | | : $N_DH$ = | | | at/$cm^3$ | | : μ = | | $cm^2$/V-s | | | |
| .72 | 0.643 | 0.295 | | | | 06.99 | 27.00 | -5 | 0 | | | 2.530 | |
| Sample ASGA9MIN.3 | | | Tsubs = 750.0 °C | | | | | | | | | | |
| Thickness = | | | : $N_DH$ = | | | at/$cm^3$ | | : μ = | | $cm^2$/V-s | | | |
| .72 | | | | | | 14.30 | 74.60 | -5 | 0 | | | 1.350 | |
| .72 | | | | | | 08.90 | 74.60 | -1 | 0 | | | | |
| .72 | | | | | | 10.90 | 74.60 | -4 | -2 | | | | |
| Sample EP18MIN.3 | | | Tsubs = 750.0 °C | | | | | | | | | | |
| Thickness = | | | : $N_DH$ = | | | at/$cm^3$ | | : μ = | | $cm^2$/V-s | | | |
| .72 | 0.315 | 0.133 | | | | 15.40 | 99.00 | -5 | 0 | | | 1.166 | |
| .72 | 0.192 | 0.133 | | | | 12.00 | 99.00 | -1 | 0 | | | | |
| .72 | 0.270 | 0.133 | | | | 15.50 | 99.00 | -3 | 0 | | | | |
| Sample 2AS9MIN.1 | | | Tsubs = 750.0 °C | | | | | | | | | | |
| Thickness = | | | : $N_DH$ = | | | at/$cm^3$ | | : μ = | | $cm^2$/V-s | | | |
| .72 | 0.514 | 0.199 | | | | 03.18 | 58.00 | -5 | 0 | | | 0.960 | |

TABLE I.1 (Continued)

| Ea | $W_0$ | $W_1$ | Rs | Rsh | Js | $N_T$ | $N_D$ | $V_0$ | $V_1$ | n | $\phi_b$ | $V_b$ | %err |
|---|---|---|---|---|---|---|---|---|---|---|---|---|---|
| eV | μm | μm | Ω | Ω | $A/cm^2$ | $at/cm^3$ | $at/cm^3$ | Volt | Volt | | eV | eV | $V_b$ & $n*\phi_b$ |
| | | | | E6 | E-9 | E14 | E15 | | | | | | |
| Sample S29E12 | | | | Tsubs = 797.0 °C | | | | | | | | | |
| Thickness = 22.0 μm | | | | : $N_DH$ = 4.68E16 $at/cm^3$ | | | | | | : μ = 3430 $cm^2/V-s$ | | | |
| .72 | 0.738 | 0.416 | | | | 2.990 | 07.05 | -2 | 0 | 1.082 | 0.800 | 1.070 | 23.6 |
| .72 | 0.641 | 0.356 | | | | 3.180 | 07.48 | -2 | 0 | 1.028 | 0.910 | 1.000 | 06.9 |
| .72 | 1.043 | 0.641 | | | | 1.830 | 07.90 | -7 | -2 | 1.025 | 0.910 | 0.810 | |
| .72 | 1.785 | 1.458 | | | | 0.419 | 07.37 | -0 | 0 | 1.082 | 0.380 | 1.070 | 12.4 |
| .72 | 2.226 | 1.785 | | | | 0.559 | 08.16 | -7 | -2 | 1.047 | 0.976 | 1.490 | |
| .72 | 1.817 | 1.479 | | | | 0.285 | 06.55 | -2 | 0 | 1.047 | 0.976 | 1.080 | 05.7 |
| .80 | 1.817 | 1.479 | | | | 0.287 | 06.55 | -2 | 0 | | | | |
| .72 | 2.463 | 2.257 | | | | 0.514 | 19.20 | -2 | -0 | 1.120 | 0.839 | 0.880 | 06.3 |
| .72 | 2.725 | 2.463 | | | | 0.332 | 20.90 | -7 | -2 | 1.120 | 0.839 | 1.170 | |
| .72 | 2.451 | 2.257 | | | | 0.216 | 19.10 | -2 | -0 | 1.300 | 0.792 | 0.870 | -15 |

TABLE I.1 (Continued)

| Ea | $W_0$ | $W_1$ | Rs | Rsh | Js | $N_T$ | $N_D$ | $V_0$ | $V_1$ | n | $\phi_b$ | $V_b$ | %err |
|---|---|---|---|---|---|---|---|---|---|---|---|---|---|
| eV | μm | μm | Ω | Ω | $A/cm^2$ | $at/cm^3$ | $at/cm^3$ | Volt | Volt | | eV | eV | $V_b$ & |
| | | | | E6 | E-9 | E14 | E15 | | | | | | $n*\phi_b$ |
| Sample S30R3 | | | Tsubs = 778.0 °C | | | | | | | | | | |
| Thickness = 22.0 μm | | | : $N_D$H = 2.15E16 $at/cm^3$ | | | | | | : μ = 3330 $cm^2/V-s$ | | | | |
| .72 | 0.248 | 0.238 | | | | 2.450 | 21.19 | -2 | 0 | 1.055 | 0.895 | 0.850 | 10.0 |
| .80 | 0.248 | 0.238 | | | | 0.518 | 21.19 | -2 | 0 | | | | |
| .72 | 0.695 | 0.428 | | | | 1.860 | 21.40 | -7 | -2 | 1.096 | 0.864 | 0.770 | |
| 80 | 0.695 | 0.428 | | | | 0.380 | 21.40 | -7 | -2 | | | | |
| .72 | 0.476 | 0.238 | | | | 2.200 | 21.90 | -2 | 0 | 1.096 | 0.864 | 0.840 | -11. |
| .80 | 0.476 | 0.238 | | | | 0.441 | 21.90 | -2 | 0 | | | | |
| .72 | 1.672 | 1.376 | | | | 0.546 | 09.52 | -2 | 0 | 1.080 | 0.910 | 1.140 | |
| .72 | 1.683 | 1.379 | | | | 0.542 | 09.04 | -2 | 0 | 1.131 | 0.882 | 0.920 | 07.7 |
| .72 | 2.397 | 2.235 | | | | 0.496 | 27.30 | -2 | 0 | 1.100 | 0.884 | 1.040 | 06.9 |
| 72 | 2.614 | 2 397 | | | | 0.475 | 31.10 | -7 | -2 | 1.100 | 0.884 | 1.490 | |

## APPENDIX II: Space charge region derivation for a Schottky barrier

In an n-type non degenerated and uniformly doped SC of a Schottky barrier, the Poisson equation for the space charge region can be written as (35)

$$\frac{d^2V}{dx^2} = -\frac{q}{\epsilon_s}[p(x) - n(x) + N_D] \qquad (II.1)$$

where $\epsilon_s$ is the SC permitivity, $N_D$ is the shallow donor concentration[1], and n(x) and p(x) are the electron and hole concentrations at any point x in the SC respectively, and are given by (35)

$$n(x) = n_o e^{qV(x)/kT} \qquad (II.2a)$$

and

$$p(x) = p_o e^{-qV(x)/kT} \qquad (II.2b)$$

where $n_o$ and $p_o$ are the intrinsic carrier concentrations, q is the electronic charge of an electron, k is the Boltzmann's constant, T is the absolute temperature and V(x) is the voltage an any point x in the SC.

Equation II.1 can be simplified by neglecting the contribution of carriers (p-n) to the space charge region. Thus assuming complete ionization of the impurity ($N_D^+ = N_D$), we have

---

[1] Here $N_A$ is neglected since $N_D >> N_A$.

$$\frac{d^2V}{dx^2} = -\frac{q}{\epsilon_s}N_D \qquad 0 < x < W \qquad \text{(II.3a)}$$

$$= 0 \qquad x > 0 \qquad \text{(II.3b)}$$

where $\epsilon_s$ is the semiconductor permitivity, $N_D$ the donor concentration, and n and p are the electron and hole concentration in the semiconductor respectively.

Now, referring to figure II.1 (36), we can solve the above equation by using the point form of Gauss law, $d\varepsilon/dx=(q/\epsilon_s)N_D$, as follows:

$$\int_{\varepsilon_m}^{0} d\varepsilon = \frac{-q}{\epsilon_s}N_D \int_{0}^{W} dx \qquad 0 < x < W \qquad \text{(II.4)}$$

where the solution is

$$\varepsilon_m = \frac{-q}{\epsilon_s}N_D W \qquad \text{(II.5)}$$

and

$$\varepsilon(x) = \varepsilon_m\left(1 - \frac{x}{W}\right) \qquad \text{(II.6)}$$

according to figure II.1c. Note that for the case where the electric field has to be found at $\varepsilon(W-\lambda)$, we have to change the limit of integration of equation II.3 as follows;

$$\int_{\varepsilon(W-\lambda)}^{0} d\varepsilon = \frac{-q}{\epsilon_s}N_D \int_{(W-\lambda)}^{W} dx \qquad 0 < x < W-\lambda \qquad \text{(II.7)}$$

where the solution is

$$\varepsilon(W-\lambda) = -\frac{qN_D}{\epsilon_s}\lambda \qquad (II.8)$$

With the electric field it is now possible to relate the contact potential Vi by the relation;

$$\varepsilon(x) = -\frac{dV(x)}{dx} \qquad (II.9)$$

Thus, substituting equation II.6 into equation II.9 and solving for V(x) with the boundary conditions: V = 0 at x = W we get,

$$V(x) = \int_0^x \varepsilon(x)\,dx = -\frac{qN_D}{2\epsilon_s} W^2\left(1 - \frac{x}{W}\right)^2 \qquad (II.10)$$

The contact potential is obtained for V(x) = 0 in equation II.10. Thus,

$$Vi = \frac{-q}{2\epsilon_s} N_D W^2 \qquad (II.11)$$

Rearranging equation II.11 we obtain the space charge region at zero bias as

$$W = \left[\frac{2\epsilon_s}{qN_D} Vi\right]^{1/2} \qquad (II.12)$$

Finally, with an external bias voltage V (reverse or forward), the space charge region can be written as follows (36);

$$W = \left[\frac{2\epsilon_s}{qN_D}(Vi - V)\right]^{1/2} \qquad (II.13)$$

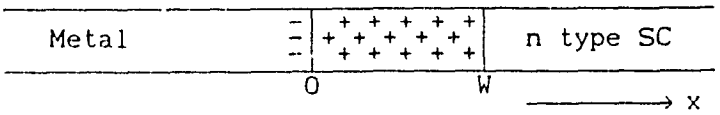


a) Transition region

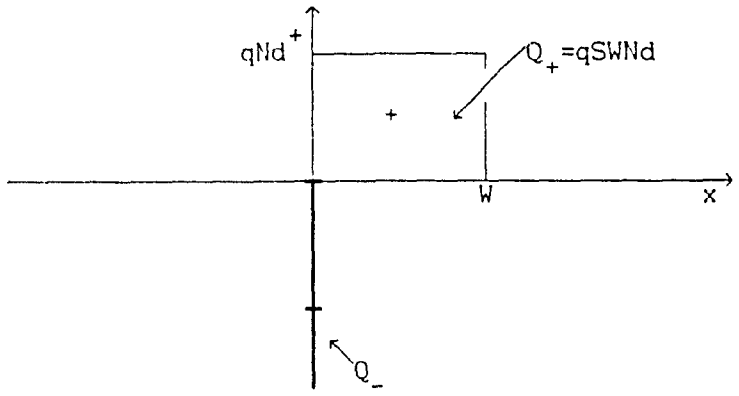


b) Charge density

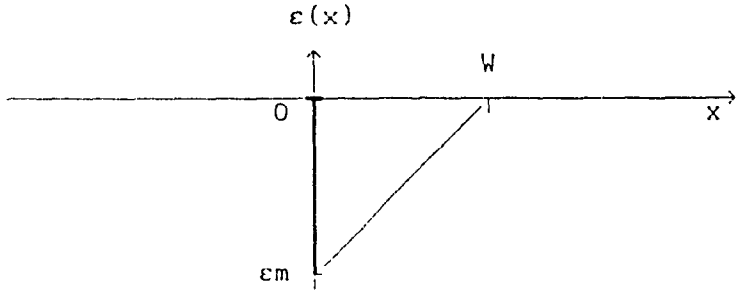


c) Electric field distribution

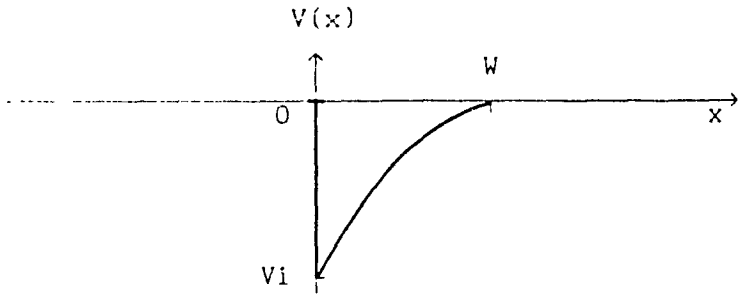


d) Potential distribution

Figure II. Schematic representation of a Schottky Barrier
a) Transition region b) charge density Q
c) Electric field dstribution
d) Potential distribution

A more accurate result is obtained when n(x) is taken into account and p(x) is neglected in equation II.1, thus (27)

$$W = \left[\frac{2\epsilon_s}{qN_D}(Vi - kT/q - V)\right]^{1/2} \qquad (II.14)$$

Now referring to figure II.1, it is seen that the charge Q in the transition region W (36) is given by

$$Q_+ = qSWN_D = S\left[2\epsilon_s qN_a(Vi - kT/q - V)\right]^{1/2} \qquad (II.15)$$

where S is the surface cross sectional area of the junction.

With the charge Q in the transition region, the capacitance of the junction is easily found by using (27) (28) the relation

$$C = dQ/dV \qquad (II.16)$$

Thus differentiating equation II.15 with respect to V we have the junction capacitance as

$$Cj = S\left[\frac{q\epsilon_s}{2[Vi-(kT/q)-V]}N_D\right]^{1/2} \qquad (II\ 17)$$

where (kT/q) is the contribution of the majority carriers to the space charge.

Is is clear here that the reverse bias structure forms a parallel plate capacitor comprising a layer of dielectric thickness W and dielectric constant $\epsilon_s$ between two conducting electrodes (28).

## APPENDIX III: The image force barrier lowering

The image force barrier lowering known as the Schottky effect can be understood by referring to figure III.1 below. If an electron is at a distance x from the metal, an electric field perpendicular to the metal surface is created. This field is calculated by assuming a positive image charge q located at a distance -x inside the metal. This creates the potential energy Fx of the electron relative to an electron at infinity. The potential energy Fx is thus added to the theoretical barrier energy -qεx giving the resultant barrier shown by the hard line on the figure. The maximum barrier height energy occurs at a distance $x_m$ from the metal surface. The barrier height is therefore lowered by an amount (39)

$$\Delta\phi_b = \left[\frac{q^3 N_D}{8\pi^2 \epsilon_s^3} (V_i - V)\right]^{1/4} \qquad \text{(III.1)}$$

where $\epsilon_s$ is the permitivity and V the applied voltage.

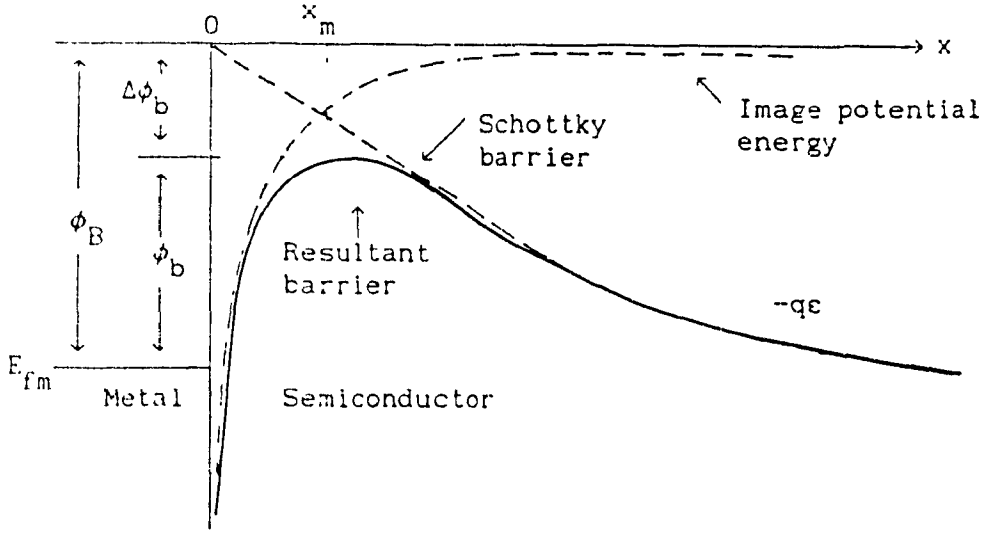


Fig. V.1 Diagram of the image force lowering of the barrier

## Appendix IV: Emission rate at thermal equilibrium

An electron trap exchange carriers with the conduction band and a hole trap exchange carriers with the valence band. For the case of an electron trap, equation 4.1 can be rewritten as

$$\frac{dn_T}{dt} = nC_n(N_T - n_T) - e_n n_T \qquad (IV.1)$$

At *thermal equilibrium* the probability $f_T$ that the state is occupied is given by the ratio of the concentration of defects occupied by electrons $n_T$ to the total trap concentration $N_T$, thus (50)

$$f_T = \frac{n_T}{N_T} \qquad (IV.2)$$

which can be described by the Fermi-Dirac statistics

Recalling for the present case, that the Fermi-Dirac statistic states the probability that an energy level Er is occupied by an electron at a given temperature T (50), thus

$$f_T = \frac{1}{1 + g_n^{\bullet} e^{-\{(E_F - E_T)/kT\}}} \qquad (IV\ 3)$$

where $g_n^{\bullet}$ is the degeneracy factor and $E_F$ is the Fermi level.

Now, substituting equation IV.2 into equation IV.1 we get

$$\frac{df_T}{dt} = -e_n f_T + nC_n(1 - f_T) \qquad (IV.4)$$

Consequently, the value of the emission rate $e_n$ can be found by using the principle of detailed balance, which states that in thermal equilibrium the carrier capture and the emission for each electron state must be equal (16) (54). Thus, at equilibrium $df_T/dt = 0$ and equation IV.4 becomes

$$e_n f_T = nC_n(1 - f_T) \qquad \text{(IV.5)}$$

Substituting equation IV.5 into equation IV.3 and solving for $e_n$ we obtain

$$e_n = nC_n g_n^{\bullet} e^{-((E_F-E_T)/KT)} \qquad \text{(IV.6)}$$

where the electron concentration n is given by (57)

$$n = N_c e^{[-(E_c-E_F)/kT]} \qquad \text{(IV.7)}$$

with $N_c$ the effective density of states at the conduction band edge given by (57)

$$N_c = 2\left(\frac{2\pi m_n^{\bullet} kT}{h^2}\right)^{3/2} \qquad \text{(IV.8)}$$

where h is the Plank's constant. Now with $C_n=\sigma_n\langle V_{th_n}\rangle$ and IV.7 into equation IV.6 we find the required value of $e_n$ as (16)(17)(54)

$$e_n = 1/\tau_n = N_c\sigma_n\langle V_{th_n}\rangle g_n^{\bullet} e^{-(E_D/kT)} \qquad \text{(IV.9)}$$

where $E_D$ is the Gibbs free energy of transition between the energy levels $E_T$ and $E_c$ ($E_D = E_c - E_T$).

Similarly, for an hole trap we obtain;

$$e_p = 1/\tau_p = N v \sigma_p \langle V th_p \rangle (g_p^*)^{-1} e^{(-E_D/kT)} \qquad (IV.10)$$

## Appendix V: Determination of the transition region λ

The transition region λ can be found by integrating Poisson's equation where λ is defined in the space charge region as shown in figure 4.2b After some mathematical manipulations, equation II.3 an be rewritten as

$$\frac{d}{dx}\left(x\,\frac{dV}{dx} - V\right) = -\,x\,\frac{\rho(x)}{\varepsilon dx} \qquad (V.1)$$

Integrating the above equation from (W-λ) to W we find λ as follows;

$$\left[x\,\frac{dV}{dx} - V\right]_{(W-\lambda)}^{W} = -\,\frac{1}{\epsilon}\int_{(W-\lambda)}^{W} x\,\rho(x)dx \qquad (V.2)$$

which leads to

$$V(W-\lambda) - V(W) + (W-\lambda)\varepsilon(W-\lambda) = \frac{qN_D}{2\epsilon}\{W^2 - (W-\lambda)^2\} \qquad (V.3)$$

Now, from figure 4.2 it can be seen that {V(W-λ) - V(W)} correspond to [(EF-ET)/q] and ε(W-λ) is simply equal to (qNdλ/ϵ) (equation II.8 appendix II). Therefore,

$$\frac{(E_F - E_T)}{q} - (W-\lambda)\frac{-2qN_D\lambda}{2\epsilon} = \frac{qN_D}{2\epsilon}[W^2 - (W-\lambda)^2] \qquad (V.4)$$

By simplifying this equation we obtain the transition region λ as (56)

$$\lambda = \left[\frac{2\epsilon}{q^2 N_D}(E_F - E_T)\right]^{1/2} \qquad (V.5)$$

## APPENDIX VI: Determination of ΔC/Co

In order to find ΔC/Co, we have to find the variation of the defect concentration between the limits ($W_1-\lambda_1$) and ($W_o-\lambda_o$) as shown in figure 4.4c. This is done by solving Poisson's equation or equation V.1 with the limits shown in figure 4.4c. Thus, we have

$$V(t) = \int_0^{W_o} x\frac{q}{\epsilon_s}N_D\,dx + \int_0^{W_1-\lambda_1} x\frac{q}{\epsilon_s}N_T\,dx + \int_{W_1-\lambda_1}^{W_o-\lambda_o} x\frac{q}{\epsilon_s}N_T(1-e^{-t/\tau_n})\,dx \qquad (VI.1)$$

The solution of the above equation is therefore

$$V(t) = \frac{q}{2\epsilon_s}N_D\,W_o^2 + \frac{q}{2\epsilon_s}N_T\,(W_1-\lambda_1)^2 + \frac{q}{2\epsilon_s}N_T\,[(W_o-\lambda_o)^2-(W_1-\lambda_1)^2](1-e^{-t/\tau_n})] \qquad (VI.2)$$

At t=0, the initial condition, we consider the initial width Wo, the capacitance Co and ($W_1-\lambda_1$) = $x_o$. Therefore equation VI.2 is rewritten as

$$V(0) = \frac{q}{2\epsilon_s}N_D\,W_o^2 + \frac{q}{2\epsilon_s}N_T\,(W_1-\lambda_1)^2 = \frac{q}{2\epsilon_s}N_D\,W_o^2 + \frac{q}{2\epsilon_s}N_T\,x_o^2 \qquad (VI.3)$$

At V(0) we have an initial value of (Vi + Vo) as shown in figure 4.4a which is therefore replaced in equation VI.3. We can rearrange the above equation in the following form as

$$\frac{2(V_o+V_i)\epsilon_s}{qN_DW_o^2} = \left[1 + \frac{N_T}{N_D}\left(\frac{x_o}{W_o}\right)^2\right] \qquad (VI.4)$$

Now with Co equals to $\epsilon_s/W_o$ substituted in equation VI.4 we obtain

$$Co\left[\frac{2(Vo+Vi)}{qN_D\epsilon_s}\right]^{1/2} = \left[1 + \frac{N_T}{N_D}\left(\frac{x_o}{W_o}\right)^2\right]^{1/2} \qquad (VI.5)$$

The root of the right hand side of this equation can be eliminated by expanding it in binomial expansion (59) and keeping the first order term since the total trap concentration is a lot smaller than the shallow donor concentration (i.e. $N_T << N_D$). Therefore, equation VI.5 becomes

$$Co\left[\frac{2(Vo+Vi)}{qN_D\epsilon_s}\right]^{1/2} \simeq \left[1 + \frac{N_T}{2N_D}\left(\frac{x_o}{W_o}\right)^2\right] \qquad (VI.6)$$

Now, at some value of t we consider the value of Vo + Vi constant since the variation in voltage is negligible due to the small change in $n_{T_e}$ between $(W_o-\lambda_o)$ and $(W_1-\lambda_1)$ (i.e. $V(t)\simeq(Vo+Vi)$). Thus proceeding the same ways as the above we obtain

$$C^2\left[\frac{2(Vo+Vi)}{qN_D\epsilon_s}\right] = 1 + \frac{N_T}{N_D}\left(\frac{x_o}{W_o}\right)^2 + \frac{N_T}{N_D}\frac{\{(W_o-\lambda_o)^2-W_1-\lambda_1)^2\}}{W_o^2}\,(1-e^{-t/\tau_n}) \qquad (VI.7)$$

Now, using the binomial expansion in equation VI.7 and keeping the first order term we get

$$C\left[\frac{2(Vo+Vi)}{qN_D\epsilon_s}\right]^{1/2} = \left[1 + \frac{N_T}{2N_D}\left(\frac{x_o}{W_o}\right)^2\right] + \frac{N_T}{2N_D}\frac{\{(W_o-\lambda_o)^2-(W_1-\lambda_1)^2\}}{W_o^2}\,(1-e^{-t/\tau_n}) \qquad (VI.8)$$

We notice that the first two terms in the square bracket on the right hand side of the above equation is equation VI.6. This leads to

$$(C - Co)\left[\frac{2(Vo+Vi)}{qN_D\epsilon_s}\right]^{1/2} = \frac{N_T}{2N_D}\,\frac{\{(W_o-\lambda_o)^2-(W_1-\lambda_1)^2\}}{W_o^2}\,(1-e^{-t/\tau_n}) \quad (VI.9)$$

Finally, the term inside the left hand side bracket in equation VI.9 is the value of 1/Co by comparing to equation II.17. This is justified by rewriting equation VI.6 in the following form;

$$Co = \left[\frac{q\epsilon_s}{2(Vo+vi)}\left\{N_D + N_T\left(\frac{x_o}{W_o}\right)^2\right\}\right] \quad (VI.10)$$

Since $N_T << N_D$ and $x_o << W_o$, $N_D$ remains and $N_T$ is neglected. Therefore, equation VI.9 becomes (58)

$$\frac{\Delta C}{Co} = \frac{C - Co}{Co} = \frac{N_T}{2N_D}\,\frac{\{(W_o-\lambda_o)^2-(W_1-\lambda_1)^2\}}{W_o^2}\,(1-e^{-t/\tau_n}) \quad (VI.11)$$

which the normalized variation of the capacitance between $(W_o-\lambda_o)$ and $(W_1-\lambda_1)$ due to trap defect when a bias pulse is applied to the Schottky barrier under reverse bias.

## APPENDIX VII: Arrhenius Plot and Rate Window

### VII.1 Arrhenius plot

The relation $1/\tau_n$ was given by equation 4.14 Now rewriting equation 4.14 and taking the natural logarithm on both sides we get

$$\ln(1) = \ln\left[\tau_n N_c \sigma_n \langle V_{th} \rangle e^{-Ea/kT}\right] \qquad \text{(VII.1)}$$

The above equation can be rearranged by multiplying it by $T^2/T^2$ inside the bracket of the right hand side, thus we obtain

$$\ln(\tau_n T^2) = \frac{Ea}{kT} - \ln\left(\frac{N_c \sigma_n \langle V_{th} \rangle}{T^2}\right) \qquad \text{(VII.2)}$$

where Nc and $\langle V_{th} \rangle$ can be simplified as $\alpha T^{3/2}$ and $\beta T^{1/2}$ respectively where

$$\alpha = 2\left(\frac{2\pi m_n^* k}{h^2}\right)^{3/2} \quad \text{and} \quad \beta = \{3K/m_n^*\}^{1/2} \qquad \text{(VII.3)}$$

Therefore, the second term of the right hand side in equation VII.2 is independent of the temperature, thus

$$\ln(\tau_n T^2) = \frac{Ea}{kT} - \ln\{\alpha\beta\sigma_n\} \qquad \text{(VII.4)}$$

Thus, the slope $\ln(\tau_n T^2)$ vs (1000/T) is called the Arrhenius plot (6). Its slope allow us to find the apparent activation energy Ea of the deep level trap and the capture cross section is obtain by the intercept with the y axis.

In fact, equation VII.4 is a straight line of the form y = ax + b where x represents 1/T. The slope is then given by

$$a = Ea/k \qquad \text{(VII.5a)}$$

and the intercept;

$$b = -\ln\{\alpha\beta\sigma_n\} \qquad \text{(VII.5b)}$$

which cuts the y axis. We recall here that a and b can be found from the least square method (31).

VII.2 Rate window

The rate window $\tau_n$ can be found by differendiating the normalized value of the DLTS peak S(T)/Co and equate it to zero in order to find its maximum. Thus,

$$\frac{S(T)}{Co} = \left[\frac{N_T}{2N_D}\,\frac{\{(W_o-\lambda)^2-(W_1-\lambda)^2\}}{W_o^2}\right]\left(e^{-t_1/\tau_n} - e^{-t_2/\tau_n}\right) \qquad \text{(VII.6)}$$

or

$$\frac{S(T)}{Co} = \left[\frac{N_T}{2N_D}\,\frac{\{(W_o-\lambda)^2-(W_1-\lambda)^2\}}{W_o^2}\right]\left(e^{-t_1 e_n(T)} - e^{-t_2 e_n(T)}\right) \qquad \text{(VII.7)}$$

Thus, differentiating with respect to temperature T we have

$$\frac{d}{dT}\frac{S(T)}{Co} = \frac{d}{dT}\left[\frac{N_T}{2N_D}\,\frac{\{(W_o-\lambda)^2-(W_1-\lambda)^2\}}{W_o^2}\right]\left(e^{-t_1 e_n(T)} - e^{-t_2\, e_n(T)}\right) = 0 \qquad \text{(VII.8)}$$

Therefore

$$\frac{d}{dT}\frac{S(T)}{Co} = \left[-t_1\frac{de_n(T)}{dT}\, e^{-t_1 e_n(T)} + t_2\frac{de_n(T)}{dT}\, e^{-t_2 e_n(T)}\right] = 0 \qquad \text{(VII.9)}$$

thus

$$\frac{de_n(T)}{dT}\left[-t_1\, e^{-t_1 e_n(T)} + t_2\, e^{-t_2 e_n(T)}\right] = 0 \qquad \text{(VII.10)}$$

We can now rewrite the above equation as follows

$$t_1\, e^{-t_1 e_n(T)} = t_2\, e^{-t_2 e_n(T)} \qquad \text{(VII.11)}$$

or

$$t_2/t_1 = e^{e_n(T)[t_2 - t_1]} \qquad \text{(VII.12)}$$

Finally, rearranging the above equation we obtain the rate window as

$$\tau_n = 1/e_n = \frac{[t_2 - t_1]}{\ln(t_2/t_1)} \qquad \text{(VII.13)}$$

## APPENDIX VIII: Summary on epitaxial layer grown by CSVT technique

The closed space vapor transport (CSVT) is a chemical transport between source and substrate separated by a fused silica spacer plate. For GaAs, water is used as the transport reagent operating at atmospheric pressure and moderates temperatures which make a cost effective procedure. The reaction used for the transport of GaAs is (5)(62)

$$2GaAs_{(s)} + H_2O_{(g)} \rightleftarrows Ga_2O_{(g)} + As_{2(g)} + H_{2(g)} \qquad \text{(VIII.1)}$$

The source and substrate may be both semi-insulating (SI) type or Si-doped GaAs n-type. For the epitaxial growth of GaAs on GaAs, this reaction is happening at two places in the system; on the surface of GaAs source at temperature $T_1$ and, on the surface of GaAs substrate at temperature $T_2$. The source temperature is higher than the temperature substrate by 40°C and the equilibrium is displaced to the left onto the substrate surface resulting in GaAs deposition onto the epitaxial layer.

The epitaxial layer set-up consists of a rectangular cross section (6.8 X 6.8 $cm^2$) fused silica chamber containing two graphite blocks as heat susceptors sandwiching between them the GaAs source and substrate separated by a thin fused silica spacer on the order of 0.3mm. One end of this reaction chamber, designed to accommodate 5cm diameter slice, is sealed while the other side is equipped with a fused silica taper joint containing the gas and thermocouple connections. The heat source is a set of 2KW globar (SiC) heating elements. The temperatures are

controlled by two thermocouples positioned in appropriate wells inside of the graphite blocks. The transport agent is wet hydrogen containing triply distilled water vapor corresponding to a saturator temperature of 0°C. The diagram of the CSVT system used for the growth of GaAs epitaxial layer is shown in figure VIII.1 (62).

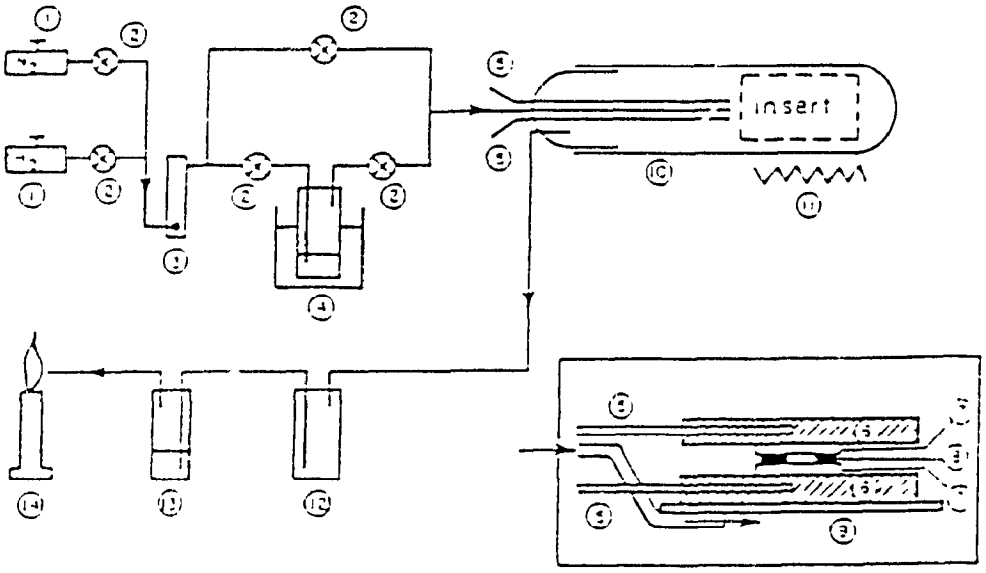


Fig VIII.1 Diagram of the CSVT system: (1) $N_2$ and $H_2$ gas cylinders; (2) valves; (3) fluxmeter; (4) water saturator; (5) thermocouples; (6) graphite blocs; (7) GaAs source and substrate; (8) fused silica spacer; (9) fused silica supporting plate; (10) fused silica reactor; (11) 2000W tungsten-hallogen lamp; (12) trap; (13) glycerol bubbler; (14) burner.

## Appendix IX: Results for temperature regulator for DLTS

TABLE IX.1: Readings for R at the cryostat tail and at the sample

| Cryostat R1 (Ω) | Sample R2 (Ω) | % error R1 & R2 | Cryostat R1 (Ω) | Sample R2 (Ω0 | % error R1 & R2 |
|---|---|---|---|---|---|
| 21.6 | 23.9 | -9.62 | 88.0 | 87.86 | 0.46 |
| 22.0 | 24 2 | -9.10 | 90 0 | 89.5 | 0.56 |
| 27.0 | 27.4 | -1.46 | 95.0 | 94 5 | 0 53 |
| 30.0 | 29.9 | 0.33 | 97.0 | 96.6 | 0.62 |
| 33.0 | 32.7 | 0.92 | 100.0 | 99.1 | 0.91 |
| 36.0 | 35.6 | 1.23 | 103.0 | 102 1 | 0.88 |
| 40.0 | 39.4 | 1.52 | 105 0 | 104.1 | 0.86 |
| 44.0 | 43.5 | 1.15 | 108.0 | 107.2 | 0.75 |
| 47.0 | 46.4 | 1.29 | 110.0 | 109 2 | 0 73 |
| 50.0 | 49.3 | 0.02 | 113.0 | 112.1 | 0.80 |
| 53.0 | 52.4 | 1.34 | 115 0 | 114 1 | 0 79 |
| 55.0 | 54.4 | 1 10 | 118.0 | 117.1 | 0.77 |
| 58.0 | 57.5 | 0.87 | 121.0 | 120.0 | 0.83 |
| 61.0 | 60.5 | 0.83 | 123 0 | 121.9 | 0.90 |
| 65.0 | 64.5 | 0.77 | 125.0 | 123 9 | 0.89 |
| 70.0 | 69.5 | 0.72 | 127.0 | 125.9 | 0 87 |
| 75.0 | 74.5 | 0.67 | 130 0 | 128.8 | 0.93 |
| 79.0 | 80.7 | -2.10 | 133.0 | 131.7 | 0.99 |
| 80.0 | 81.8 | -2.2 | 135 0 | 133.6 | 1.05 |
| 82.0 | 83.7 | -2.03 | 139.0 | 137.4 | 1.16 |
| 84.0 | 84.6 | -0.71 | 142.0 | 140.4 | 1.14 |
| 86.0 | 84.5 | 0.58 | 145.0 | 143.3 | 1.18 |

TABLE IX.2: Results from circuit of fig. IX.II

| V1 (-) volt | V2 (+) volt | V3 volt | DT (K) | \|V1-V2\| volt | V1 (-) volt | V2 (+) volt | V3 volt | DT (K) | \|V1-V2\| volt |
|---|---|---|---|---|---|---|---|---|---|
| 2.89 | 2.81 | 9.90 | 1.21 | -0.08 | 6.60 | 6.54 | 9.44 | 1.88 | -0.06 |
| 3.05 | 3.05 | 13.90 | 1.28 | -0.00 | 6.75 | 6.69 | 9.90 | 1.86 | -0.06 |
| 3.22 | 3.20 | 12.20 | 1.51 | -0.02 | 6.90 | 6.85 | 10.83 | 1.81 | -0.05 |
| 3.40 | 3.37 | 10.04 | 2.00 | -0.03 | 7.00 | 6.95 | 11.25 | 1.80 | -0.05 |
| 3.58 | 3.50 | 9.66 | 2.34 | -0.08 | 7.20 | 7.16 | 11.45 | 1.87 | -0.04 |
| 3.76 | 3.68 | 9.66 | 2.49 | -0.08 | 7.35 | 7.30 | 10.57 | 1.91 | -0.05 |
| 3.90 | 3.81 | 9.71 | 2.40 | -0.09 | 7.50 | 7.44 | 10.14 | 1.94 | -0.06 |
| 4.00 | 3.93 | 9.46 | 2.22 | -0.07 | 7.60 | 7.54 | 9.98 | 1.93 | -0.06 |
| 4.15 | 4.10 | 10.30 | 2.05 | -0.05 | 7.75 | 7.69 | 10.36 | 1.86 | -0.06 |
| 4.27 | 4.23 | 10.68 | 1.99 | -0.05 | 7.90 | 7.85 | 11.00 | 1.82 | -0.05 |
| 4.46 | 4.41 | 9.80 | 2.04 | -0.05 | 8.10 | 8.04 | 10.44 | 1.78 | -0.06 |
| 4.65 | 4.59 | 9.27 | 2.07 | -0.06 | 8.30 | 8.26 | 11.36 | 1.78 | -0.04 |
| 4.88 | 4.82 | 9.37 | 2.03 | -0.06 | 8.50 | 8.47 | 11.70 | 2.19 | -0.03 |
| 5.00 | 4.95 | 9.90 | 2.00 | -0.05 | 8.60 | 8.57 | 11.79 | 2.08 | -0.03 |
| 5.20 | 5.15 | 10.50 | 1.96 | -0.05 | 8.70 | 8.67 | 12.22 | 1.97 | -0.03 |
| 5.36 | 5.30 | 10.47 | 1.97 | -0.06 | 8.90 | 8.88 | 12.34 | 1.90 | -0.02 |
| 5.50 | 5.45 | 10.85 | 2.00 | -0.05 | 9.10 | 9.06 | 11.45 | 1.95 | -0.04 |
| 5.73 | 5.67 | 9.96 | 2.02 | -0.06 | 9.40 | 9.38 | 12.20 | 3.62 | ---- |
| 5.93 | 5.86 | 9.96 | 2.00 | -0.07 | 9.60 | 9.58 | 12.10 | 3.15 | -0.02 |
| 6.00 | 5.95 | 9.85 | 1.98 | -0.05 | 9.70 | 9.67 | 11.64 | 2.45 | -0.03 |
| 6.25 | 6.19 | 9.90 | 1.93 | -0.06 | 9.80 | 9.76 | 11.40 | 2.23 | -0.04 |
| 6.42 | 6.36 | 9.51 | 1.92 | -0.06 | 9.90 | 9.85 | 11.63 | 2.10 | -0.05 |

TABLE IX.2: (continued)

| V1 (-) volt | V2 (+) volt | V3 volt | DT (K) | \|V1-V2\| volt | V1 (-) volt | V2 (+) volt | V3 volt | DT (K) | \|V1-V2\| volt |
|---|---|---|---|---|---|---|---|---|---|
| 10.00 | 9.69 | 11.8 | 2.01 | -0.04 | 12.80 | 12.80 | 16.10 | 1.31 | 0.00 |
| 10.10 | 10.60 | 11.60 | 1.85 | -0.04 | 12.90 | 12.94 | 15.80 | 1.30 | 0.04 |
| 10.30 | 10.26 | 11.70 | 1.69 | -0.04 | 13.10 | 13.04 | 10.06 | 1.50 | -0.06 |
| 10.50 | 10.45 | 11.09 | 1.61 | -0.05 | 13.40 | 13.34 | 13.26 | 1.26 | -0.06 |
| 10.60 | 10.54 | 10.19 | 1.56 | -0.06 | 13.45 | 13.50 | 18.20 | 1.02 | 0.05 |
| 10.80 | 10.77 | 12.58 | 1.40 | -0.03 | 13.55 | 13.58 | 16.50 | 1.11 | 0.03 |
| 10.90 | 10.89 | 14.07 | 1.45 | -0.01 | 13.70 | 13.65 | 10.14 | 1.22 | -0.05 |
| 11.00 | 11.00 | 14.42 | 1.48 | 0.00 | 13.80 | 13.71 | 10.16 | 1.44 | -0.09 |
| 11.10 | 11.09 | 12.50 | 1.51 | -0.01 | 13.90 | 13.88 | 13.75 | 1.45 | -0.02 |
| 11.30 | 11.23 | 9.86 | 1.62 | -0.07 | 14.00 | 14.02 | 16.34 | 1.32 | 0.02 |
| 11.50 | 11.43 | 10.70 | 1.48 | -0.07 | 14.10 | 14.13 | 17.32 | 1.31 | 0.03 |
| 11.60 | 11.58 | 13.50 | 1.25 | -0.02 | 14.25 | 14.31 | 18.30 | 1.95 | 0.06 |
| 11.70 | 11.67 | 12.40 | 1.20 | -0.03 | 14.40 | 14.36 | 11.70 | 2.01 | -0.04 |
| 11.80 | 11.76 | 12.46 | 1.23 | -0.04 | 14.55 | 14.42 | 9.31 | 2.08 | -0.13 |
| 11.90 | 11.85 | 10.94 | 1.29 | -0.05 | 14.60 | 14.47 | 9.38 | 2.03 | -0.13 |
| 12.00 | 11.96 | 11.58 | 1.35 | -0.04 | 14.70 | 14.63 | 11.32 | 1.44 | -0.07 |
| 12.10 | 12.08 | 12.90 | 1.35 | -0.02 | 14.75 | 14.73 | 14.55 | 1.11 | -0.02 |
| 12.20 | 12.22 | 15.68 | 1.36 | 0.02 | 14.80 | 14.86 | 19.29 | 0.81 | 0.06 |
| 12.30 | 12.31 | 13.96 | 1.40 | 0.01 | 14.85 | 14.96 | 19.27 | 1.01 | 0.01 |
| 12.45 | 12.41 | 11.30 | 1.53 | -0.04 | 15.00 | 15.04 | 19.29 | 1.46 | 0.04 |
| 12.60 | 12.51 | 10.07 | 1.63 | -0.09 | 15.10 | 15.15 | 15.41 | 1.76 | 0.05 |
| 12.70 | 12.65 | 11.50 | 1.50 | -0.05 | 15.20 | 15.18 | 13.26 | 1.96 | -0.02 |

TABLE IX.2: (continued)

| V1 (-) volt | V2 (+) volt | V3 volt | D1 (K) | \|V1-V2\| volt | V1 (-) volt | V2 (+) volt | V3 volt | DT (K) | \|V1-V2\| volt |
|---|---|---|---|---|---|---|---|---|---|
| 15.30 | 15.26 | 12.43 | 1.90 | -0.04 | 17.30 | 17.31 | 16.30 | 0.97 | 0.00 |
| 15.40 | 15.37 | 13.29 | 1.52 | -0.03 | 17.40 | 17.53 | 19.26 | 0.83 | 0.13 |
| 15.45 | 15.44 | 14.40 | 1.42 | -0.01 | 17.50 | 17.61 | 19.26 | 1.11 | 0.11 |
| 15.50 | 15.51 | 15.38 | 1.25 | 0.01 | 17.60 | 17.68 | 19.27 | 1.28 | 0.08 |
| 15.55 | 15.57 | 16.18 | 1.12 | 0.02 | 17.70 | 17.78 | 19.26 | 1.55 | 0.08 |
| 15 60 | 15 62 | 16.27 | 1.13 | 0.02 | 17.80 | 17.99 | 19.24 | 2.56 | 0.19 |
| 15.70 | 15.71 | 14 44 | 1.18 | 0 01 | 17.85 | 18.05 | 19.25 | 2.27 | 0.10 |
| 15.85 | 15.77 | 9.57 | 1.24 | -0.08 | 17.86 | 18.14 | 19.25 | 2.27 | 0.28 |
| 15.90 | 15.81 | 9.64 | 1.21 | -0.09 | | | | | |
| 15.95 | 15.99 | 17.38 | 0.88 | 0.04 | | | | | |
| 16.00 | 16.04 | 17.90 | 0.84 | 0.04 | | | | | |
| 16.10 | 16.14 | 17.83 | 0.92 | 0.04 | | | | | |
| 16.15 | 16.20 | 18.68 | 1.17 | 0.05 | | | | | |
| 16.20 | 16.25 | 18.34 | 1.35 | 0.05 | | | | | |
| 16.30 | 16.33 | 15.40 | 1.52 | 0.03 | | | | | |
| 16.40 | 16.36 | 12.57 | 1.63 | -0.04 | | | | | |
| 16.50 | 16.47 | 12.90 | 1.55 | -0.03 | | | | | |
| 16.60 | 16.63 | 16.77 | 1.15 | 0.03 | | | | | |
| 16.70 | 16.68 | 12.87 | 1.15 | -0.02 | | | | | |
| 16.80 | 16.77 | 12.80 | 1.13 | -0.03 | | | | | |
| 16.90 | 16.99 | 15.79 | 0.90 | 0.00 | | | | | |
| 17.00 | 17.04 | 17.90 | 0.84 | 0.04 | | | | | |

# TEMPERATURE REGULATOR FOR DLTS

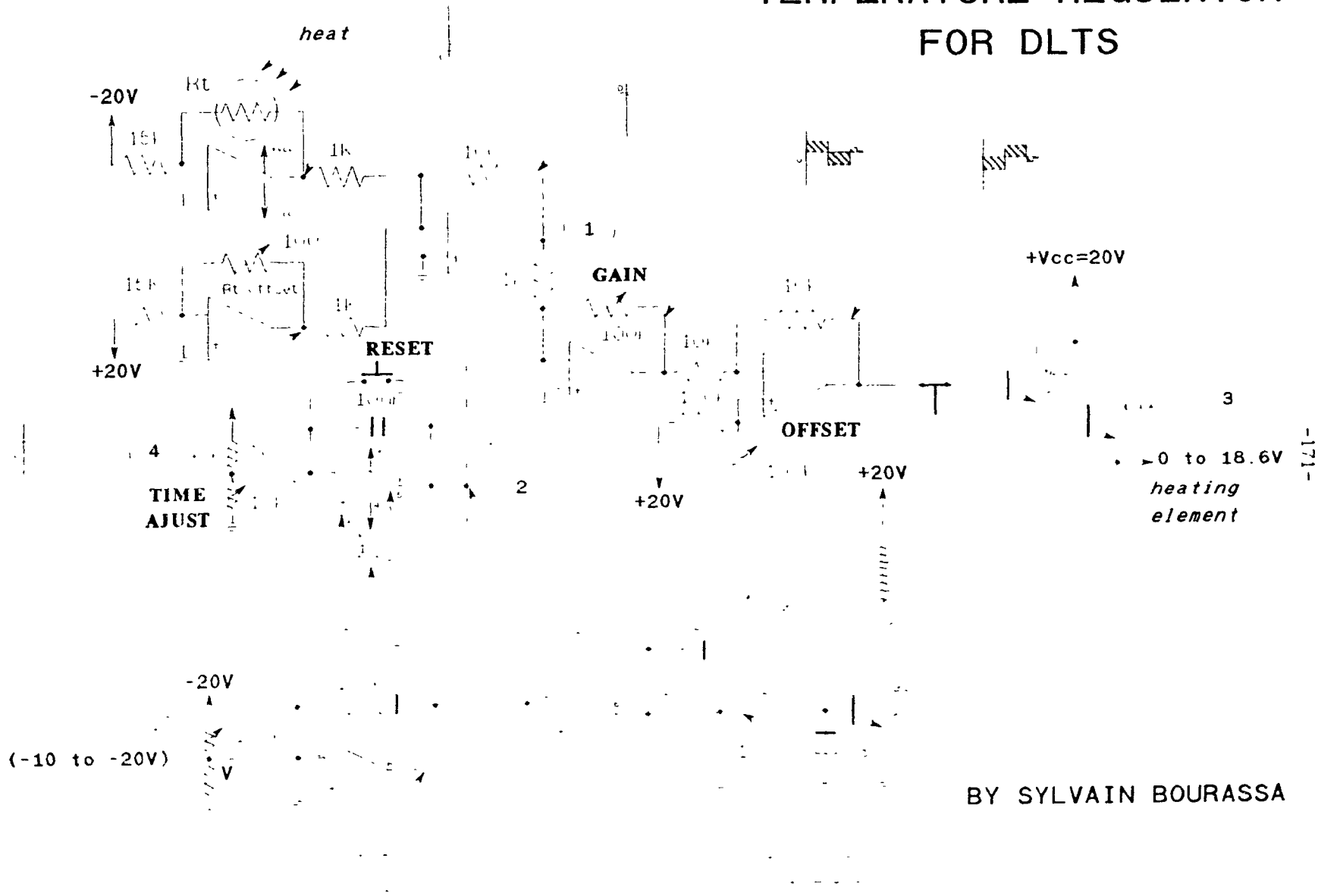


Figure IX.1

BY SYLVAIN BOURASSA

## APPENDIX X: Schottky barrier fabrication

This appendix gives the steps to follow for the fabrication of a Schottky barrier diode on a GaAs epitaxial layer at Concordia University in the Electrical Engineering Solid State Device Research Laboratory.

A- Sample cleaning procedure

1- Rinse the slice in boiling trichloroethane for five minutes.

2- Rinse the slice in boiling acetone for five minutes.

3- Rinse the slice in boiling methanol ($CH_3OH$) for five minutes.

4- Dip the slice in HF 20% (HF + distilled water) for 30 sec.

5- Rinse the slice in running deionized water for 30 sec.

6- Dry with gas nitrogen.

B- Annealing for ohmic contact

1- Put the sample inside the glass oven.

2- Let the nitrogen (gas) flow through the oven for 30 sec. The flow rate is 30. DO NOT FORGET TO LIGHT UP THE GAS BURNER.

3- Heat up the heating element for five min. under nitrogen (put the variac to 20).

4- While heating up, plug in the thermocouple.

5- Put hydrogen (for about two min.) and then increase the variac to maximum until, 20mV (500°C) is red on the voltmeter.

6- Keep the 20mV reading constant for 2min. (Readjust the variac if necessary).

7- Turn off the variac and the hydrogen and put back the nitrogen (gas) and let it cool off for 20 minutes.

8- Check the ohmic contact with the curve tracer.

C- Pd-Al Schottky contact

**i) Photo resist**

1- Clean up the sample: repeat step **A**.

2- Meanwhile, prepare the negative photo resist under yellow light : **two** negative photo resist for **one** thinner .

3- Adjust the temperature of the oven to 120°C and turn on the UV mask aligner.

4- Put the sample in the oven for **five** min.

5- Take out the sample of the oven and apply the photo resist:

-Put a piece of tape on the spinner and lay the sample on it.

-Dry the sample with nitrogen (gas) before applying the photo resist.

-Put a few drops of negative photo resist on the sample and spin at 3000 rpm for 15 sec.

-**Clean up** the spinner.

6- Put the sample back into the oven at 80°C for 15 min.

7- Take the sample out of the oven and align the dots on the sample using the mask aligner (UV for 15 sec.).

8- Then develop into the developer for **30 sec.** and more if necessary.

9- Rinse in running water (90°C) for one minute or more if necessary and dry with nitrogen (gas).

10- Put the sample back into the oven at 80°C for **15 min.**

**ii) Electroless solution preparation**

1- a) Prepare the $PdCl_2$ electroless solution:

-Dissolve 0.3 g of $PdCl_2$ in 9ml of HCl concentrate.

-Mix the above solution in 9ml of deoinized water.

-Poor the obtained solution in 864ml of acetic acid.

-Add 28ml of HF 49%.

b) Poor the electroless solution in a beecher and steer slowly with a magnetic agitator.

2- Prepare three beecher with --> 1-HCl, 2-DI water, 3-DI water.

a- Dip in HCl for **one min.**

b- Dip in water to stop the reaction.

c- Rinse in water for **30 sec.**

d- Dry the sample with nitrogen (gas).

3- Put the sample on the support and soak in the solution for **four min.** without agitating.

4- Rinse in DI water and repeat step 2 b, c, and d.

**iii) Evaporation**

1- Put the sample on the special support for evaporation purpose.

2- Starting off the evaporation with the EDWARDS vacuum evaporator:

a- The three valves of the evaporator are closed and the water is running then switch to **rotary pump.**

b- Open the **backing valve** to a minimum of 30 min. before performing the evaporation. -->clean up the oil.

c- Put to **diff rot pump** and wait for vacuum.

3- Install the support inside the bell jar:

a- Let the air flow in the bell jar by opening the **air**

valve.

b- Place an Al-pellet on the heating element and put the support inside the bell jar.

c- Put the bell jar to its original place.

d- Close the air valve and open the roughing valve.

e- While the vacuum is taking place, poor some liquid nitrogen in the liquid nitrogen trap on the left side of the evaporator and wait for the primary vacuum inside the bell jar ($>10^{-2}$torr).

f- When primary vacuum is done, close the roughing valve.

g- Open the main valve and wait until the secondary vacuum is reached to a maximum ($10^{-6}$ to $10^{-7}$ torr).

4- Performing the evaporation:

a- When the secondary vacuum is reached, add more liquid nitrogen. Heat up the element by increasing slowly the potentiometer. Check so that the vacuum (scale) remains as low as possible when increasing the current flowing through the heating element. Set up the potentiometer until the current element reaches 30A and let evaporate for 20 sec.

b- To cool down the sample wait 15 min. under vacuum.

c- Close the main valve and open the air valve. Let the air flow in until it is possible to remove the bell jar from the evaporator case. Then remove the sample.

d- When the evaporation experiment is finished:

A- <u>If by pass</u>

-Close the air valve and the main valve.

-Open the roughing valve.

-Switch off the **Diff-pump**.

B- <u>If for a long period of time</u>

-Close the air valve and the main valve.

-Open the roughing valve.

-Switch off the diff-pump.

-Wait half a day.

-Close the main valve.

-Close the backing valve.

-Switch off the rotary pump.

-Turn off the running water.

**iv) Photo resist removal**

1- Dip the sample in hot trichloroethane for a few minutes until flaws are observed on the photo resist surface.

2- Take a swab-stick and rub gently until the photo resist is completely removed (if necessary).

3- Finally, check the electrical properties of the Schottky barrier has been made.

S.B.